Prom. Nr. 3525

Theoretical Estimation of Dynamic Forces and Vibratory Stresses for a Turbine Blade

THESIS

presented to the Swiss Federal Institute of Technology, Zürich
for the Degree of Doctor of Technical Science

By

MOUSTAFA NAGUIB MAHMOUD NAGUIB

B. Sc. Cairo University

Citizen of the U A R

Accepted on the Recommendation of:

Professor Dr. W. Traupel and Professor Dr. Chr. Wehrli

Juris-Verlag Zürich
1965

Leer - Vide - Empty

Preface

The investigation described in this thesis was inspired by Prof. Dr. W. Traupel. I remain indebted to him for his constant encouragement and assistance, without which it would have been difficult to complete the work. I should like also to thank Prof. Dr. Chr. Wehrli for having recommended the acceptance of this thesis.

My thanks are also due to my colleague Mr. G. Mucklow for his help in preparing the final text of the manuscript.

Finally I must express my gratitude to the Government of the United Arab Republic (Egypt) for having endowed the scholarship which made it possible to continue my studies in Zürich.

Leer - Vide - Empty

CONTENTS

NOMENCLATURE

In this thesis it has been necessary to use a large number of symbols, and it was sometimes impossible to avoid using the same character with more than one meaning. The use of subscripts prevents ambiguity in the analysis, and it is to be hoped that no difficulty or misunderstanding will be caused by using this system of notation.

Since mainly non-dimensional analysis is used in the text and since the results are always presented in non-dimensional form, it is possible to avoid specifying any particular system of units. Symbols having dimensions are therefore given in the following list without their units.

Symbols:

a_n	non-dimensional Fourier coefficient for the expression of the velocity distribution at entrance to the moving row of blades.
a_n^*	Fourier coefficient for the expression of the velocity distribution at entrance to the moving row of blades.
a_ν	Amplitude of the ν th order of the dynamic force on the suction side of the blade.
A_n	non-dimensional Fourier coefficient for the expression of the mean velocity at entrance to the moving row of blades.
$\dot{A}_n$	non-dimensional Fourier coefficient for expressing the rate of change of the mean velocity at entrance to the moving row of blades.
b	blade channel width, see fig. 2.2.
b_n	similar to a_n.
b_n^*	similar to a_n^*.
b_ν	amplitude of the ν th order of the dynamic force on the pressure side of the blade.
B	non-dimensional blade-channel width.
B_n	similar to A_n.
$\dot{B}_n$	similar to $\dot{A}_n$.
c	absolute flow velocity.
c_n	similar to a_n.

c_n^*	similar to a_n^*.
C	non-dimensional absolute flow velocity.
C_n	similar to A_n.
$\dot{C}_n$	similar to $\dot{A}_n$.
d_n	similar to a_n.
d_n^*	similar to a_n^*.
D_n	similar to A_n.
$\dot{D}_n$	similar to $\dot{A}_n$.
$D_{n\ max}$	dynamic factor.
E	amplitude of the harmonic changes in cot β_2 , also Young's modulus of elasticity.
f	force acting on the moving blade.
F	non-dimensional force acting on the moving blade.
F_n	non-dimensional Fourier coefficient for the combined expression used in equation (2.64).
F_n & F'_n	Fourier coefficients for the expression of the dynamic force on the moving-blades.
F_n^*	harmonic coefficient of the dynamic force when divided by the steady force component at the mean radius.
g	total pressure.
G_n	similar to F_n in equation (2.64).
H_n	a factor depending on the shape and dynamic properties of the vibrating blade, see eqn. 3.22.
I	cross-section moment of inertia of the moving blade.
I_0	moment of inertia of the moving-blade hub section.
K	blade form parameter.
K_n	constant of proportionality as given in eqn. 3.11.
l^*	reference blade length.
M_{bn}	dynamic bending moment.
M_{bs}	static bending moment.

N	number of terms in the Fourier series.
p	static pressure.
P	non-dimensional static pressure.
P_1	harmonic coefficient in the Fourier expression for W_1^*.
q	deflection at the tip of the vibrating blade.
q_0	maximum deflection at the tip of the vibrating blade, also dynamic pressure.
Q_1	similar to P_1.
r	radius, also resultant of the harmonic coefficients, as given by eqn. 4.7.
r_m^*	mean radius at the reference plane.
R	pitch ratio.
R_n	relative amplitude of the harmonic coefficients of the dynamic force.
s	curvilinear coordinate along the mean stream line.
$\hat{s}$	distance along the mean stream line as shown in fig. 2.2.
S	non-dimensional curvilinear coordinate along the mean stream line.
$\hat{S}$	non-dimensional distance along the mean stream line.
S_n	dynamic stimulating factor or stimulus.
t	time.
t^*	reference time.
T'	stationary-blades pitch.
T''	moving-blades pitch.
$\hat{T}'$	non-dimensional pitch.
u	blade peripheral speed.
u_m^*	reference speed.
u_n	non-dimensional blade deflection.
w	relative flow velocity.
W	non-dimensional relative flow velocity.
W^*	velocity component responsible for unsteady directional changes in the exit flow.

x	distance coordinate used either along tangential flow direction or along the moving-blade length.
x_p	coordinate perpendicular to absolute flow direction at entrance.
x'	coordinate of the blade profile.
y_n	blade dynamic deflection at any instant t.
y'_p	blade-profile pressure-side coordinate.
y'_s	blade-profile suction-side coordinate.
Y_n	maximum dynamic deflection of the blade.
α	absolute flow angle.
α_n	harmonic coefficient in the product of two Fourier series.
β	relative flow angle.
β_n	similar to α_n.
γ	angle between the axial direction and the second principal plane of the turbine blade hub-section.
γ_o	blade chord angle.
δ	logarithmic decrement.
ζ	total-pressure-loss coefficient.
ν	ratio of moments of inertia I / I_0.
μ	non-dimensional peripheral speed of the blade.
ξ	non-dimensional coordinate used either along tangential flow direction or for distance along the moving-blade length.
ρ	density of flow medium.
σ	stress.
τ	non-dimensional time.
φ	geometric pitch angle.
φ_n	harmonic phase angle.
φ_ν	harmonic phase angle.
χ	non-dimensional coordinate along the tangential flow direction.
ψ_ν	harmonic phase angle.

ψ	harmonic phase angle for changes in cot β_2.
ψ_n	potential energy of the vibrating blade.

Subscripts etc.:

a	axial.
b	bending.
c	continuity.
e	energy.
l	lower.
m	mean and momentum.
n	harmonic order.
p	perpendicular to absolute flow direction.
s	static.
t	tangential.
u	upper.
ν	harmonic order.
0	before stationary row of blades.
1	before moving row of blades.
2	behind moving row of blades.
—	mean value.
'	first derivative.
"	second derivative.

1. INTRODUCTION

The turbine designer is faced with the challenge of a very wide variety of problems requiring the application of scientific ingenuity and knowledge. There are so many design problems in this field that it would be difficult to pick out a single feature in the turbine design and label it as the one which requires the most engineering skill and experience in its solution. However, if a list was to be made of design problems it is certain that turbine blades would appear near the top. Blade design covers a large range of scientific and engineering knowledge, and involves cooperative efforts in several scientific fields such as fluid flow, heat transfer, strength of materials and vibration.

The vibration of blades is a very important topic in the design of turbines. Not only blades of variable-speed turbines but also those of constant-speed ones suffer from the difficulty of being perfectly tuned. It is very often that a row of blades runs in resonance with an exciting harmonic force. The energy added to the blade during resonance is large enough to produce relatively high stresses. The alternating character of these stresses is very dangerous to the blades and can cause fatigue failures. Noticing that most blade failures are due to fatigue, we can see the importance of studying the character and level of these vibratory stresses.

There are many different causes for exciting a turbine blade into vibration, and a good review about them is given by A. Sabastiuk and F. Sisto [1][1)]. The object of this thesis is to study the problem of forced vibration due to non-uniform flow through turbine stages with full admission.

1.1. Analysis of the problem

The wakes shed from a stationary row of blades are considered as excitation to some modes of vibration of the moving blades. Since these wakes have a periodic nature they may be analysed into different harmonic components, which cause a periodically varying force to act on the moving blades. If one of these force harmonic-components coincides with one of the blades natural frequencies, it will lead to vibration and consequently cause high alternating stresses. The purpose of this study is to calculate first of all the magnitude of these exciting forces, and secondly, to calculate the vibratory stresses resulting in case of resonance.

In the first part of this work it is assumed that the velocity distribution before the moving row of blades is known. This can be achieved either by direct measurements, or analytically, by using boundary layer theory to find the shape of the wake.

---

1) numbers in squared brackets refer to references listed under Bibliography on page 116

This velocity distribution is considered to vary along the radial direction of the blade, according to the shape and configuration of both the stationary and the moving blades. The turbine moving blade is divided along its length into a sufficient number of sections to ensure an acceptable accuracy in representing the radial distribution of the resulting forces. Considering one of these sections, and choosing a proper control volume, we can apply the simplified momentum and energy equations to it; we will assume in this analysis a quasi one-dimensional flow, and neglect effects of viscosity and compressibility. In this way, two expressions are established for the axial and tangential components of the dynamic force on the turbine blade.

It is found that the value of the dynamic force depends upon the aerodynamic conditions before the moving blades (e.g. pressure and velocity distribution in the wake), and after them, also upon the shape and configuration of both the moving and the stationary blades. The periodic velocity distribution at entrance to the moving row of blades is expressed as a harmonic series, and then substituted in the expressions for the axial and tangential components of the dynamic force. The resulting dynamic force will thus be expressed in terms of a harmonic series, and we may then use this result to calculate the vibratory stresses. It might also be expected that the dynamic force depends on the flow direction at exit from the moving row of blades, which is found to vary periodically with time according to the periodical variation in the direction of the flow before this row. It is, however, difficult to establish the exact relationship between these two periodical flow variations. If we allow the velocity disturbances causing directional changes at entrance to the moving row of blades to pass totally undamped through this row to the exit plane, we can calculate one extreme value for the flow directional changes at exit; the calculation of the dynamic force based on this assumption is considered as an upper limit. The lower limit can then be calculated by assuming that the exit flow angle remains constant, i.e. that the velocity disturbances mentioned above are totally damped in passing through the moving row. In this case the angle of potential flow at exit from the moving blades row can be used.

The dynamic force is calculated for each one of the radial sections chosen, thus establishing the distribution of the dynamic force along the blade length. This method also yields the amplitudes and phase angles of the different harmonic orders of the exciting force along the blade length. By using this general form for the dynamic force distribution, it is possible to calculate the vibratory stresses with a better accuracy than has been achieved up to now.

In the second part of the work, the results obtained in the first one are applied to calculate the vibratory stresses in a turbine blade. In this study the blade is assumed to vibrate independently from the adjacent ones. The method of calculation

is given by Traupel [2], and has been extended so that it is valid for the general conditions in our case. Resonance is assumed to take place between one of the exciting-force harmonics and a natural frequency of the blade. By equating the work done by this harmonic force component on the vibrating blade to the sum of the potential and kinetic energy, increased by the amount of energy dissipated in heat, we can calculate the maximum blade deflection. This blade deflection depends on the mode of vibration, the damping capacity of the blade, as well as the distribution of the exciting force along the blade length. The maximum dynamic bending moment is assumed to occur at the blade-hub section, and is calculated by considering the blade deflection at resonance; in this way the vibratory bending-stresses at the hub section may be calculated. A dynamic stimulating factor or stimulus is obtained, and is found to depend largely on the radial distribution of the amplitudes and phase angles of the exciting harmonic component of the dynamic force. It depends as well on the dynamic deflection line of the vibrating blade.

The method established can be used for any type of blade, since it does not assume any restrictions to the blade form. It can also be applied to compressor blades, however the numerical solution is relatively long and requires the use of electronic computing machines. Simpler methods can be used for compressor blade vibration, e. g. [3]. For turbine blades which will, in general, be tapered and twisted, it is essential to use the method given here.

1.2. Comparison with recent researches

For a long time, the design of turbine blades from the point of view of vibration has been based on statistical experience with previous designs. It has been assumed that the steady bending stresses due to fluid flow are magnified by a certain factor in case of resonance, and the turbine designer used a factor of safety to avoid this stress-magnification effect. The calculation of this factor of safety has been based on very simplified assumptions. Values of between 8 and 10 have been proposed by Noland [4] and Forshaw [5]. Other authors, Trumpler and Owens [6], have proposed the use of a magnification factor depending on the natural mode of frequency of the blade.

With the development of modern electronic computers, several attempts have been made to calculate the vibratory stresses more accurately. Methods of calculation have been developed and used for single blades and for blades packed together into groups, and have been very successful in estimating the vibratory stresses e.g. [7] and [8]. However, in these studies the exciting force, which is considered as the decisive factor in determining the stress level during vibration, has always been

assumed, and not calculated. Moreover, the amplitudes and phase angles of the different harmonic components of the dynamic force were considered, in all previous researches, to be constant along the blade length. These simplifying assumptions allow only a very appoximate study of the stresses in the vibrating blade, even though computers were used.

This is the reason why the present work is mainly directed at investigating the actual character of the dynamic force using a general velocity distribution before the moving row of blades, and finding the general form of the radial distribution of its various harmonic components.

The analytical solution which is developed here will be applied to an actual example of a turbine blade, where the dynamic forces and the vibratory stresses will be calculated.

2. CALCULATION OF THE DYNAMIC FORCES

2.1. General

Owing to the non-uniform character of the flow from the stationary row of blades, each blade in the following moving row is subjected to an exciting force which varies periodically with time, one complete force period corresponding to one pitch of the stationary blades. This non-uniform and unsteady character of the flow depends on the viscosity of the medium, the existing aerodynamic conditions, as well as the geometry and configuration of the stationary blades. It might also be slightly affected by the following moving row of blades.

The value of the dynamic force depends also on the geometry and configuration of the moving row of blades, as well as the aerodynamic conditions at exit from this row. The effect of the following stages on the aerodynamic conditions behind the moving blades is neglected in the analysis, in order to avoid unnecessary complications; in any case, it is usually small.

The blade geometry and row configuration are assumed to take any general form for both the moving and the stationary rows. One limitation should be made here, even though it does not affect the calculation of the dynamic force: it is assumed that there are neither bands nor lacing wires connecting the blades together.

It is very difficult and complicated to try to solve the problem under the most general aerodynamic conditions. A solution applying the general three-dimensional theory of unsteady fluid flow and considering viscosity and compressibility effects will certainly be mathematically tedious, and complicated. Moreover, the results would be so involved that the solution would lose any physical or practical meaning. It is best therefore to use simplifying assumptions for the aerodynamic conditions in the solution of the problem. These assumptions and their influence on the accuracy of the results are now discussed.

First of all, we will assume the flow of the medium through the turbine stages to be incompressible. This assumption is usually adopted in any preliminary study of fluid flow in turbomachines, and is justified by the small density changes across the blade row or stage being examined. Using incompressible flow analysis will not endanger the accuracy of our results in any way, especially with subsonic conditions.

The dynamic forces on a turbine blade depend on the unsteady static-pressure distribution along both the pressure and suction sides of the blade, and it is known that this is slightly affected by the boundary-layer thickness or, in other words, by fluid friction (except in the case of boundary layer separation which is beyond the scope of our investigation); we will assume, therefore that the flow through the moving row

of blades is frictionless. Frictionless analysis will also simplify the solution of the problem to a great extent. However, it should be stated here that it is the viscosity of the working medium (fluid friction) which is the main cause of the non-uniform character of the flow entering the moving blades. This, however, is a question of the fluid friction in the stationary row and does not directly affect the calculation of the dynamic force on the moving blades. It is, of course, this fluid friction which controls the shape of the velocity wakes, and, since we assume their shape to be quite general in the calculation, we are indirectly taking it into account in the analysis.

Thirdly, we assume that the flow through the moving row of blades can be divided along the length of the blade into a finite number of conical surfaces of flow. We treat the flow along each one of these surfaces as quasi one-dimensional for the mean stream line between two adjacent blades, but maintaining at the same time its unsteady character. By dividing the length of the blade into a sufficient number of these conical surfaces we can estimate the radial distribution of the dynamic force along the blade length. This quasi one-dimensional analysis along each of the flow surfaces simplifies the solution and can be expected to give a reasonably accurate estimation of the dynamic force. It fails, however, to give the point of application of the forces, which is only necessary for calculating the torque on the blades. This point of application of the forces can only be calculated by using complicated two-dimensional theories for each surface of flow.

These are the main assumptions required for the solution of the problem of the dynamic forces. It is further assumed that the velocity distribution before the moving row of blades is known at a distance which is far enough from the blade leading edge to ensure a constant distribution of the static pressure along the pitch. However, this static pressure can vary in the radial direction along the length of the blade, according to the stage design. The velocity distribution can either be measured directly in an actual stage or can be estimated theoretically using boundary layer theory.

The following method of determining the dynamic forces on a turbine blade is applicable for both the stationary and the moving blades. Although it is deduced here for a moving blade, the reader can easily make the changes necessary for applying it to a stationary blade. A moving blade has been chosen because it is subject in addition to centrifugal stresses giving the most severe loading conditions.

2.2. Method of Calculation

In estimating the dynamic force on a turbine blade under the assumptions given in 2.1., we will apply the equations of fluid dynamics (continuity, energy and momen-

tum). Resolving the dynamic force into two main components, axial and tangential, we can use

1. The unsteady energy equation to calculate the static pressure drop across the blade row.
2. The unsteady rate of change of axial momentum equation, together with the calculated static pressure drop, to calculate the axial component of the dynamic force (that component of the dynamic force which acts in a direction parallel to the turbine axis).
3. The unsteady rate of change of tangential momentum equation to calculate the tangential component of the dynamic force (that component of the dynamic force which acts in a direction tangential to the direction of rotation of the turbine, and perpendicular to the axial component defined in 2.).

These equations are applied to each conical flow surface along the blade length. It is thus necessary to specify the boundaries of the control volume and control surface for each flow surface, before applying the fluid dynamic equations stated above.

2.2.1. Choice of control volume and control surface

Let us consider the flow through a turbine stage (one stationary and one moving row of blades) to be divided, along the blade length, into a finite number of conical surfaces as assumed in 2.1. and as shown in fig. 1.a. We can choose as our control volume that volume enclosed by a) the inside and outside surfaces of two adjacent blades, b) two parallel planes placed before and after the moving row of blades and perpendicular to the axis of the turbine (indicated by the two lines 1-1 and 2-2 in fig. 1.a), and c) two parallel surfaces distance dr apart and enclosing the flow surface as shown in fig. 1.a.

Fig. 1.b shows the limits of the control volume along the flow surface, and which is denoted by the line ABCDEFGHA. In choosing this control volume we have to consider the following:

1. The two planes of the control surface (by control surface is meant that surface given by the line ABCDEFGHA and having a depth of dr), which enclose our control volume and are denoted in fig. 1.b. by AB and FE, lie along the two parallel planes 1-1 and 2-2 (see fig. 1.a.). It is assumed further that the static pressure along these two planes (AB and FE) does not vary with the pitch and is denoted by p_1 and p_2 respectively.

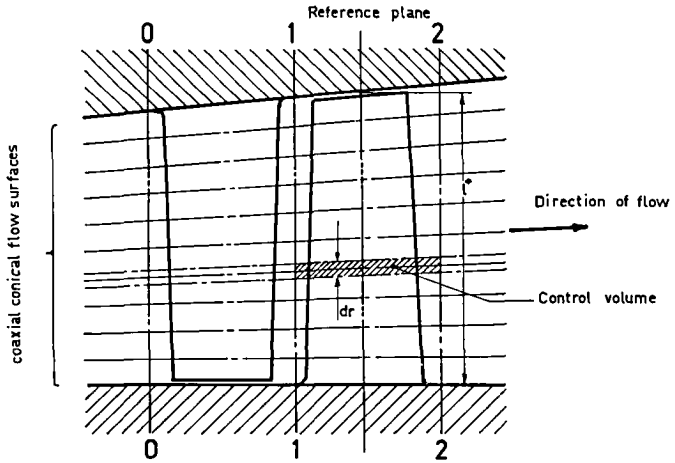

a. coaxial flow surfaces & control volume

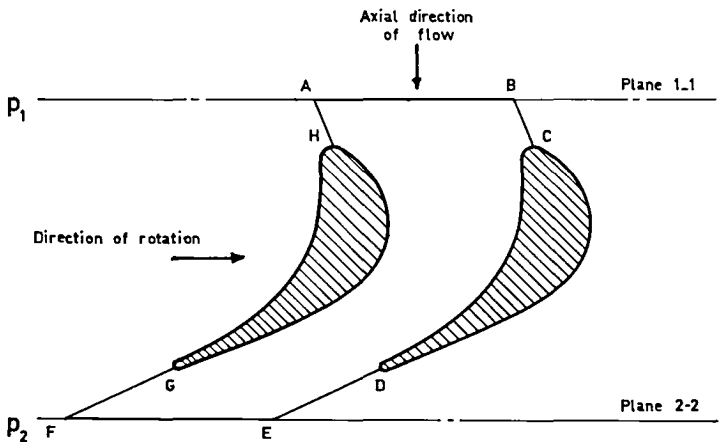

b. limits of control volume along flow surfaces

Fig. 2.1. Choice of control volume for force calculation

2. The lines AH, BC, DE and GF represent stream lines along the flow surface, although this can only be an approximation, considering the unsteady character of the flow. However, they may be chosen according to the steady potential flow theory without large error, since they represent only a relatively small portion of the control surface.
3. We neglect any radial force components on our control volume which might result from a difference of pressure above and below the control volume. This is justified by the fact that such force components do not have any great effect on the blade.
4. It is assumed that the velocity distribution is known at entrance to the control volume (along AB), for all flow surfaces.
5. Positive directions for flow velocities, pressures and forces are assumed to be along the axial direction of flow, and the tangential direction of blade rotation respectively.

2.2.2. Calculation of the axial component

To calculate the axial component of the dynamic force on the control volume chosen and analysed in 2.2.1 we use the unsteady energy equation for quasi one-dimensional flow [9], and the unsteady momentum equation [10], together with the continuity equation to establish a simple expression for this axial component. The quasi one-dimensional concept which is applied here can be considered to be a mean between simple one-dimensional analysis and two-dimensional analysis, or rather a simplified two-dimensional concept. However, we must not forget that this applies only to the control volume chosen, which has an infinitesimal depth dr in the radial direction. Having calculated the dynamic forces on the different surfaces along the blade length, we can finally derive the radial distribution of the dynamic force along the blade length.

Let us consider the curved line y-y in fig. 2 to be the mean stream line along the flow surface given by ABCDEFGHA, with s giving the distance along this line from a fixed point O. The width of the channel between two adjacent blades, and along a potential line x-x, is given by b . In general this channel width b can be assumed to vary along the mean stream line, according to blade shape and configuration. The moving blades are assumed to have a pitch T'' , which is considered to be related to the pitch of the stationary-blades T' by the pitch ratio R ($R = T''/T'$). We shall consider the flow field from a point which is fixed to the moving blades, and this requires the analysis of the relative flow field. The flow medium enters the control volume through AB with velocity $\bar{w}_1$, which is

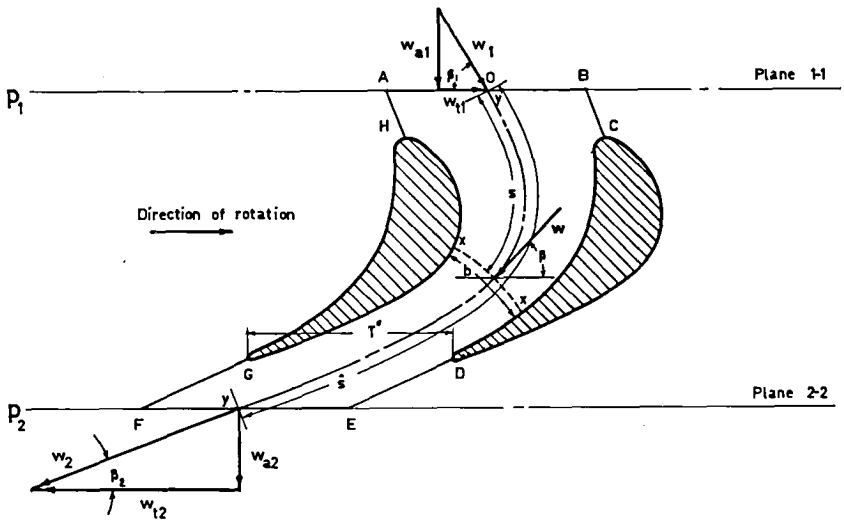

Fig. 2.2. Diagram for calculation of dynamic forces

assumed to be the mean value of the velocity distribution along AB (one complete moving-blade pitch), and at an angle of flow β_1 (see fig. 2). Similarly, at exit from the control volume FE we have $\bar{w}_2$ and β_2 respectively. Inside the blade channel and between entrance and exit we can consider the mean flow velocity, which is tangential to the direction of the stream line y-y, to be $\bar{w}$, having a flow angle β, as shown in fig. 2. All flow angles are given relative to the tangential direction. Further, it is assumed that all flow velocities, entering, leaving, or inside the control volume, are functions of time, thus establishing the unsteady character of the solution.

The curvilinear coordinate s along the mean stream line is supposed to vary between zero and $\hat{s}$, as shown in fig. 2. $\hat{s}$ is the total length of the mean stream line between entrance and exit of the control volume, and depends on the shape and configuration of the blades.

Formulating the continuity condition between the entrance and exit planes AB and FE respectively, we can write

$$\overline{w}_{a2} = \overline{w}_{a1} \tag{1}$$

and for the exit plane FE we can also write

$$\overline{w}_{t2} = \overline{w}_{a2} \cot \beta_2$$

or using equation (1), we can transform the last equation into

$$\overline{w}_{t2} = \overline{w}_{a1} \cot \beta_2 \tag{2}$$

Equations (1) and (2) establish the relation between the exit flow-velocity components and the velocity components at entrance to the control volume. Noticing that we have assumed in 2.2.1. that the flow velocity at entrance is known, we have thus expressed the exit flow-velocity components in terms of known functions. However, the exit flow angle is allowed to change with time, depending also on the known conditions at entrance to the control volume. Details about this latter relationship will be discussed later, in the mean time we will consider β_2 simply as a function of time.

The static pressure drop Δp ($\Delta p = p_1 - p_2$) between AB and FE, which is considered in this case of unsteady flow conditions to be a function of time, can be given in the form of the unsteady pressure equation (energy equation). Formulating this energy equation for our control volume, we can express the unsteady pressure drop across the moving row of blades as

$$\Delta p = \varrho \left[\frac{(\overline{w}_2^2 - \overline{w}_1^2)}{2} + \int_0^{\hat{s}} \left(\frac{\partial \overline{w}}{\partial t}\right) ds \right] \tag{3}$$

Here we use the unsteady momentum equation [10] as applied to the axial direction, for the simplified case of quasi one dimensional flow. Neglecting the effect of gravitational force we can describe the axial component of the dynamic force f_a by the following expression

$$f_a = T'' \left[\Delta p - \varrho \frac{\partial}{\partial t} \int_0^{\hat{s}} b\, \overline{w}(s,t) \sin \beta \, ds \right] \tag{4}$$

The integral on the right hand side of this equation gives the effect of the unsteady flow velocity inside the blade channel on the axial component of the dynamic force.

From the velocity triangles in fig. 2 we can deduce the following trigonometric relations at both entrance and exit planes respectively (AB and FE),

$$\bar{w}_1^2 = \bar{w}_{a1}^2 + \bar{w}_{t1}^2 \quad ; \quad \bar{w}_2^2 = \bar{w}_{a2}^2 + \bar{w}_{t2}^2$$

Substituting equations (1) and (2) in the above expressions we can write

$$\left(\bar{w}_2^2 - \bar{w}_1^2\right) = \bar{w}_{a1}^2 \cot^2 \beta_2 - \bar{w}_{t1}^2 \tag{5}$$

The right hand side of equation (5) depends on the axial and tangential velocity components at entrance to the control volume in fig. 2, and also the exit flow angle β_2.

In order to avoid the complications resulting from using different dimensions, and so that we can apply the solution obtained to all geometrically similar blades and row configurations, we will use the method of non-dimensional analysis. For this purpose, we must choose reference parameters for the velocity, length and time.

Fig. 3 describes the position of the reference plane, which is considered as a radial plane passing through the centre of gravity of the blade hub section. The choice of this reference plane is more important in the calculation of the vibratory stresses than in the calculation of the dynamic force as will be seen later. Our reference length l^* will be defined as the blade length along this reference plane (see fig. 3), and the peripheral speed of the blade section at the mean radius u_m^* is considered as the reference speed. For the reference time t^* we use

$$t^* = \frac{l^*}{u_m^*}$$

Using these parameters, we can define the following non-dimensional variables,

$$\left.\begin{aligned} \overline{W} &\equiv \frac{\bar{w}}{u_m^*} \quad ; \quad S \equiv \frac{s}{l^*} \\ \tau &\equiv \frac{t}{t^*} = \frac{t}{(l^*/u_m^*)} \quad \text{and} \quad F_a \equiv \frac{f_a}{\frac{\rho}{2} u_m^{*2} l^*} \end{aligned}\right\} \tag{6}$$

in addition we define

$$\hat{T}' \equiv \frac{T'}{l^*} \quad ; \quad R \equiv \frac{T''}{T'} \quad \text{and} \quad B(S) \equiv \frac{b(s)}{T'} \tag{7}$$

Substituting equation (5) in (4) and changing the variables according to equations (6) and (7), we get the following non-dimensional form for the axial component of the dynamic force

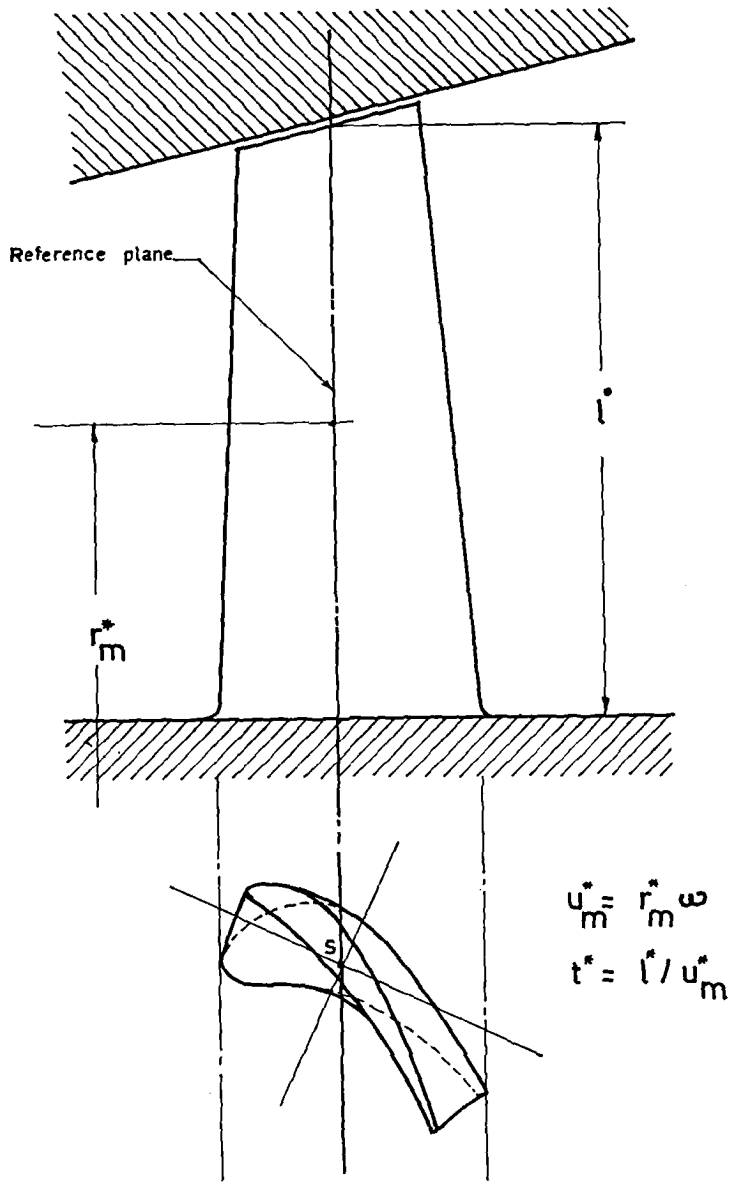

Fig. 2.3. Reference plane and reference parameters for nondimensional analysis

$$F_a = \hat{T}' \left\{ R \left[\overline{W}_{a1}^2 \cot^2 \beta_2 - \overline{W}_{t1}^2 \right] + 2R \frac{\partial}{\partial \tau} \int_0^{\hat{S}} \overline{W}(S,\tau) \left[R - B \sin \beta \right] dS \right\} \quad (8)$$

The velocity $\overline{W}(S,\tau)$ under the sign of integration in the right hand side of equation (8) depends on the position S along the mean stream line, as well as on the time τ. This difficulty in the integration can be avoided if we consider the continuity condition between any section x-x along the mean stream line fig. 2, and the entrance section AB

$$\overline{w}(s,t) = \overline{w}_{a1} \frac{T''}{b(s)}$$

or in non-dimensional form,

$$\overline{W}(S,\tau) = \overline{W}_{a1}(\tau) \frac{R}{B(S)} \quad (9)$$

In equation (9) the function $\overline{W}(S,\tau)$ is expressed as the product of two other functions, each of which depends on only one variable. The choice of R and $B(S)$ is necessary to establish the relation between configurations of moving and stationary blades, which in turn is necessary in the expression for the mean velocity distribution at entrance to the control volume.

Substituting equation (9) in (8) we find the following expression for the axial component of the dynamic force per unit blade length:

$$F_a = \hat{T}' \left\{ R \left[\overline{W}_{a1}^2 \cot^2 \beta_2 - \overline{W}_{t1}^2 \right] + 2R \frac{d\overline{W}_{a1}}{d\tau} \int_0^{\hat{S}} \left[\frac{R}{B} - \sin\beta \right] dS \right\} \quad (10)$$

It can be seen from the above equation that the axial component of the dynamic force is finally expressed in terms of the known aerodynamic conditions at entrance to the control volume of the moving blades, the exit flow angle β_2, and a term which depends on the shape of the moving blades and the configuration of the moving and stationary blades. This last term, which appears in the last part of the right hand side of equation (10), can be calculated by means of drawing the steady potential-flow pattern for the moving-blades configuration and then evaluating the integral $\int_0^{\hat{S}} \left[\frac{R}{B} - \sin\beta \right] dS$ numerically. This, however, is only an approximation, since the unsteady potential and stream lines also depend on time. However, it is considered as a good approximation especially as we only need the integral value given above.

In order to simplify the above equation (10) let us introduce the form-parameter for the axial component of the dynamic force K_a, which is defined as follows:

$$K_a \equiv 2\,R \int_0^{\hat{S}} \left[\frac{R}{B} - \sin\beta\right] dS \qquad (11)$$

Substituting this in equation (10) we find

$$F_a = \hat{T}' \left\{ R \left[\overline{W}_{a1}^2 \cot^2\beta_2 - \overline{W}_{t1}^2\right] + K_a \frac{d\overline{W}_{a1}}{d\tau} \right\} \qquad (12)$$

This represents the simplified form of the expression for the axial component of the dynamic force on a turbine blade, per unit blade length.

2.2.3. Calculation of the tangential component

In the calculation of the tangential component of the dynamic force we shall use the same control volume as was used for the axial component, we can as well use the same figures. Here we use the general form of the unsteady momentum equation [10], applied to the tangential direction for simplified quasi one-dimensional flow.

Neglecting the effect of gravitational forces we can write this equation of tangential momentum as

$$f_t = \rho \left\{ \left[\overline{w}_{t2}\,\overline{w}_{a2} - \overline{w}_{t1}\,\overline{w}_{a1}\right] T'' + \frac{\partial}{\partial t} \int_0^{\hat{s}} b\,\overline{w}(s,t) \cos\beta\, ds \right\} \qquad (13)$$

where f_t is the tangential component of the dynamic force per unit blade length for a control volume as shown in fig. 1. In equation (13), we notice that the tangential component is the sum of two terms, the first of which represents the difference between the tangential momentum at inlet and exit of the control volume, and the second represents the effect of the unsteady velocity changes inside the control volume on the tangential component of the dynamic force.

Defining the non-dimensional tangential component of the dynamic force per unit blade length F_t by a similar expression to before

$$F_t \equiv \frac{f_t}{\frac{\rho}{2} u_m^{*2}{}_{1^*}}$$

we can rewrite equation (13) with the parameters of equation (6) as follows

$$F_t = 2\,\hat{T}' \left\{ R \left[\overline{W}_{t2}\,\overline{W}_{a2} - \overline{W}_{t1}\,\overline{W}_{a1}\right] + \frac{\partial}{\partial\tau} \int_0^{\hat{S}} B(S)\,\overline{W}(S,\tau) \cos\beta\, dS \right\} \qquad (14)$$

Combining equation (14) with equations (1), (2), (7) and (9) we find

$$F_t = 2\hat{T}' \left\{ R \left[\overline{W}_{a1}^2 \cot \beta_2 - \overline{W}_{a1} \overline{W}_{t1} \right] + R \frac{d\overline{W}_{a1}}{d\tau} \int_0^{\hat{S}} \cos \beta \, dS \right\} \quad (15)$$

As in 2.2.2, it can be seen from this equation that the tangential component of the dynamic force is expressed in terms of the aerodynamic conditions at entrance to the control volume of the moving blades, the exit flow angle β_2, and also a form parameter which appears in the last term of the right hand side of equation (15). This form parameter can be calculated numerically as in the first case, and depends on the geometry and configuration of the blades.

In order to simplify equation (15) we introduce, as before, the form-parameter for the tangential component of the dynamic force K_t, which is defined as follows,

$$K_t \equiv 2R \int_0^{\hat{S}} \cos \beta \, dS \quad (16)$$

Substituting it in equation (15) we may write

$$F_t = \hat{T}' \left\{ 2R \left[\overline{W}_{a1}^2 \cot \beta_2 - \overline{W}_{a1} \overline{W}_{t1} \right] + K_t \frac{d\overline{W}_{a1}}{d\tau} \right\} \quad (17)$$

This represents the simplified form of the expression for the tangential component of the dynamic force, per unit blade length.

2.2.4. Discussion of the approximations used

In the above analysis we have assumed an elementary one dimensional flow. This means that the complex velocity distribution across the width of the moving-blades channel is replaced by its mean value across the channel-width. The equations of such a theory are to be considered as relationships between integral values. However, it is considered as an approximation to the exact conditions in which minute details are neglected. Let us now consider whether these approximations are plausible, and in what way they can affect the result.

It is possible to deduce a mean value of the axial and tangential components of the flow velocity based on each of the three concepts of continuity, momentum, and energy. We must decide, therefore, upon which of these three concepts we will base our mean value; the simplest is the continuity condition, and it will be used throughout the analysis.

Before considering our analysis of the dynamic force in greater detail, we should examine the validity of the continuity mean value of the flow velocity when used in either the momentum or energy equations. In other words we must compare the mean values obtained according to each of the three concepts mentioned above.

Considering the absolute flow at entrance to the moving row of blades, which varies periodically with the stationary blades pitch T' as period, we can write

$$c_1 = c_{10} + \Delta c_1 \tag{18}$$

where c_{10} is a constant main flow velocity with the perturbation component Δc_1 as a function of the tangential direction along the pitch x. It can be assumed that this perturbation component is relatively small with respect to the main flow component c_{10}. A further condition to the definition of equation (18) is that

$$\int_0^{T'} \Delta c_1 \, dx = 0$$

In order to analyse the mean velocity components across the entrance plane to the moving blades we must consider now the following relative velocity components

$$w_{a1} = c_1 \sin \alpha_1 = (c_{10} + \Delta c_1) \sin \alpha_1 \tag{19}$$

and

$$w_{t1} = c_1 \cos \alpha_1 - u_1 = (c_{10} + \Delta c_1) \cos \alpha_1 - u_1 \tag{20}$$

We can form the mean value of the flow velocity according to the continuity condition at entrance to the moving blade (subindex c stands for continuity). Thus

$$\bar{w}_{a1_c} \equiv \frac{1}{T''} \int_0^{T''} w_{a1} \, dx$$

and substituting equation (19) in the above expression we find

$$\bar{w}_{a1_c} = \left[c_{10} + \frac{1}{T''} \int_0^{T''} \Delta c_1 \, dx \right] \sin \alpha_1 \tag{21}$$

If we now calculate the same mean value from the momentum condition (subindex m stands for momentum) we can write

$$\bar{w}_{a1_m} \equiv \frac{\int_0^{T''} w_{a1}^2 \, dx}{\int_0^{T''} w_{a1} \, dx}$$

and, substituting w_{a1} from equation (19), we get

$$\bar{w}_{a1_m} = \sin \alpha_1 \frac{\int_0^{T''} \left[c_{10}^2 + 2 c_{10} \Delta c_1 + \Delta c_1^2 \right] dx}{\int_0^{T''} (c_{10} + \Delta c_1) dx}$$

Since the velocity perturbation components are small, we can neglect higher orders of Δc_1 (i. e. second and higher orders). Thus the above equation may be written in the form

$$\bar{w}_{a1_m} = \sin \alpha_1 \frac{c_{10} \int_0^{T''} (c_{10} + \Delta c_1) dx + c_{10} \int_0^{T''} \Delta c_1 dx}{\int_0^{T''} (c_{10} + \Delta c_1) dx}$$

$$= \sin \alpha_1 \left\{ c_{10} + \frac{1}{T''} \int_0^{T''} \Delta c_1 dx \left[\frac{c_{10}}{c_{10} + \frac{1}{T''} \int_0^{T''} \Delta c_1 dx} \right] \right\} \quad (22)$$

A similar analysis for the tangential component using the following two definitions

$$\bar{w}_{t1_c} \equiv \frac{1}{T''} \int_0^{T''} w_{t1} dx \quad \text{and} \quad \bar{w}_{t1_m} \equiv \frac{\int_0^{T''} w_{a1} w_{t1} dx}{\int_0^{T''} w_{a1} dx}$$

and equations (19) and (20) yields

$$\bar{w}_{t1_c} = \cos \alpha_1 \left[c_{10} + \frac{1}{T''} \int_0^{T''} \Delta c_1 dx \right] - u_1 \quad (23)$$

and

$$\bar{w}_{t1_m} = \cos \alpha_1 \left\{ c_{10} + \frac{1}{T''} \int_0^{T''} \Delta c_1 dx \left[\frac{c_{10}}{c_{10} + \frac{1}{T''} \int_0^{T''} \Delta c_1 dx} \right] \right\} - u_1 \quad (24)$$

From equation (21):

$$\bar{w}_{a1_c}^2 = \left[c_{10} + \frac{1}{T''} \int_0^{T''} \Delta c_1 \, dx \right]^2 \sin^2 \alpha_1$$

Assuming that $\left[\frac{1}{T''} \int_0^{T''} \Delta c_1 \, dx \right]^2$ is also small relative to c_{10}^2 we can write

$$\bar{w}_{a1_c}^2 \approx \left[c_{10}^2 + \frac{2c_{10}}{T''} \int_0^{T''} \Delta c_1 \, dx \right] \sin^2 \alpha_1 \qquad (25)$$

According to the energy condition, however, we have for the mean value of the axial component of flow velocity (subindex e stands for energy).

$$\bar{w}_{a1_e}^2 \equiv \frac{\int_0^{T''} w_{a1}^3 \, dx}{\int_0^{T''} w_{a1} \, dx}$$

Substituting equation (19) in the above expression and making the necessary changes after neglecting higher orders of the small perturbation velocities we can derive

$$\bar{w}_{a1_e}^2 = \sin^2 \alpha_1 \left\{ c_{10}^2 + \frac{2c_{10}}{T''} \int_0^{T''} \Delta c_1 \, dx \left[\frac{c_{10}}{c_{10} + \frac{1}{T''} \int_0^{T''} \Delta c_1 \, dx} \right] \right\} \qquad (26)$$

A similar analysis for the tangential component using the definition

$$\bar{w}_{t1_e}^2 \equiv \frac{\int_0^{T''} w_{a1} \, w_{t1}^2 \, dx}{\int_0^{T''} w_{a1} \, dx}$$

and the equations (19) and (20) give

$$\bar{w}_{t1_c}^2 = \cos^2 \alpha_1 \left[c_{10}^2 + \frac{2c_{10}}{T''} \int_0^{T''} \Delta c_1 \, dx \right] + u_1^2 - 2u_1 \cos \alpha_1 \left[c_{10} + \frac{1}{T''} \int_0^{T''} \Delta c_1 \, dx \right] \qquad (27)$$

and

$$\bar{w}_{t1_e}^2 = \cos^2\alpha_1 \left\{ c_{10}^2 + \frac{2c_{10}}{T''} \int_0^{T''} \Delta c_1 \, dx \left[\frac{c_{10}}{c_{10} + \frac{1}{T''} \int_0^{T''} \Delta c_1 \, dx} \right] \right\} + u_1^2$$

$$-2 u_1 \cos\alpha_1 \left\{ c_{10} + \frac{1}{T''} \int_0^{T''} \Delta c_1 \, dx \left[\frac{c_{10}}{c_{10} + \frac{1}{T''} \int_0^{T''} \Delta c_1 \, dx} \right] \right\} \qquad (28)$$

Studying now equations (21) - (28) we can see that if

$$\frac{c_{10}}{c_{10} + \frac{1}{T''} \int_0^{T''} \Delta c_1 \, dx} \approx 1 \qquad (29)$$

then we can say that it is plausible to use the mean value based on the continuity condition in both the energy and the momentum equations. From equation (21) it is clear that for small perturbation velocities Δc_1, the value of the quotient cannot differ greatly from unity (the difference depends also on the pitch ratio R). In certain cases it can even be exactly unity.

We can, therefore, conclude, that in such an estimation theory as ours it is very plausible to use these approximations in order to achieve simplicity. Moreover, as shown above, the accuracy of the results is not endangered.

A second point requiring attention is the method of deducing the axial and tangential components of the dynamic force on the blade, for which the momentum and energy equations are used. The basic analysis of this problem has been given in chapters 2.2.2. and 2.2.3, however, without studying the actual conditions very deeply.

Considering fig. 4 we can see that the control volume ABCDEFGHA acts on both the adjacent blades with a certain force having both axial and tangential components as follows

$$F_a = - (F_{as} - F_{ap})$$

and (30)

$$F_t = - (F_{tp} - F_{ts})$$

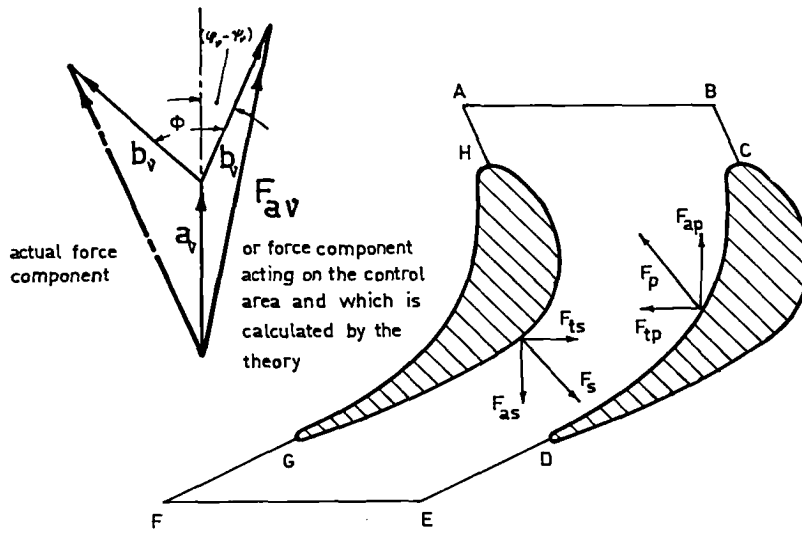

Fig. 2.4 Relationship between actual and calculated components of dynamic force

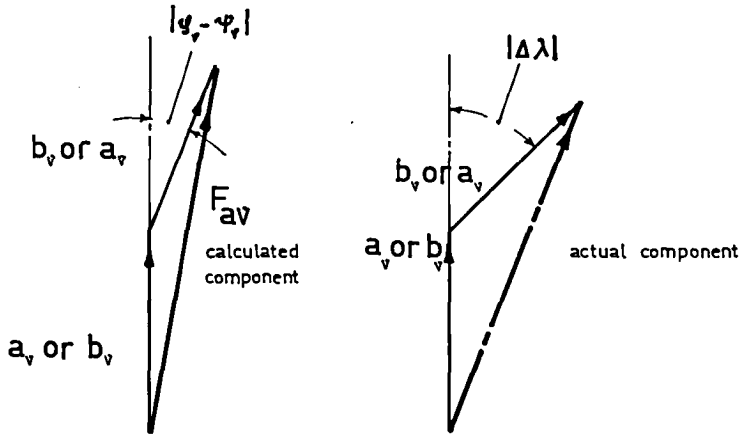

Fig. 2.5 Comparison between amplitudes of actual & calculated components of dynamic force

On the right hand side of these expressions are the components of the dynamic force acting on both the pressure and the suction sides of the two adjacent blades. Considering the axial component (first expression in equation (30)), and expressing the force on the control volume as a Fourier series, we can write

$$F_{as} = a_0 + \sum_{\nu} a_\nu \sin(\omega_\nu t - \varphi_\nu)$$

and (31)

$$F_{ap} = b_0 + \sum_{\nu} b_\nu \sin(\omega_\nu t - \psi_\nu)$$

Considering both the equations (30) and (31), we can represent the amplitude of the ν th order of the resulting axial component of the dynamic force as shown in fig. 4. This component is not, however, the actual force on the blade. If we consider the phase shift between two adjacent control volumes to be Φ , we can then draw the actual amplitude of the axial component of the dynamic force as shown in fig. 4. We approximate in our theory by substituting the vector $F_{a\nu}$ for the actual force component (represented by the chain-dotted line in fig. 4).

In order to study the effect of this approximation let us consider fig. 5, in which we compare the calculated with the actual conditions.

The calculated amplitude of the force is equal to or greater than the actual amplitude if

$$|\Delta \lambda| \geq |\varphi_\nu - \psi_\nu|$$

whereas the critical case, in which the calculated amplitude is smaller than the actual amplitude, occurs if

$$|\varphi_\nu - \psi_\nu| > |\Delta \lambda|$$

This last condition means that the absolute value of the phase shift of the forces inside the control volume is larger than the phase shift between the forces on the pressure and suction sides of a given blade. This is the case, for example, if both moving and stationary blade pitches are equal ($T' = T''$), and the calculation yields in this case a zero amplitude of the dynamic force. On the other hand, if T' is many times T'', then $|\varphi_\nu - \psi_\nu|$ tends to zero, and the first condition, in which the calculated amplitude is larger than the actual amplitude, is fulfilled. A similar analysis can be made for the tangential component.

The aim of this work is to estimate the magnitude of the force amplitude acting on the turbine blade. To achieve this, let us consider the following analysis. Assuming $\frac{\Delta w}{\bar{w}}$ to be the relative amplitude of the velocity variations and $\Delta F/\bar{F}$ to be

the calculated relative amplitude of the dynamic force, then, by varying R , we will find cases in which the calculated value of the force amplitude agrees with the actual value, and other cases where the agreement is not sufficient. Now we assume that the largest actual amplitude of the force that might occur for any given values of $\frac{\Delta w}{\bar{w}}$ cannot be larger than the maximum calculated amplitude (with the worst pitch ratio R). This analysis is not rigorous but is considered to be perfectly plausible.

A more accurate calculation of the amplitudes of the dynamic force is not possible without a detailed two dimensional flow solution along the control volume. In such a solution we have to obtain the exact velocity field inside the blade channel, from which we may calculate the force components on the pressure and suction sides of the blade separately. This method was tried at the beginning and was found to be very complex. It was therefore considered better to attempt to obtain a simpler theory which allows an estimation of the dynamic force and which can produce practical results.

It is now necessary to choose a suitable form for expressing the velocity distribution at entrance to the control volume, $\bar{w}_{a1}$ and $\bar{w}_{t1}$, and the exit flow angle β_2, which are required in the equations (12) and (17).

2.3. Velocity distribution at entrance to the row of blades

Due to skin friction along the pressure and suction sides of the stationary blades, the velocity distribution behind a row of blades is not uniform, but is composed of different wakes periodically displaced along the periphery, as shown in fig. 6. These wakes repeat themselves at intervals equal to the pitch of the preceding row (stationary row of blades) and are assumed to be similar. In fact, they differ slightly from each other, but this difference is of no importance in our analytical study, and can be neglected. The shape of a single wake is as shown in fig. 6, and is assumed to be non-symmetrical about the mean flow direction, due to the difference between the boundary-layer thicknesses at the pressure and suction sides of the trailing edge of the blade. The wake is assumed also to change its strength and shape along the blade length, especially at the ends of the blade, where its shape is affected by the boundary-layer along both casing and hub walls. Most important, however, is the possibility that the position of this wake relative to a fixed radial axis might vary according to the shape of the stationary blade or, to be more accurate, according to the position of the trailing-edge of the stationary blade in space, relative to this fixed radial axis. Hence in expressing the velocity distribution behind the stationary row of blades, we must consider a certain axis along a fixed radial direction, to which

the position of the wakes is referred. The velocity distribution along the plane 1-1 in fig. 6 is assumed to be known over a complete period T' and for different sections along the blade length (i.e. along the conical flow surfaces discussed in 2.2.1 and

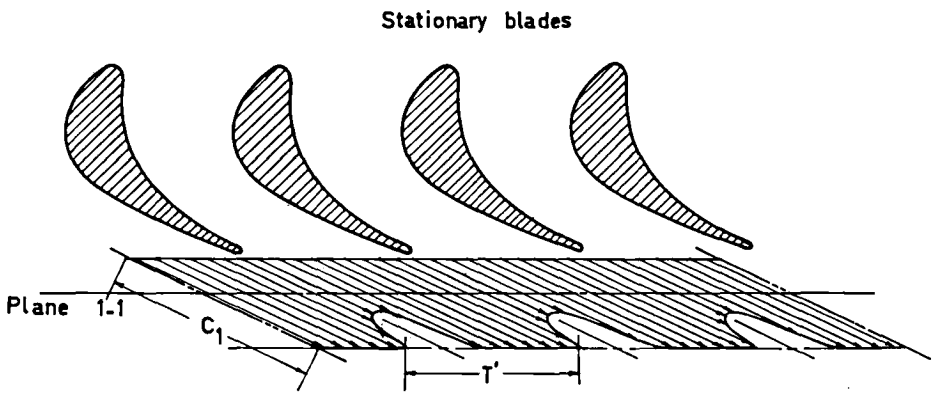

Fig. 2.6 Wake pattern behind a stationary row of turbine blades

shown in fig. 1). Let us now consider the control volume ABCDEFGHA shown in fig. 1: since we know the velocity distribution along AB relative to the moving blades, which is needed for the calculation of the dynamic forces, we can analyse the problem in the following manner. Considering this non-uniform velocity distribution before the moving row of blades from a point fixed to this row, it is evident that each moving blade will be washed periodically by the wakes of the non-uniform flow entering it.

This will result in a periodically unsteady and non-uniform flow through the moving blades or in other words, at our control volume. The general character of the position of the wake relative to the fixed radial axis, which is discussed above and which depends on the configuration of the stationary blades, will cause a phase shift between the washing action of the wakes at different radial sections, according to the position in space of the leading edge of the moving blades. This phase shift has always been neglected in recent researches but will be considered here.

The steady flow relative to the stationary row can be transformed to the unsteady flow relative to the moving row by means of the following simple relationship

$$W(\xi) = W(x - ut) \tag{32}$$

where u is the peripheral speed of the moving blades at the section where the velocity $W(\xi)$ is required.

2.3.1. Harmonic analysis of the velocity distribution

In choosing the method of expressing the periodical character of the flow velocity entering the moving row of blades, we must refer to blade vibration. A blade will be excited to vibrate in one of its natural modes, and will continue to vibrate with dangerous amplitudes, if this mode coincides with one of the harmonic components of the dynamic force. Because our ultimate aim is to study the vibration and vibratory stresses when this resonance occurs, we must express the dynamic force in terms of its different harmonic components. Thus it will be expedient to express the periodical velocity distribution required for our study as a harmonic series, by means of harmonic or Fourier analysis.

For the axial and tangential components of the velocity at entry to the control volume at AB (fig. 2), and assuming x to be the direction coordinate along the plane 1-1, we can write the following harmonic series

$$w_{a1}(x,t) = w_{a10} + \sum_{n=1}^{N} \left\{ a_n^* \cos \left[2\pi n \left(\frac{x-ut}{T} \right) \right] + b_n^* \sin \left[2\pi n \left(\frac{x-ut}{T} \right) \right] \right\} \tag{33}$$

and

$$w_{t1}(x,t) = w_{t10} + \sum_{n=1}^{N} \left\{ c_n^* \cos \left[2\pi n \left(\frac{x-ut}{T} \right) \right] + d_n^* \sin \left[2\pi n \left(\frac{x-ut}{T} \right) \right] \right\} \tag{34}$$

The series is terminated after a finite number of terms N, as only the first few harmonic components of the dynamic force are considered to be dangerous for vibration. Using the non-dimensional analysis in 2.2.2 and introducing further

$$\chi \equiv \frac{x}{l^*}$$

we can rewrite both equation (33) and (34) as follows

$$W_{a1}(\chi,\tau) = W_{a10} + \sum_{n=1}^{N} \left\{ a_n \cos \left[2\pi n \left(\frac{\chi - \mu\tau}{\hat{T}} \right) \right] + b_n \sin \left[2\pi n \left(\frac{\chi - \mu\tau}{\hat{T}} \right) \right] \right\} \qquad (35)$$

and

$$W_{t1}(\chi,\tau) = W_{t10} + \sum_{n=1}^{N} \left\{ c_n \cos \left[2\pi n \left(\frac{\chi - \mu\tau}{\hat{T}} \right) \right] + d_n \sin \left[2\pi n \left(\frac{\chi - \mu\tau}{\hat{T}} \right) \right] \right\} \qquad (36)$$

We should notice here that the relation between the harmonic coefficients in equations (35) and (36), and those in equations (33) and (34) is established by

$$a_n \equiv \frac{a_n^*}{u_m^*} \quad ; \quad b_n \equiv \frac{b_n^*}{u_m^*} \quad ; \quad c_n \equiv \frac{c_n^*}{u_m^*} \quad \text{and} \quad d_n \equiv \frac{d_n^*}{u_m^*}$$

and also that $\mu \equiv \frac{u}{u_m^*}$

defines the ratio of the control volume peripheral speed u to the reference peripheral speed u_m^*.

2.3.2. Velocity distribution for the quasi one-dimensional analysis

The quasi one-dimensional analysis as discussed before neglects the variation in the instantaneous velocity distribution along the width of the channel between two adjacent blades (along x-x in fig. 2), and assumes in the solution the mean velocity across the channel width to be representative of the flow. For the entrance section AB in fig. 2 we require the mean values of the velocity-component along this line, which has a length equal to the pitch of the moving-blades, T''. For $\overline{W}_{a1}$ and $\overline{W}_{t1}$, the mean axial and tangential components of the velocity across AB respectively, we can write the following expressions:

$$\overline{W}_{a1}(\tau) = \frac{1}{\hat{T}''} \int_0^{\hat{T}''} W_{a1}(\chi, \tau)\, d\chi = \frac{1}{\hat{T}'R} \int_0^{\hat{T}'R} W_{a1}(\chi, \tau)\, d\chi \qquad (37)$$

$$\overline{W}_{t1}(\tau) = \frac{1}{\hat{T}''} \int_0^{\hat{T}''} W_{t1}(\chi, \tau)\, d\chi = \frac{1}{\hat{T}'R} \int_0^{\hat{T}'R} W_{t1}(\chi, \tau)\, d\chi \qquad (38)$$

Substituting equation (35) in (37), and integrating, we find

$$\overline{W}_{a1}(\tau) = W_{a10} + \sum_{n=1}^{N} \left\{ A_n \cos\left(2\pi n \frac{\mu}{\hat{T}'}\tau\right) + B_n \sin\left(2\pi n \frac{\mu}{\hat{T}'}\tau\right) \right\} \qquad (39)$$

where

$$A_n \equiv \frac{\sin(\pi n R)}{\pi n R} \left\{ a_n \cos(\pi n R) + b_n \sin(\pi n R) \right\}$$

and (40)

$$B_n \equiv \frac{\sin(\pi n R)}{\pi n R} \left\{ a_n \sin(\pi n R) - b_n \cos(\pi n R) \right\}$$

Similarly, substituting equation (36) in (38) and integrating, we find

$$\overline{W}_{t1}(\tau) = W_{t10} + \sum_{n=1}^{N} \left\{ C_n \cos\left(2\pi n \frac{\mu}{\hat{T}'}\tau\right) + D_n \sin\left(2\pi n \frac{\mu}{\hat{T}'}\tau\right) \right\} \qquad (41)$$

where

$$C_n \equiv \frac{\sin(\pi n R)}{\pi n R} \left\{ c_n \cos(\pi n R) + d_n \sin(\pi n R) \right\}$$

and (42)

$$D_n \equiv \frac{\sin(\pi n R)}{\pi n R} \left\{ c_n \sin(\pi n R) - d_n \cos(\pi n R) \right\}$$

Examining equations (39) and (41), which represent the axial and tangential components of the mean velocity at entrance to the control volume, we find

1. Both expressions for the velocity distribution are functions of time alone.
2. They are periodical functions, repeating themselves at time intervals corresponding to one stationary-blade pitch and the peripheral speed at the given section.
3. The two functions have steady mean values W_{a10} and W_{t10}, corresponding to the steady flow axial and tangential velocity-components respectively.

However, it is important to notice that these time functions (equations (39) and (41)) can be independent of the time under certain special conditions. These conditions will apply if the values of the harmonic coefficients A_n , B_n , C_n and D_n , defined by equations (40) and (42), are such that

$$A_n = B_n = C_n = D_n = 0 \qquad (43)$$

In this case, equations (39) and (41) give expressions for $\bar{W}_{a1}$ and $\bar{W}_{t1}$ corresponding to the steady state velocity components W_{a10} and W_{t10} respectively. This means that the quasi one-dimensional velocity distribution at entrance to the moving-blades control-volume is independent of the time.

From the form of both equations (40) and (42) for the harmonic coefficients, it can be seen that there are several cases when the above harmonic coefficients vanish simultaneously, and thus fulfil equation (43). However, in this analysis it is only important to discuss those cases having a certain physical meaning. These cases can be summarised as follows:

1. The harmonic coefficients A_n , B_n , C_n and D_n fulfil equation (43) for all harmonic orders (all values of n), if the pitch ratio R (ratio of moving-blades pitch to stationary-blades pitch) is equal to a whole number $(0, 1, 2, \ldots)$. The term sin (π n R) vanishes in both equations (40) and (42), and thus the harmonic coefficients A_n , B_n , C_n and D_n become zero. The zero value of the pitch ratio R is meaningless for any turbine design and need not be considered, but R=1 occurs often in practical applications, and R=2 is sometimes used in turbine stages of the impulse type (zero reaction).
2. The harmonic coefficients A_n , B_n , C_n and D_n fulfil equation (43) for certain harmonic orders (certain values of n), if the pitch ratio R is such that the product nR is equal to a whole number, in which case the term sin (π nR)

vanishes in both the equations (40) and (42). This case covers a large range of practical pitch ratios.

These two cases for which the harmonic coefficients A_n , B_n , C_n and D_n vanish simultaneously are very important for the calculation of the dynamic force on a turbine blade, as will be seen later.

2.4. Limits of the dynamic force

It is essential to decide upon the necessary expressions for the velocity distribution at entrance to the control volume before proceeding further with the calculation of the dynamic force itself. Referring to equations (12) and (17) in 2.2, which express the axial and tangential components of the dynamic force respectively, we see that both have a similar character. They contain in their right hand sides either functions which are known ($\bar{W}_{a1}$ and $\bar{W}_{t1}$) or form parameters (K_a and K_t), which can be easily calculated for any blade type. The only variable in the right hand side which is not yet known or explained is cot β_2, which depends on the flow direction at exit from the control volume chosen. According to previous analysis, the flow direction at exit can vary with time. This variation should, however, be periodical since it is dictated by periodical changes. In accordance with the general equations of fluid mechanics, it is not possible to find any definite conditions under which the exit flow direction can be determined. However, we shall consider the following two cases which are supposed to limit the variation in the exit flow direction:

1. In the first case, which sets the lower limit to the dynamic force, we assume that the perturbations in the flow velocity entering the blade channel, and causing time changes in the flow direction at entrance, are totally damped while passing through this channel. This results in a constant exit flow angle $\bar{\beta}_2$, and the flow at exit will follow the same direction as for a steady potential flow through the moving row of blades.
2. On the other hand, if these velocity perturbations or some of their harmonic components are allowed to have their full effect on the exit flow direction, i.e. to pass completely undamped to the exit flow plane, we get the other extreme, or the upper limit to the dynamic force.

What actually happens in a turbine is somewhere between these two limits; in other words, the velocity perturbations causing periodical changes in the entrance flow direction are partially damped in passing through the blade channel. In calculating the upper and lower limits of the dynamic force we get a range in which the

actual value of the force lies. The difference between these two limits is expected to be small.

2.4.1 Calculation of the lower limit

For the calculation of the lower limit, we assume that the direction of the flow at exit is the same as that resulting from a steady potential flow through the given moving-blade configuration. This direction does not, in general, coincide with the geometric angle of the blade trailing-edge, but even if the latter is assumed for the exit flow angle, it will not seriously affect the results. It should be mentioned here that, to calculate the form parameters K_a and K_t, we are usually obliged to draw an approximate potential flow pattern from which we can easily calculate the exit flow angle required. Assuming for the exit flow angle when calculating the lower limit the constant value $\bar{\beta}_2$, and substituting it in equations (12) and (17) we get

$$F_{a1} = \hat{T}' \left\{ R \left[\overline{W}_{a1}^2 \cot^2 \bar{\beta}_2 - \overline{W}_{t1}^2 \right] + K_a \frac{d\overline{W}_{a1}}{d\tau} \right\} \tag{44}$$

$$F_{t1} = \hat{T}' \left\{ 2R \left[\overline{W}_{a1}^2 \cot \bar{\beta}_2 - \overline{W}_{a1} \overline{W}_{t1} \right] + K_t \frac{d\overline{W}_{a1}}{d\tau} \right\} \tag{45}$$

Equations (44) and (45) represent the lower limit of the dynamic force on a turbine moving-blade.

2.4.2. Calculation of the upper limit

If on the other hand we allow the first order harmonic component of the velocity perturbation at entry, which is responsible for variations in the direction of flow, to pass through the blade channel undamped, we will expect as a result a first order harmonic change in the exit flow direction. This variation can be represented by the simple expression

$$\cot \beta_2 = \cot \bar{\beta}_2 + E \sin \left(2\pi \frac{\mu}{T'} \tau + \psi \right) \tag{46}$$

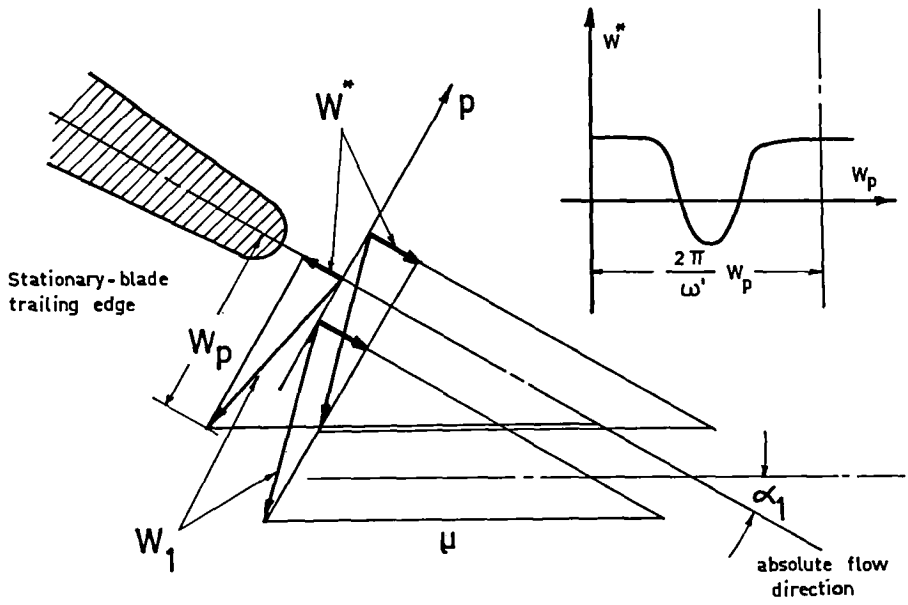

Fig. 2.7 Velocity component "W^*" causing changes in flow direction at entrance to the moving row of blades

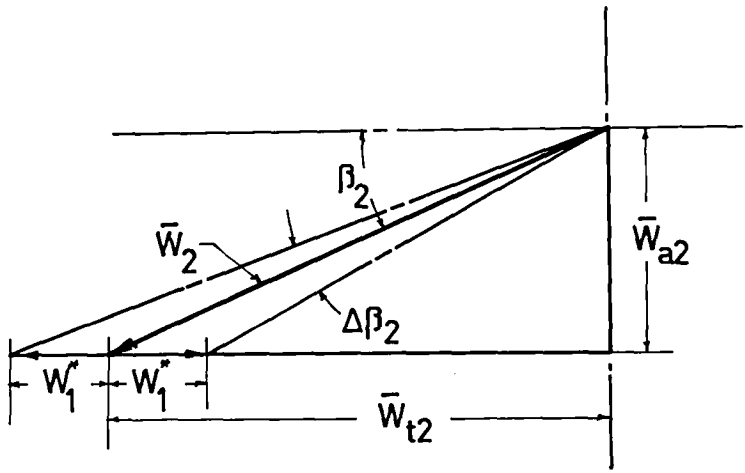

Fig. 2.8 Exit-flow direction-changes for the upper limit of the dynamic force

where the second term in the right hand side of the above equation represents the first order periodical change in the exit flow direction $\bar{\beta}_2$ as discussed in 2.4.1. Harmonic orders higher than the first in the above velocity perturbation are very small and are probably damped. In equation (46) there are two unknowns which have to be calculated. These are the amplitude E and the phase angle ψ of the first order harmonic variation in cot β_2 .

Let us resolve the entrance velocity W_1 into two components as shown in fig. 7, one component parallel to the absolute flow direction and the other perpendicular to it (W^* and W_p). We can prove that the perpendicular component W_p is constant and therefore has no effect on the variation of the flow direction at entrance, whereas the other component W^* is found to vary periodically as shown in fig. 7. Applying the same harmonic analysis used before to this periodical function W^* we can write

$$W^* = W_0^* + \sum_{n=1}^{N} W_n^* \sin \left(\frac{n\omega'}{W_p} \chi_p + \varphi_n \right) \tag{47}$$

Let us assume that the first order harmonic of this velocity component W_1^* passes through the moving row of blades undamped and affects the flow direction at exit as shown in fig. 8. It can be seen too from fig. 8 that the whole effect is assumed to take place along the tangential component of the flow velocity at exit, since any effect on the axial component contradicts the continuity condition in equation (1). W_1^* can be calculated from the known velocity distribution at entrance to the control volume of the moving row of blades, using the above harmonic series.

Referring to equation (46) we can write for the maximum value of cot β_2

$$(\cot \beta_2)_{max} = \cot \bar{\beta}_2 + E \tag{48}$$

and from fig. 8 we can write for the same exit angle

$$(\cot \beta_2)_{max} = \frac{\bar{W}_{t2} + W_1^*}{\bar{W}_{a2}} = \cot \bar{\beta}_2 + \frac{W_1^*}{\bar{W}_{a2}} \tag{49}$$

By comparing equations (48) and (49) and noticing that $\bar{W}_{a2} = \bar{W}_{a1}$ according to equation (1), we can then write for the amplitude of the variation in cot β_2 the following expression

$$E = \frac{W_1^*}{\bar{W}_{a1}} \tag{50}$$

As for the phase angle ψ given in equation (46) we can vary it between O and 2π, and calculate the corresponding effect on the dynamic force. We can then choose the maximum value calculated to represent the upper limit. It should be pointed out here that the variation in the exit flow direction discussed above might be such that, for certain values of the phase angle ψ, the resulting dynamic force lies even below the lower limit. However, we are interested only in the maximum value of the upper limit, corresponding to a certain phase angle which we can call ψ_{max}.

We can write for the exit flow angle

$$\cot \beta_2 = \cot \bar{\beta}_2 + \left(\frac{W_1^*}{\bar{W}_{a1}}\right) \sin \left(2\pi \frac{\mu}{\hat{T}'} \tau + \psi_{max}\right) \tag{51}$$

Substituting equation (51) in equations (12) and (17), and simplifying, we get

$$F_{au} = \hat{T}' \left\{ R \left[\bar{W}_{a1}^2 \cot^2 \bar{\beta}_2 + 2 \bar{W}_{a1} \cot \bar{\beta}_2 W_1^* \sin \left(2\pi \frac{\mu}{\hat{T}'} \tau + \psi_{max}\right) + W_1^{*2} \sin^2 \left(2\pi \frac{\mu}{\hat{T}'} \tau + \psi_{max}\right) - \bar{W}_{t1}^2 \right] + K_a \frac{d\bar{W}_{a1}}{d\tau} \right\} \tag{52}$$

$$F_{tu} = \hat{T}' \left\{ 2R \left[\bar{W}_{a1}^2 \cot \bar{\beta}_2 + \bar{W}_{a1} W_1^* \sin \left(2\pi \frac{\mu}{\hat{T}'} \tau + \psi_{max}\right) - \bar{W}_{a1} \bar{W}_{t1} \right] + K_t \frac{d\bar{W}_{a1}}{d\tau} \right\} \tag{53}$$

Comparing the upper and lower limits together by inspecting equations (44), (45), (52), and (53), we can write the relationship between the two limits as

$$F_{au} = F_{al} + \Delta F_a \tag{54}$$

$$F_{tu} = F_{tl} + \Delta F_t \tag{55}$$

The differences between the upper and lower limits of the axial and tangential components of the dynamic force ΔF_a and ΔF_t respectively are then found by comparing equations (54) and (55) with (52) and (53) respectively:

$$\Delta F_a = \hat{T}'R \left[2 \bar{W}_{a1} \cot \bar{\beta}_2 W_1^* \sin \left(2\pi \frac{\mu}{\hat{T}'} \tau + \psi_{max}\right) + W_1^{*2} \sin^2 \left(2\pi \frac{\mu}{\hat{T}'} \tau + \psi_{max}\right)\right. \quad (56)$$

$$\Delta F_t = 2 \hat{T}'R \bar{W}_{a1} W_1^* \sin \left(2\pi \frac{\mu}{\hat{T}'} \tau + \psi_{max}\right) \quad (57)$$

2.5. Harmonic analysis of the dynamic forces

It is required that we should express the directional components of the dynamic force in the form of a Fourier series with the different orders of exciting harmonics. For this reason we have expressed the velocity distribution at entrance to the moving-blades row in the form of a harmonic series (see equations (39) and (41)). However, it can be seen from the expressions for the dynamic force (equations (12) and (17)) that they contain terms which are squares of the velocity components ($\bar{W}_{a1}^2$ and $\bar{W}_{t1}^2$), and products of them ($\bar{W}_{a1} \cdot \bar{W}_{t1}$) . This means that two such harmonic series must be multiplied together when equations (39) and (41) are substituted for the velocities. We will discuss first, therefore, the multiplication of two harmonic series as applied to our problem and also some other mathematical analysis which will be required in the study.

2.5.1. Multiplication of harmonic series

The problem of multiplying two harmonic series together, and the special case of squaring a harmonic series, which are required for the calculation of the dynamic force, has been considered by Tolstow [11]. The product of two harmonic series of order N and having the same period is a third harmonic series having 2N terms, whose coefficients are series combinations of the coefficients of the original harmonic series. It is, however, assumed there that the periodical functions expressed by the original series have equal periods, and are continuous and differentiably smooth functions. All of these conditions are satisfied by the functions $\bar{W}_{a1}$ and $\bar{W}_{t1}$. It is not the scope of this work to discuss the details of harmonic series multiplication, and reference will be made to Tolstow [11]. However, we shall briefly indicate the different product forms used when calculating the dynamic force.

We apply the method given in [11] for the multiplication of harmonic series, and neglect harmonic orders higher than N in the resulting series, since they have only little effect on the results, especially for the first few orders (1, 2 and 3). We can write for the square of the axial component of the entrance-velocity $\bar{w}_{a1}^2$ the following expression

$$\bar{w}_{a1}^2 = \frac{\alpha_{a0}}{2} + \sum_{n=1}^{N} \left\{ \alpha_{an} \cos\left(2\pi n \frac{\mu}{\hat{T}'} \tau\right) + \beta_{an} \sin\left(2\pi n \frac{\mu}{\hat{T}'} \tau\right) \right\} \tag{58}$$

where the harmonic coefficients α_{a0} , α_{an} , and β_{an} are series combinations defined by

$$\left.\begin{aligned} \alpha_{a0} &\equiv 2 w_{a10}^2 + \sum_{n=1}^{N} \left[A_n^2 + B_n^2\right] \\ \alpha_{an} &\equiv w_{a10} A_n + \frac{1}{2} \sum_{m=1}^{N} \left\{ A_m \left(A_{m+n} + A_{m-n}\right) + B_m \left(B_{m+n} + B_{m-n}\right) \right\} \\ \beta_{an} &\equiv w_{a10} B_n + \frac{1}{2} \sum_{m=1}^{N} \left\{ A_m \left(B_{m+n} - B_{m-n}\right) - B_m \left(A_{m+n} - A_{m-n}\right) \right\} \end{aligned}\right\} \tag{59}$$

It should be noticed here, when evaluating numerically those cases for which (m-n) is negative, that the following relations are applied, in accordance with the properties of harmonic functions

$$A_k = A_{-k} \quad \text{and} \quad B_k = -B_{-k} \tag{60}$$

Similarly we may write for the square of the tangential component of the entrance-velocity $\bar{w}_{t1}^2$ the following harmonic series

$$\bar{w}_{t1}^2 = \frac{\alpha_{t0}}{2} + \sum_{n=1}^{N} \left\{ \alpha_{tn} \cos\left(2\pi n \frac{\mu}{\hat{T}'} \tau\right) + \beta_{tn} \sin\left(2\pi n \frac{\mu}{\hat{T}'} \tau\right) \right\} \tag{61}$$

where

$$\left.\alpha_{t0} \equiv 2 w_{t10}^2 + \sum_{n=1}^{N} \left[C_n^2 + D_n^2\right] \right|$$

$$\left.\begin{aligned} \alpha_{tn} &\equiv W_{t10}\, C_n + \frac{1}{2} \sum_{m=1}^{N} \left\{ C_m \left(C_{m+n} + C_{m-n} \right) + D_m \left(D_{m+n} + D_{m-n} \right) \right\} \\ \beta_{tn} &\equiv W_{t10}\, D_n + \frac{1}{2} \sum_{m=1}^{N} \left\{ C_m \left(D_{m+n} - D_{m-n} \right) - D_m \left(C_{m+n} - C_{m-n} \right) \right\} \end{aligned}\right\} \quad (62)$$

noticing as before that

$$C_k = C_{-k} \quad \text{and} \quad D_k = -D_{-k} \quad (63)$$

In equation (45), expressing the lower limit of the dynamic force F_{a1}, we find the expression

$$\bar{W}_{a1} \left[\bar{W}_{a1} \cot \bar{\beta}_2 - \bar{W}_{t1} \right]$$

which is the product of two harmonic series; one of these is the composite series $\bar{W}_{a1} \cot \bar{\beta}_2 - \bar{W}_{t1}$, which may be written as

$$\bar{W}_{a1} \cot \bar{\beta}_2 - \bar{W}_{t1} = \frac{F_0}{2} + \sum_{n=1}^{N} \left\{ F_n \cos \left(2\pi n \frac{\mu}{\hat{T}'} \tau \right) + G_n \sin \left(2\pi n \frac{\mu}{\hat{T}'} \tau \right) \right\} \quad (64)$$

Comparing equations (39) and (41) with this equation, and noticing that $\cot \bar{\beta}_2$ is constant, we can write for the harmonic coefficients in equation (64)

$$\left.\begin{aligned} F_0 &\equiv 2 \left(W_{a10} \cot \bar{\beta}_2 - W_{t10} \right) \\ F_n &\equiv \left(A_n \cot \bar{\beta}_2 - C_n \right) \\ G_n &\equiv \left(B_n \cot \bar{\beta}_2 - D_n \right) \end{aligned}\right\} \quad (65)$$

Forming the product of the harmonic expression for $\bar{W}_{a1}$ and the expression in (64), we find

$$\bar{W}_{a1}\left[\bar{W}_{a1}\cot\bar{\beta}_2 - \bar{W}_{t1}\right] = \frac{\alpha_0}{2} + \sum_{n=1}^{N}\left\{\alpha_n \cos\left(2\pi n \frac{\mu}{\hat{T}'}\tau\right) + \beta_n \sin\left(2\pi n \frac{\mu}{\hat{T}'}\tau\right)\right\} \tag{66}$$

where

$$\left.\begin{aligned} \alpha_0 &\equiv W_{a10} F_0 + \sum_{n=1}^{N}\left[A_n F_n + B_n G_n\right] \\ \alpha_n &\equiv W_{a10} F_n + \frac{1}{2}\sum_{m=1}^{N}\left\{A_m\left(F_{m+n} + F_{m-n}\right) + B_m\left(G_{m+n} + G_{m-n}\right)\right\} \\ \beta_n &\equiv W_{a10} G_n + \frac{1}{2}\sum_{m=1}^{N}\left\{A_m\left(G_{m+n} - G_{m-n}\right) - B_m\left(F_{m+n} - F_{m-n}\right)\right\} \end{aligned}\right\} \tag{67}$$

in which as before

$$F_k = F_{-k} \quad \text{and} \quad G_k = -G_{-k} \tag{68}$$

In calculating the upper limit of the dynamic force we must evaluate the following term

$$W_{a1}\left[W_1^* \sin\left(2\pi \frac{\mu}{\hat{T}'}\tau + \psi_{max}\right)\right]$$

which is also a product of two harmonic series in a simplified form, the second series containing only the first harmonic order. To simplify the calculation we may transform the second series according to the following relation

$$W_1^* \sin\left(2\pi \frac{\mu}{\hat{T}'}\tau + \psi_{max}\right) = P_1 \cos\left(2\pi \frac{\mu}{\hat{T}'}\tau\right) + Q_1 \sin\left(2\pi \frac{\mu}{\hat{T}'}\tau\right) \tag{69}$$

where

$$\left.\begin{aligned} P_1 &\equiv W_1^* \sin\psi_{max} \\ Q_1 &\equiv W_1^* \cos\psi_{max} \end{aligned}\right. \tag{70}$$

Using the previous procedure for multiplication, and substituting equation (69) we may write

$$\bar{w}_{a1}\left[w_1^* \sin\left(2\pi \frac{\mu}{\hat{T}'}\tau + \psi_{max}\right)\right] = \frac{\alpha_0^*}{2} + \sum_{n=1}^{N}\left\{\alpha_n^* \cos\left(2\pi n \frac{\mu}{\hat{T}'}\tau\right) + \beta_n^* \sin\left(2\pi n \frac{\mu}{\hat{T}'}\tau\right)\right\} \tag{71}$$

where

$$\left.\begin{aligned} \alpha_0^* &\equiv P_1 A_1 + Q_1 B_1 \\ \alpha_1^* &\equiv \frac{1}{2}\left\{P_1 (A_2 + A_0) + Q_1 (B_2 + B_0)\right\} \\ \beta_1^* &\equiv \frac{1}{2}\left\{P_1 (B_2 - B_0) - Q_1 (A_2 - A_0)\right\} \end{aligned}\right\} \tag{72}$$

In the above equation, it can be easily proved that harmonic orders higher than the first are negligibly small. This is very important, as it means that the harmonic component of the velocity considered in the calculation of the upper limit has an effect which is negligible in the results for harmonic orders of the dynamic force higher than the first. It is sufficient, therefore, to consider only the first harmonic order of the upper limit.

2.5.2. Further mathematical analysis

In order to complete the mathematical analysis required for the solution of the problem, let us refer to equations (12) and (17). The term $d\bar{w}_{a1}/d\tau$ which appears in both equations implies the differentiation of a harmonic series. Assuming that the function $\bar{w}_{a1}$ is continuous and differentiably smooth we can differentiate equation (39), and write

$$\frac{d\bar{W}_{a1}}{d\tau} = \frac{d}{d\tau}\left\{ W_{a10} + \sum_{n=1}^{N} \left\{ A_n \cos\left(2\pi n \frac{\mu}{\hat{T}'}\tau\right) + B_n \sin\left(2\pi n \frac{\mu}{\hat{T}'}\tau\right)\right\}\right\}$$

$$= \sum_{n=1}^{N} \left\{ \left(-2\pi n \frac{\mu}{\hat{T}'} A_n\right) \sin\left(2\pi n \frac{\mu}{\hat{T}'}\tau\right) + \left(2\pi n \frac{\mu}{\hat{T}'} B_n\right) \cos\left(2\pi n \frac{\mu}{\hat{T}'}\tau\right)\right\}$$

$$= \sum_{n=1}^{N} \left\{ \dot{A}_n \cos\left(2\pi n \frac{\mu}{\hat{T}'}\tau\right) + \dot{B}_n \sin\left(2\pi n \frac{\mu}{\hat{T}'}\tau\right)\right\} \qquad (73)$$

where

$$\dot{A}_n \equiv 2\pi n \frac{\mu}{\hat{T}'} B_n \quad \text{and} \quad \dot{B}_n \equiv -2\pi n \frac{\mu}{\hat{T}'} A_n \qquad (74)$$

Further, in equation (56) expressing the axial component of the upper limit of the dynamic force, we find the term

$$W_1^{*2} \sin^2\left(2\pi \frac{\mu}{\hat{T}'}\tau + \psi_{max}\right)$$

This term can be simplified as follows

$$W_1^{*2} \sin^2\left(2\pi \frac{\mu}{\hat{T}'}\tau + \psi_{max}\right) = \frac{W_1^{*2}}{2} + \left[A_2^* \cos\left(4\pi \frac{\mu}{\hat{T}'}\tau\right) + B_2^* \sin\left(4\pi \frac{\mu}{\hat{T}'}\tau\right)\right] \qquad (75)$$

where

$$A_2^* \equiv \frac{W_1^* \cos 2\psi_{max}}{2}$$

$$B_2^* \equiv \frac{W_1^* \sin 2\psi_{max}}{2} \qquad (76)$$

It can be seen that this term affects only the zero and second order harmonics and is expected to have little effect on the first order harmonic of the dynamic force.

2.5.3. Results of the harmonic analysis for the dynamic force

We may now apply the results obtained in 2.5.1 and 2.5.2 to the expressions for the upper and lower limits of the dynamic force, in order to find the final harmonic series for these expressions. Substituting equations (58), (61) and (73) in equation (44) we get

$$F_{al} = \hat{T}' \left\{ \frac{R}{2} \left(\alpha_{a0} \cot^2 \bar{\beta}_2 - \alpha_{t0} \right) + \sum_{n=1}^{N} \left[\left\{ R \left(\alpha_{an} \cot^2 \bar{\beta}_2 - \alpha_{tn} \right) + \right. \right. \right.$$

$$\left. \left. \left. + K_a \dot{A}_n \right\} \cos \left(2\pi n \frac{\mu}{\hat{T}'} \tau \right) + \left\{ R \left(\beta_{an} \cot^2 \bar{\beta}_2 - \beta_{tn} \right) + K_a \dot{B}_n \right\} \sin \left(2\pi n \frac{\mu}{\hat{T}'} \tau \right) \right] \right\} \tag{77}$$

Similarly substituting equations (66) and (73) in equation (45) we find

$$F_{tl} = \hat{T}' \left\{ R \alpha_0 + \sum_{n=1}^{N} \left[\left\{ 2R\alpha_n + K_t \dot{A}_n \right\} \cos \left(2\pi n \frac{\mu}{\hat{T}'} \tau \right) + \left\{ 2R \beta_n + \right. \right. \right.$$

$$\left. \left. \left. + K_t \dot{B}_n \right\} \sin \left(2\pi n \frac{\mu}{\hat{T}'} \tau \right) \right] \right\} \tag{78}$$

For the upper limit we substitute equations (71) and (75) in equation (56), and neglect orders higher than the first

$$\Delta F_a = \hat{T}' R \left\{ \left(\alpha_0^* \cot \bar{\beta}_2 + \frac{W_1^*}{2} \right) + 2 \left[\alpha_1^* \cos \left(2\pi \frac{\mu}{\hat{T}'} \tau \right) + \beta_1^* \sin \left(2\pi \frac{\mu}{\hat{T}'} \tau \right) \right] \right.$$

$$\left. \cot \bar{\beta}_2 \right\} \tag{79}$$

Similarly, substituting equation (71) in (57), we find

$$\Delta F_t = \hat{T}' R \left\{ \alpha_0^* + 2 \left[\alpha_1^* \cos \left(2\pi \frac{\mu}{\hat{T}'} \tau \right) + \beta_1^* \sin \left(2\pi \frac{\mu}{\hat{T}'} \tau \right) \right] \right\} \tag{80}$$

On inspection, we see that not only the first order harmonic is present in equations (79) and (80) but also the zero order, i.e. the steady part of the dynamic force. This, however, is expected to be negligible, since it is caused by disturbances of the first harmonic order as assumed.

2.6. Conclusion

The dynamic force acting on a turbine blade has been studied and expressed as a harmonic (Fourier) series which is suitable for further studies on blade vibration and vibratory stresses. This force has been calculated at different positions along the blade length, and is given in the form of the radial distribution of the dynamic force per unit blade length. By considering the general form of the velocity distribution and allowing variations of its amplitude and phase angle along the length of the blade, the force has been expressed in its most general form. The expression derived for the axial and tangential components of the dynamic force per unit blade length can be summarised as follows

$$F_{al} = F_{a0} + \sum_{n=1}^{N} \left\{ F_{an} \cos \left(2\pi n \frac{\mu}{\hat{T}'} \tau \right) + F'_{an} \sin \left(2\pi n \frac{\mu}{\hat{T}'} \tau \right) \right\} \qquad (81)$$

$$F_{tl} = F_{t0} + \sum_{n=1}^{N} \left\{ F_{tn} \cos \left(2\pi n \frac{\mu}{\hat{T}'} \tau \right) + F'_{tn} \sin \left(2\pi n \frac{\mu}{\hat{T}'} \tau \right) \right\} \qquad (82)$$

These two equations give the lower limit of the dynamic force and are harmonic series. The resulting force varies periodically with time with a period corresponding to the pitch of the stationary-blades $\hat{T}'$. The amplitudes and phase angles of the different harmonics are represented by the coefficients F_{an}, F'_{an}, F_{tn} and F'_{tn}, which depend on different factors and parameters, and which can be studied by comparing equations (77) and (78) with equations (81) and (82) respectively. On inspection we find the following relations.

$$\begin{aligned}
F_{an} &\equiv \hat{T}' \left[R \left(\alpha_{an} \cot^2 \bar{\beta}_2 - \alpha_{tn} \right) + K_a \dot{A}_n \right] \\
F'_{an} &\equiv \hat{T}' \left[R \left(\beta_{an} \cot^2 \bar{\beta}_2 - \beta_{tn} \right) + K_a \dot{B}_n \right] \\
F_{tn} &\equiv \hat{T}' \left[2R \alpha_n + K_t \dot{A}_n \right] \\
F'_{tn} &\equiv \hat{T}' \left[2R \beta_n + K_t \dot{B}_n \right]
\end{aligned} \qquad (83)$$

Thus we see that the harmonic coefficients depend not only on the stationary-blades pitch $\hat{T}'$, but also on the pitch ratio R and the form parameters K_a and K_t . We notice too that this pitch ratio R is contained in the harmonic coefficients in the right-hand sides of the expressions in equation (83). These coefficients α_{an}, α_{tn}, α_n, β_{an}, β_{tn}, β_n, $\dot{A}_n$ and $\dot{B}_n$ are different combinations of the harmonic coefficients of the velocity distribution A_n, B_n, C_n and D_n. We see too from equations (40) and (42) that these latter coefficients depend on the velocity distribution before the moving-blades (a_n, b_n, c_n and d_n) as well as on the pitch ratio R , and this establishes the indirect, but more important, effect of the pitch ratio on the harmonic components of the dynamic force. It is also very important to notice that the different harmonic components of the lower limit of the dynamic force vanish under the same conditions as were discussed in 2.3.2. This can be proved very simply by expressing the harmonic coefficients F_{an}, F'_{an}, F_{tn}, and F'_{tn} in terms of the mean velocity harmonic coefficients A_n, B_n, C_n and D_n .

The steady component of the lower limit (zero order) can be written as

$$F_{a0} = \frac{\hat{T}'R}{2} \left[\alpha_{a0} \cot^2 \bar{\beta}_2 - \alpha_{t0}\right]$$

$$F_{t0} = \hat{T}'R \, \alpha_0 \tag{84}$$

It can be proved that these values are very approximately the same as if the forces were calculated for steady mean flow conditions W_{a10} and W_{t10} . This could be done by substituting the values of α_{a0}, α_{t0} and α_0 from equations (59), (62) and (67), neglecting the effect of higher harmonics on them. Thus we can write, instead of equation (84)

$$F_{a0} = \hat{T}'R \left[W_{a10}^2 \cot^2 \bar{\beta}_2 - W_{t10}^2\right]$$

$$F_{t0} = 2\,\hat{T}'R\,W_{a10} \left[W_{a10} \cot \bar{\beta}_2 - W_{t10}\right] \tag{85}$$

Substituting now the continuity condition in equation (1), and equation (2), and also the definition of the pitch ratio R , we can rewrite equation (85) as

$$F_{a0} = \hat{T}'' \left[W_{20}^2 - W_{10}^2 \right]$$

$$F_{t0} = 2 \hat{T}'' W_{a10} \left[W_{t20} - W_{t10} \right] \qquad (86)$$

where W_{20} is the mean steady velocity-component at exit from the moving row of blades. Equation (86) represents the same results as if the force was calculated for a moving blade exposed to steady flow conditions W_{10} and W_{20} , and having the same shape and configuration considered here.

It can be seen from the above analysis that the steady part of the lower limit of the dynamic force depends on the shape and configuration of the moving-blades, and the steady flow velocity-components at entrance.

The upper limit of the dynamic force, in the calculation of which we have neglected all disturbances of harmonic orders higher than the first, will have negligible effect on the steady component, as shown in 2.5.2.

Referring now to equations (79) and (80), we may write

$$\Delta F_a = \Delta F_{a0} + \Delta F_{a1} \cos \left(2 \pi \frac{\mu}{\hat{T}'} \tau \right) + \Delta F'_{a1} \sin \left(2 \pi \frac{\mu}{\hat{T}'} \tau \right) \qquad (87)$$

$$\Delta F_t = \Delta F_{t0} + \Delta F_{t1} \cos \left(2 \pi \frac{\mu}{\hat{T}'} \tau \right) + \Delta F'_{t1} \sin \left(2 \pi \frac{\mu}{\hat{T}'} \tau \right) \qquad (88)$$

If we now compare these two equations (87) and (88) with equations (79) and (80), we see that

$$\Delta F_{a0} \equiv \hat{T}' R \left[\alpha_0^* \cot \bar{\beta}_2 + \frac{W_1^*}{2} \right]$$

$$\Delta F_{a1} \equiv 2 \hat{T}' R \, \alpha_1^* \cot \bar{\beta}_2 \quad ; \quad \Delta F'_{a1} \equiv 2 \hat{T}' R \, \beta_1^* \cot \bar{\beta}_2 \qquad (89)$$

$$\Delta F_{t0} \equiv \hat{T}' R \, \alpha_0^*$$

$$\Delta F_{t1} \equiv 2 \hat{T}' R \, \alpha_1^* \quad ; \quad \Delta F'_{t1} \equiv 2 \hat{T}' R \, \beta_1^*$$

The effect of the upper limit on the steady component can be neglected by equating ΔF_{a0} and ΔF_{t0} to zero. The upper limit of the dynamic force depends as shown here on the harmonic component of the velocity, which is allowed to pass undamped through the moving row of blades to the exit plane, where it causes changes in the flow direction.

We may conclude this chapter by stating that the dynamic force distribution along a turbine blade has been expressed in terms of harmonic series. The expressions derived allow for any variation of amplitudes and phase angles of the different harmonic components of this force along the blade length, according to the general form of the velocity distribution at entrance to the moving row of blades. The upper and lower limits of the dynamic force per unit blade length may be calculated from the equations (81), (82), (87) and (88), at a sufficient number of sections along the blade length to establish an accurate radial distribution.

3. CALCULATION OF THE VIBRATORY STRESSES

3.1. General

If an alternating component of the dynamic force falls into resonance with one of the natural modes of vibration of the blade subject to this force, it will cause the blade to vibrate. This forced vibration has large amplitudes and consequently leads to large vibratory stresses. The magnitude of these stresses depends on the work done by the exciting force on the vibrating blade.

The condition and character of these vibratory stresses will be studied here, and a method of calculating them will be established, using the results obtained in chapter 2 for the radial distribution of the dynamic force. This study is considered important for the turbine moving-blades since some of them, in order to fulfil their aerodynamic requirements, are run in resonance with one of the harmonic components of the exciting force.

It is also necessary to discuss the conditions and assumptions under which we are going to calculate these vibratory stresses. This is essential, since a turbine blade, which in general will be tapered and even twisted, is such a complicated body that no full and exact theory can be established for its vibration. It is, therefore, more important to develop a method of calculation which is relatively simple, but still capable of yielding an accurate estimation of the vibratory stresses. In order to establish such a method, let us consider the following assumptions and simplifying conditions:

1. The moving blade, exposed to the exciting force, and for which we calculate the vibratory stresses, is assumed to move with a constant speed relative to the stationary row of blades.

2. Owing to the non-uniform character of the flow entering the moving row of blades, each blade in itself is subjected to an exciting force which varies periodically with time. One complete force period corresponds to one pitch of the stationary row of blades. This exciting force can be resolved into axial and tangential components, and each one of these directional components can be resolved into a series of harmonic components.

3. The stationary blades are assumed to be uniformly spaced in order to avoid any irregularities in the period of the exciting force. The moving blades are also assumed to be uniformly spaced to ensure the equality of the dynamic force acting on each one of them.

4. A condition of resonance is assumed to exist between the given harmonic of the dynamic force and a natural mode of vibration of the blade in question. In this case the exciting force is assumed to compensate the friction or damping forces so that the natural vibration takes place.

5. The amplitude and phase angle of the given harmonic can vary along the blade length. (The variations in the amplitudes and phase angles of the dynamic force have already been considered in chapter 2.).

6. The work done on the vibrating blade is equal to the sum of the kinetic and potential energy of the blade, increased by the amount of energy dissipated into heat.

7. A turbine blade can vibrate with different modes, in either the stiff or the flexible direction (along the two principal axes). When the blade is twisted however, vibrations in the stiff and flexible directions no longer take place independently, but become coupled together and give rise to complex modes [12]. This coupling affects the form of the vibration and must be considered in the calculation of the vibratory stresses.

8. In the case of coupled vibrations of twisted blades, the bending stresses along the stiff direction of the hub section are neglected relative to those along the flexible direction. This is justified in most cases by the large ratio of the moments of inertia along both principal axes of a turbine-blade section.

9. The largest vibratory stresses are assumed to take place in the blade hub section. This is usually the case in most turbine designs and is justified by the severe bending conditions at this section caused by the superposition of all bending effects due to the radial distribution of the dynamic force. At this section too there are severe stress concentration conditions.

3.2. Reduction of the forces

It has been shown in chapter 2 how the dynamic force on a turbine blade can be calculated, and expressed as a harmonic series. Equations (2.81) and (2.82) give the form of these harmonic series for the lower limit of the axial and tangential components of the dynamic force per unit blade length respectively, and equations (2.87) and (2.88) describe the upper limit in the same way. These different harmonic-components considered above can be the cause of excitation to some modes of vibration of the blade. The resulting vibratory stresses in the hub section of a moving

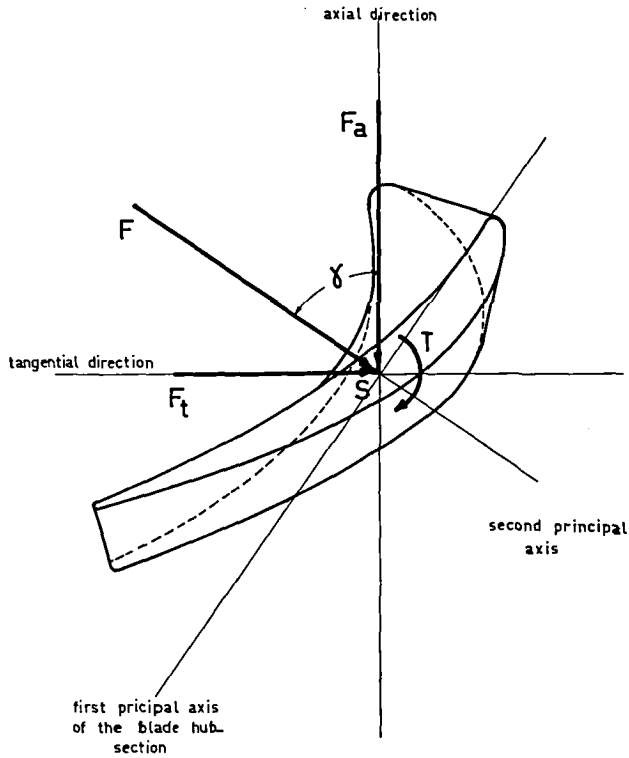

Fig. 3.1 Forces reduction-diagram for the dynamic force-components acting on a turbine blade

blade, which is subject to such an exciting-force distribution, will be calculated in this chapter. Before beginning with the actual analysis, it is convenient to reduce the given components of the force to a form which is more easily applied to the conditions at the blade hub-section, according to the assumptions in 3.1.

Considering the axial and tangential components of the dynamic force as given by equations (2.81) and (2.82) and referring to fig. 1, we can resolve these two components into two other components acting in two perpendicular planes through the centre of gravity of the hub section S , together with a torque T . Choosing these

two perpendicular planes to be the principal planes of moment of inertia of the hub section, and assuming an angle γ between the second principal plane and the axial direction, we can write for the lower limit of the dynamic force

$$F_l = F_0 + \sum_{n=1}^{N} \left\{ F_n \cos \left(2\pi n \frac{\mu}{\hat{T}'} \tau \right) + F'_n \sin \left(2\pi n \frac{\mu}{\hat{T}'} \tau \right) \right. \tag{1}$$

Equation (1) represents the lower limit of the component of the dynamic force in the direction along the second principal axis (see fig. 1). The relations between the coefficients in equation (1) and those of equations (2.81) and (2.82) are

$$\begin{aligned} F_0 &\equiv F_{a0} \cos \gamma + F_{t0} \sin \gamma \\ F_n &\equiv F_{an} \cos \gamma + F_{tn} \sin \gamma \\ F'_n &\equiv F'_{an} \cos \gamma + F'_{tn} \sin \gamma \end{aligned} \tag{2}$$

Similarly for the upper limit we can write

$$\Delta F = \Delta F_0 + \Delta F_1 \cos \left(2\pi \frac{\mu}{\hat{T}'} \tau \right) + \Delta F'_1 \sin \left(2\pi \frac{\mu}{\hat{T}'} \tau \right) \tag{3}$$

where according to equations (2.87) and (2.88) we have

$$\begin{aligned} \Delta F_0 &\equiv \Delta F_{a0} \cos \gamma + \Delta F_{t0} \sin \gamma \\ \Delta F_1 &\equiv \Delta F_{a1} \cos \gamma + \Delta F_{t1} \sin \gamma \\ \Delta F'_1 &\equiv \Delta F'_{a1} \cos \gamma + \Delta F'_{t1} \sin \gamma \end{aligned} \tag{4}$$

Equations (1) and (3) give the dynamic force responsible for the excitation of vibrations along the plane of weakest resistance of the blade hub section (along the second principal axis). In the case of untwisted blades these are considered the only force components which will cause vibration, since modes in the stiff direction of the blade (along the first principal axis) do not take place with the same frequency.

With the twisted blades, the first mode of vibration will nearly coincide with the direction of the second principal axis, whereas second and higher modes usually deviate from this direction [12]. This deviation depends on the total angle of blade twist, and in such cases the vibration is a coupled one, which can be resolved into two components along the two principal axes of the hub section. We can then assume that the stresses resulting from the vibration component along the axis of greatest resistance can be neglected in comparison with those resulting from the vibration component along the axis of weakest resistance. This is justified by the fact that the ratio of the principal inertias of a turbine blade is usually very large, moreover it is expected that the component of the dynamic force in the direction of the largest resistance is small and can be neglected compared to the one perpendicular to it.

With this analysis it is possible to apply the method given in this chapter to any type of blades. We assume therefore that the energy added to the blades by the exciting force component along the first principal axis is negligible compared to the energy added by its component F, along the second principal axis.

The torque T, which results from reducing the system of the resulting forces, as calculated in chapter 2, to the new system, is responsible for excitation of torsional vibrations. It is not possible, however to determine the point of application of the dynamic forces by means of the analysis in chapter 2, we cannot, therefore, calculate this torque T. It is possible to assume extreme conditions for the position of the point of application (e.g. the assumption made by Prohl [7], that this point of application lies at a distance equal to half the blade width from the centre of gravity S), in which case we get only very approximate results for the value of the actual torque.

3.3. Method of calculation

The method used here to calculate the vibratory stresses is similar to the one used by Traupel [2]; we consider for the calculation of the stresses in the hub section only the vibration along the plane of weakest resistance. This vibration can be represented for any mode by the dynamic deflection line (see fig. 2).

For any mode of vibration n and at any time t, the position of the dynamic deflection line relative to the neutral axis can be given by

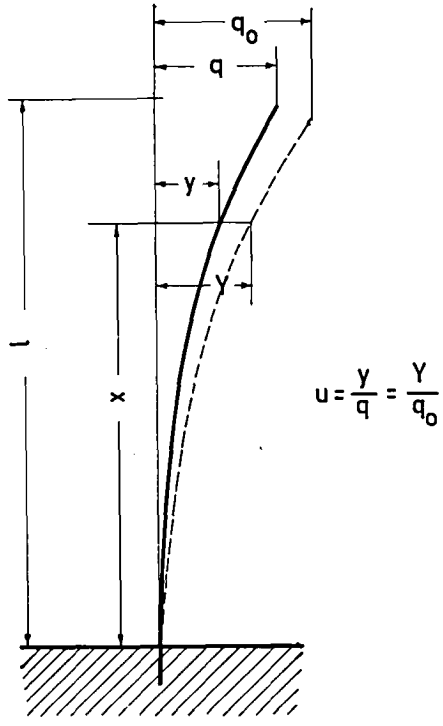

Fig. 3.2 Blade deflection-line for calculation of the vibratory stresses

$$y_n = Y_n(x) \cos \omega_e t \tag{5}$$

where Y_n represents the fully deflected line.

We assume for our analysis that this deflection line passes through the point S , fig. 1 (this is the reason for choosing the reference plane as mentioned in 2.2.2 and shown in fig. 2.3). We assume also that a certain harmonic component of the dynamic force, represented by

$$F = F_n \cos \left(2\pi n \frac{\mu}{\hat{T}'} \tau\right) + F_n' \sin \left(2\pi n \frac{\mu}{\hat{T}'} \tau\right)$$

is applied to the given blade along the plane of vibration. At resonance, by equating the work done by this force-component on the vibrating blade to the sum of the kinetic and potential energies, increased by the amount of energy dissipated into heat, we can describe the maximum deflection of the blade tip $q_{n0_{max}}$ by the relation

$$q_{n0_{max}} = \frac{\pi}{\delta K_n} \left(\frac{\rho}{2} u_m^{*2} l^* \right) \sqrt{\left[\int_0^{1^*} F_n u_n \, dx \right]^2 + \left[\int_0^{1^*} F_n' u_n \, dx \right]^2} \qquad (6)$$

In equation (6) δ represents the logarithmic decrement, which is a measure of the damping, and K_n is a constant of proportionality relating the work done on the blade in order to achieve a certain displacement to the deformation of a certain defined point (in this case the blade tip deformation q).

In order to simplify the numerical calculation, let us divide all the force harmonic-coefficients by the steady force component at the mean radius. Thus

$$F_0^* \equiv \frac{F_0}{F_{0m}} \quad ; \quad F_n^* \equiv \frac{F_n}{F_{0m}} \quad \text{and} \quad F_n^{*'} \equiv \frac{F_n'}{F_{0m}} \qquad (7)$$

let us introduce also the non-dimensional form of the radial distance

$$\xi \equiv \frac{x}{l^*} \qquad (8)$$

Substituting equations (7) and (8) in equation (6) we get

$$q_{n0_{max}} = \frac{\pi}{\delta K_n} \left(\frac{\rho}{2} u_m^{*2} l^{*2} F_{0m} \right) \sqrt{\left[\int_0^1 F_n^* u_n \, d\xi \right]^2 + \left[\int_0^1 F_n^{*'} u_n \, d\xi \right]^2} \qquad (9)$$

The potential energy of the deflection line in the plane of vibration Ψ_n can be calculated according to the theory of elastic beams, if we neglect all centrifugal effects, by

$$\Psi_n = \frac{E}{2} \int_0^{1^*} \left(\frac{dy_n^2}{dx^2} \right)^2 I \, dx = \frac{E I_0}{2 l^{*3}} q_n^2 \int_0^1 \left(\frac{du_n^2}{d\xi^2} \right)^2 \vartheta \, d\xi \qquad (10)$$

where E is the Young's modulus of elasticity, and ϑ is the ratio of the moment of inertia I of the blade section at any distance x to the moment of inertia of the hub section I_0 (both being taken along the plane of vibration).

According to the definition of K_n we can write for the potential energy

$$\Psi_n = \frac{K_n}{2} \; q_n^2 \tag{11}$$

Comparing equations (10) and (11) we can derive the final expression for K_n as

$$K_n = \frac{E\, I_0}{l^{*3}} \int_0^1 \vartheta \, u_n''^2 \, d\xi \tag{12}$$

Substituting equation (12) in (9) we find

$$q_{n0_{max}} = \frac{\pi}{\delta} \left[\frac{\frac{\varrho}{2} u_m^{*2} \, l^{*5}}{E\, I_0} \right] \frac{F_{0m}}{\int_0^1 \vartheta \, u_n''^2 \, d\xi} \sqrt{\left[\int_0^1 F_n^* u_n \, d\xi \right]^2 + \left[\int_0^1 F_n^{*'} u_n \, d\xi \right]^2} \tag{13}$$

According to the theory of beams, we can write the following expression for the bending moment resulting from vibration of the turbine blade

$$M_{bn} = \frac{d^2 Y_n}{dx^2} \cdot E\, I$$

which represents the bending moment caused by a maximum deflection Y_n at any section along the blade length. Considering fig. 2 this can be written as

$$M_{bn}(\xi) = \frac{E\, I_0}{l^{*2}} \, u_n''(\xi) \, \vartheta(\xi) \, q_{n0} \tag{14}$$

For the special case of resonance, we can write for the blade hub section, at which the maximum stresses are assumed to take place,

$$M_{bn_{max}}(0) = \frac{E\, I_0}{l^{*2}} \, u_n''(0) \; q_{n0_{max}} \tag{15}$$

Substituting the expression in equation (13) for $q_{n0_{max}}$ we get the following relation for the dynamic bending moment at the blade hub-section.

$$M_{bn_{max}}(0) = \frac{\pi}{\delta}\left[\frac{\varrho}{2} u_m^{*2} l^{*3}\right] \frac{u_n''(0) F_{0m}}{\int_0^1 \vartheta u_n''^2 \, d\xi} \sqrt{\left[\int_0^1 F_n^* u_n \, d\xi\right]^2 + \left[\int_0^1 F_n^{*'} u_n \, d\xi\right]^2} \tag{16}$$

If we now consider the same blade under the action of the steady force distribution along its length, we can express the static bending moment caused by this force distribution in the hub section, as

$$M_{bs}(0) = \frac{\varrho}{2} u_m^{*2} l^{*3} F_{0m} \int_0^1 F_0^* \xi \, d\xi \tag{17}$$

Defining the dynamic factor $D_{n\,max}$ as the ratio between dynamic and static bending moments at the blade hub section ($\xi = 0$), we have

$$D_{n\,max} \equiv \frac{M_{bn_{max}}(0)}{M_{bs}(0)} \tag{18}$$

Substituting equations (16) and (17) in equation (18), we find

$$D_{n\,max} = \frac{\pi}{\delta} \cdot \frac{u_n''(0)}{\int_0^1 \vartheta u_n''^2 \, d\xi} \cdot \frac{\sqrt{\left[\int_0^1 F_n^* u_n \, d\xi\right]^2 + \left[\int_0^1 F_n^{*'} u_n \, d\xi\right]^2}}{\int_0^1 F_0^* \xi \, d\xi} \tag{19}$$

In order to be able to compare the results obtained here with those given by Traupel [2] we can rewrite equation (19) as follows

$$D_{n\,max} = \frac{\pi}{\delta} \cdot \frac{2 u_n''(0) \int_0^1 u_n \, d\xi}{\int_0^1 \vartheta u_n''^2 \, d\xi} \cdot \frac{\sqrt{\left[\int_0^1 F_n^* u_n \, d\xi\right]^2 + \left[\int_0^1 F_n^{*'} u_n \, d\xi\right]^2}}{2 \left[\int_0^1 u_n \, d\xi\right] \left[\int_0^1 F_0^* \xi \, d\xi\right]} \tag{20}$$

For simpification, let us write

$$D_{n\,max} = \frac{\pi}{\delta} H_n S_n \tag{21}$$

Comparing equation (21) with (20) we see that

$$H_n \equiv \frac{2\,u_n''(0) \int_0^1 u_n\,d\xi}{\int_0^1 \vartheta u_n''^2\,d\xi} \tag{22}$$

and

$$S_n \equiv \frac{\sqrt{\left[\int_0^1 F_n^* u_n\,d\xi\right]^2 + \left[\int_0^1 F_n^{*'} u_n\,d\xi\right]^2}}{2\left[\int_0^1 u_n\,d\xi\right] \cdot \left[\int_0^1 F_0^*\,\xi\,d\xi\right]} \tag{23}$$

In order to calculate the vibratory bending-stresses in the hub section we use equation (21), which defines the factor $D_{n\,max}$. This factor represents also the ratio between the stresses caused in the blade hub-section by the dynamic and the static bending moments, respectively. Thus the maximum vibratory stress in the hub section can be given by

$$\sigma_{bn\,max} = D_{n\,max} \cdot \sigma_{bs} \tag{24}$$

The stress ratio factor $D_{n\,max}$ can be calculated from the three equations (21), (22) and (23).

3.4. Conclusion

A general method has been found for the calculation of the vibratory stresses in a turbine blade. Equation (24) shows that the maximum vibratory stress may be evaluated by multiplying the static bending stress in the hub section by the dynamic factor $D_{n\,max}$. This factor can be calculated according to equation (21).

From equation (21) we can see that the vibratory stress depends in general on three different factors. The first depends on the damping forces acting on the blade

or the damping capacity of the blade implied by the logarithmic decrement δ . The logarithmic decrement is used here to represent the total damping in the vibrating system. There are two main types of damping available, the material damping due to internal friction in the blade material, and the structural damping due to mechanical fits and joints. It is, however, considered here that δ is a property of the material damping, since structural damping is eliminated for the most part by the centrifugal forces. It has also been assumed that no lacing wires are used, these represent usually a very important part of the structural damping. Data about the logarithmic decrement δ is available for blade materials (see [2]), but these can only be considered as approximate values compared to other properties of materials.

The factor $\frac{\pi}{\delta}$ in equation (21) can be considered as the resonance magnification factor V_{max} . This factor represents the ratio of the dynamic deflection amplitude to the deflection of the same body if acted upon by a steady force equal in magnitude to that causing the dynamic deflection.

The maximum vibratory stress depends secondly upon the factor H_n . From the form of equation (22) it can be seen that this factor depends on the mode of vibration, and the blade shape (distribution of the moment of inertia along the blade length). It can be seen too that this factor is independent of force distribution.

The last and most important factor in the calculation of $D_{n\,max}$ is the factor S_n , which is given by equation (23). We shall call it the dynamic stimulating factor or stimulus. It depends mainly on the distribution of the dynamic forces along the blade length, and also the blade deformation. Studying equation (23), we can see that the stimulus can be strongly affected by the radial distribution of the harmonic coefficients F_n^* and $F_n^{*'}$, or, in other words, the radial distribution of the amplitudes and phase angles of a certain harmonic n of the exciting force. This fact shows that the assumption used in most recent researches, that the phase angle is constant along the blade length, can be totally misleading.

In this chapter it has been shown how to calculate the maximum vibratory stresses in a turbine blade, using the results obtained in the previous chapter. These stresses might attain the amplitude level of the centrifugal stresses, especially for the first harmonic order. Superimposed together it is considered that they can be potentially very dangerous, particularly as the vibratory stresses have an alternating character.

The point should also be made here, that the results derived from this analysis are only approximate, in so far as they are subject to the assumptions stated at the beginning of this chapter. Even so, the approximation is a very good one, compared with previous methods, which assume for the stimulus S_n a certain value, estimated using a simplified dynamic force distribution (the amplitude and phase

angle of the different harmonic components being considered constant along the blade length). In this study the stimulus has been calculated, so that it takes account of the radial distribution of the dynamic force. The harmonic components of the dynamic force can be calculated according to chapter 2 and are found to vary according to the shape and configuration of the blades. Consequently, the stimulus can vary for the same blade and the same aerodynamic conditions by changing only the pitch ratio R . We can expect to have certain cases where the stimulus vanishes and others where it attains maximum values.

In the case of the first harmonic, we may calculate an upper and a lower limit for the stimulus, thus defining a certain range. These limits then correspond to the upper and lower limits of the dynamic force.

4. NUMERICAL EXAMPLE

The calculation of the dynamic force and vibratory stresses for a turbine blade has been discussed theoretically in chapters 2 and 3 respectively. In order to obtain the practical and physical meaning of the solution, we will now apply this theory to a numerical example.

It can be seen that the numerical calculations, particularly in the first part (calculation of the dynamic forces), are likely to be long and complicated, but this difficulty can be overcome by using electronic computing devices. The calculation detailed in this chapter was performed with the electronic computer of the Swiss Federal Institute of Technology in Zürich (details about this computer can be found in [13]).

4.1. Choice of example

It is very important when choosing an example for the numerical application of a theoretical study to find one which is as simple as possible, to avoid the different types of complications. At the same time, the example chosen must possess all the technical and physical requirements of the problem.

Since the velocity distribution at entrance to the moving row of blades is assumed in our solution to be known (chapter 2), we must look for an example fulfilling this requirement. Few measurements have been made under simplified aerodynamic conditions for twisted blades, especially in a real turbine. Since we tend to simplify the numerical application and for the above reasons, a simple blade form has been chosen as an example. Dettmering has published a report on some experimental work done with a turbine designed specially for the purpose of examining stage losses [14]. In this turbine, which has one stage, the velocity distribution between stationary and moving rows of blades has been measured for a complete pitch and at several radial sections. The results have been published in the report mentioned above, and are such as to fulfil the requirements for a numerical example.

In order to calculate the dynamic-force distribution on a moving blade we require the velocity distribution behind the preceding stationary row. This has been measured by Dettmering for the given blade-profile and for different configurations (pitch ratios). From the different measurements made by him we shall choose only two cases, corresponding to two different pitches. The basic condition in our choice is the ratio of the width of the velocity wake at the plane of measurement to the pitch of the stationary blades. This ratio is considered very important, since it determines the magnitude of the different harmonic components of the dynamic force, as will be seen

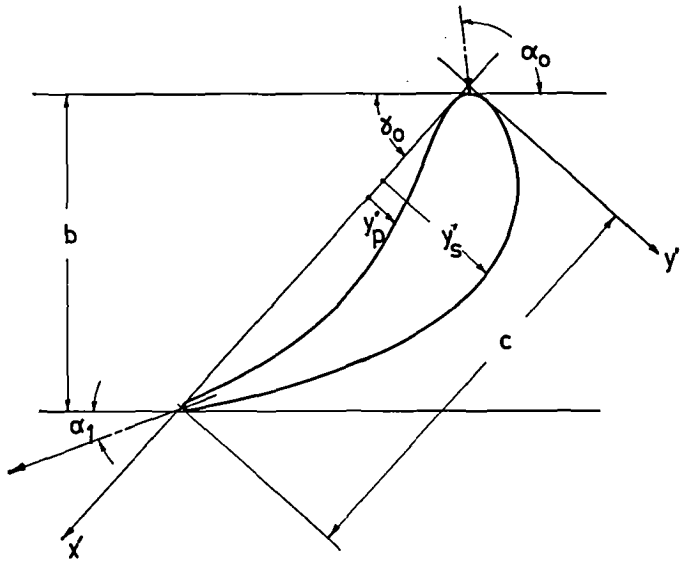

Blade chord "c" = 35.5 mm.
Blade breadth"b"= 26.6 "
Geometrical angles $\alpha_o = 96°$ $\alpha_1 = 20.5°$
$\gamma_o = 48°$

Fig. 4.1 Coordinate system and main geometrical data for Dettmering's blade-profile

later. In the first case, a small pitch is chosen, in which case the wake-width ratio is relatively large, because of boundary-layer interference from adjacent blades, whereas in the second case a relatively low ratio is achieved by choosing a larger pitch. It should be added, however, that both pitches are in the aerodynamic optimum-range for this blade configuration.

Table 1 gives the coordinates and main geometric data for the Dettmering blade used in our example, using the notation of fig. 1.

The blades in the moving and stationary rows are similar, as in the case of a typical 50 % reaction stage. The blade chord angle γ_0 is constant for both the cases used, and at all radial sections. The same profile is used along the blade length.

Table 1 Profile coordinates for Dettmering's blade

x'/c	y'_p mm	y'_s mm
0	y' = 2.15	
0.1	0.25	8.35
0.2	1.30	10.50
0.3	2.45	11.35
0.4	3.40	11.35
0.5	3.90	10.60
0.6	3.80	9.20
0.7	3.30	7.40
0.8	2.35	5.25
0.9	1.20	3.00
1.0	y' = 0.50	

The velocity behind the stationary row of blades was measured along seven different coaxial surfaces and for a complete stationary-blades pitch. This was done by means of a three-hole cylindrical probe, which measured the magnitude and direction of the absolute velocity at a small distance from the stationary-blade trailing-edge (5 mm). The axial clearance between the two rows was equal to 12 mm. The stationary row contained 40 blades in the first case, and 32 blades in the second. For simplicity we shall designate these two configurations with the following abbreviations

Dett. 40/48 for the first configuration (case)
Dett. 32/48 " " second "
(48 denoting the chord angle γ_0)

Furthermore, we will identify the coaxial surfaces along which the velocity distribution was measured by the notation MP 1-7. Table 2 shows the position of these surfaces along the blade length, as well as the corresponding blade pitch T' .

Table 2 Position and pitches of the coaxial surfaces of measurement

MP	radius r mm	r/r_m^*	T' mm		$\hat{T} = T'/l^*$	
			Dett. 40/48	Dett. 32/48	Dett. 40/48	Dett. 32/48
1	123.5	0.875	19.40	24.25	0.473	0.592
2	129.5	0.915	20.34	25.43	0.495	0.621
3	135.4	0.957	21.28	26.61	0.519	0.650
4	141.5	1.000	22.23	27.78	0.543	0.677
5	148.0	1.046	23.25	29.06	0.567	0.710
6	154.5	1.092	24.27	30.34	0.592	0.740
7	164.0	1.138	25.29	31.61	0.617	0.771

In order to use non-dimensional analysis from the beginning, we will choose our reference parameters according to 2.2.2 . The reference length l^* in this case is very simple to choose since, for cylindrical stages, it is constant along the flow direction. The experimental turbine used rotates at constant angular velocity of 8000 r.p.m. The resulting reference paramters can be given by

$$l^* = 41 \text{ mm}, \quad \text{and} \quad u_m^* = \frac{2 \pi r_m^* n}{60} = 118.59 \text{ m sec}^{-1}$$

The last two columns in table 2 give the non-dimensional pitch $\hat{T}' = T'/l^*$ for both the configurations (Dett. 40/48 and Dett. 32/48).

It should be stated that the velocity distribution behind the stationary row of blades was measured for two different conditions:

1. Without moving blades and with the rotor stationary. In this case the tip clearance of the stationary blades was zero.
2. With the rotating turbine-shaft and moving blades. In this case the radial clearance of the stationary blades was one millimeter.

The results in both cases were similar. For our example we shall consider only the second case, since it represents the actual conditions in the turbine.

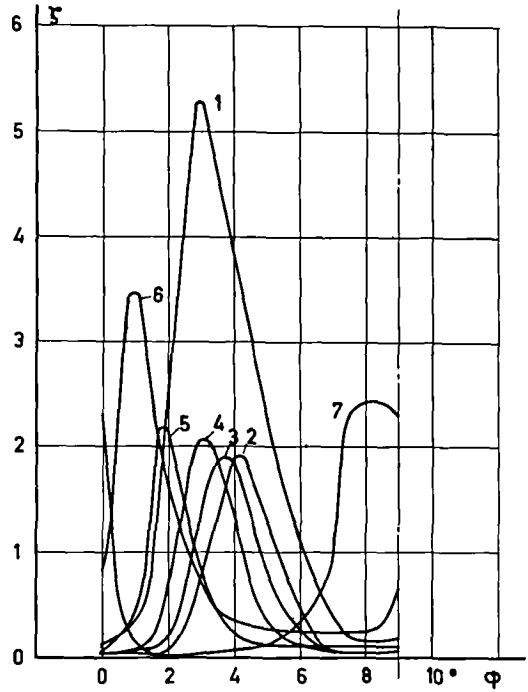

Fig. 4.2 Total-pressure-loss coefficient for stationary row of blades type Dett. 40/48 as a function of pitch-angle

4.2. Evaluation and harmonic analysis of the velocity distribution

The velocity distribution, as measured in a plane behind the stationary row of blades, is not given explicitly in Dettmering's report, but instead the distribution of the total-pressure-loss coefficient. This distribution depends on the velocity distribution required, and on the static pressure drop across the stationary row. The total-pressure-loss coefficients between two parallel planes before and after the stationary row of blades are plotted in figs. 2 and 3 for the two configurations examined. The distribution is given along one pitch, and for the seven measuring stations (MP 1-7). The pitch is transformed into pitch angle in order to give the same value at all radii.

It can be seen from these figures that the wakes at the different radial sections

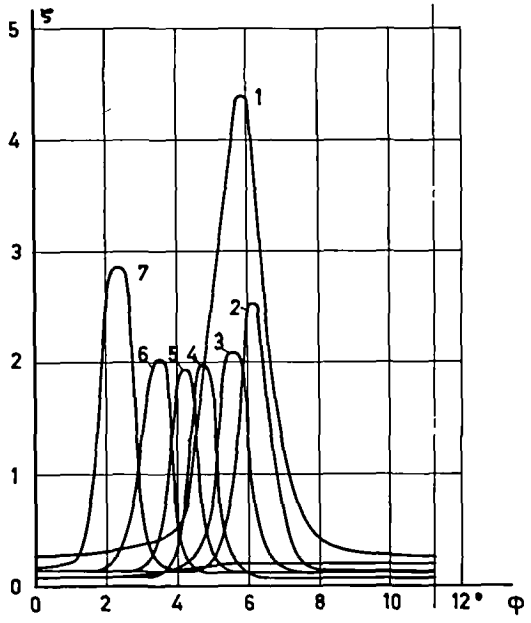

Fig. 4.3 Total-pressure-loss coefficient for stationary row of blades of the type Dett. 32/48 as a function of pitch-angle

possess a certain phase shift relative to each other, which is caused by the fact that the trailing edge of the stationary blades is inclined at a certain angle to the radial direction. We shall refer all our analysis to a fixed radial axis in order to take account of this phase shift in the calculations. On the other hand, the moving blade leading-edge takes a radial direction so that the zero-point choice of our coordinate is immaterial. The end walls (casing and hub) might also affect the position of the wakes near them, as is shown in figs. 2 and 3, and this possibility will be considered in the calculations.

The total-pressure-loss coefficient $\zeta(\varphi)$, which is considered as a function of the pitch angle φ, is defined as

$$\zeta(\varphi) \equiv \frac{g_0 - g_1(\varphi)}{q_0} \tag{1}$$

where g_0 is the total pressure before the stationary row of blades and is considered to be independent of the pitch angle φ, q_0 is the dynamic pressure in the same section (equal to $\frac{\rho}{2} c_0^2$), and g_1 is the total pressure behind the stationary row of

blades, which is considered to be a function of φ . Assuming that the static pressure before and after the stationary-blades, and at the planes where the measurements are made, is constant along the pitch, and knowing too that

$$g_0 = p_0 + q_0 = p_0 + \frac{\varrho}{2} c_0^2$$

$$g_1 = p_1 + q_1 (\varphi) = p_1 + \frac{\varrho}{2} c_1^2 (\varphi) \qquad (2)$$

$$\Delta \pi_s = \frac{p_0 - p_1}{q_0}$$

we can write for equation (1) the expression

$$\frac{c_1 (\varphi)}{c_0} = \sqrt{\Delta \pi_s + 1 - \zeta (\varphi)}$$

Inserting u_m^* as a reference velocity, we can rewrite this in non-dimensional form as

$$C_1 (\varphi) = C_0 \sqrt{\Delta \pi_s + 1 - \zeta (\varphi)} \qquad (3)$$

Equation (3) establishes the relationship between the absolute velocity $C_1 (\varphi)$ and the total-pressure-loss coefficient $\zeta (\varphi)$ which is given in figs. 2 and 3. This, however, assumes a knowledge of the static pressure drop $\Delta \pi_s$, and this was measured by Dettmering and given in his report.

In order to obtain the three velocity components W_{a1}, W_{t1} and W^*, which are required for the analysis, we can write

$$W_{a1} = C_1 \sin \alpha_1 \tag{4}$$

$$W_{t1} = C_1 \cos \alpha_1 - \mu \tag{5}$$

$$W^* = C_1 - \mu \cos \alpha_1 \tag{6}$$

The exit flow angle α_1 was also measured by Dettmering. It is given in his report as a function of the pitch angle, however the variations given are so small that we can neglect them. It is also possible that these variations were caused by the relatively large diameter of the three-hole cylindrical probe used for the measurements, particularly since the flow field inside the wake contains relatively high velocity gradients. It is assumed that α_1 is constant along the pitch and the geometric mean value will be used. Table 3 gives the value of $\Delta \Pi_s$ and $\bar{\alpha}_1$ at the different measuring sections along the blade length, as given in the report.

Table 3 Static pressure drop and flow angles at the different radial sections

MP	Dett. 40/48		Dett. 32/48	
	$\Delta \Pi_s$	$\bar{\alpha}_1$ °	$\Delta \Pi_s$	$\bar{\alpha}_1$ °
1	12.40	19.60	8.80	21.10
2	10.90	18.75	7.90	21.05
3	11.77	17.60	8.15	19.80
4	11.47	19.00	7.76	21.60
5	10.95	19.55	7.30	22.00
6	10.70	21.25	6.70	24.00
7	10.95	24.10	6.75	26.30

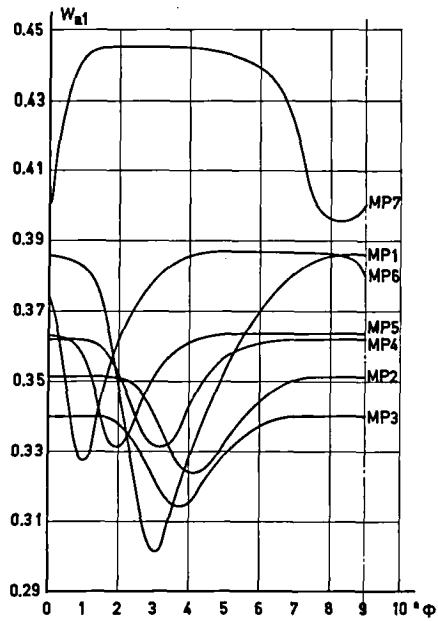

Fig. 4.4 Axial component of the flow-velocity behind a stationary row of blades of the type Dett. 40/48

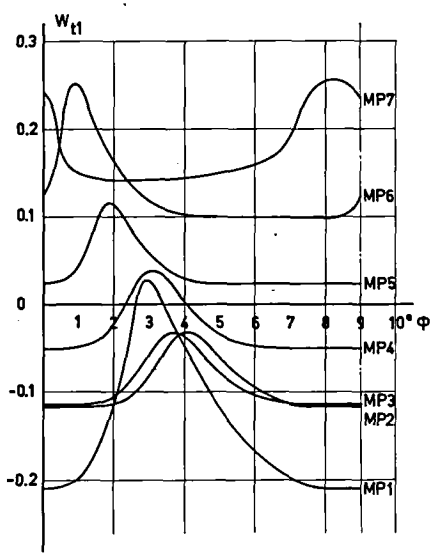

Fig. 4.5 Tangential component of the flow-velocity behind a stationary row of blades of the type Dett. 40/48

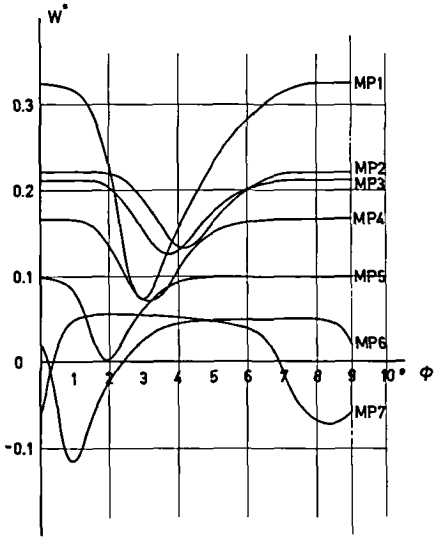

Fig. 4.6 Velocity component causing changes in flow-direction at entrance to the rotating row of blades. Stationary row of blades type Dett. 40/48

For the absolute flow velocity at entrance to the stationary row C_0 , the following values are given in Dettmering's report

Dett. 40/48	$c_0 = 37.4$ m.sec^{-1}	$C_0 = 0.3158$
Dett. 32/48	$c_0 = 43.1$ "	$C_0 = 0.3650$

The velocity components W_{a1}, W_{t1} and W^* at entrance to the moving row of blades are given for both configurations in figs. 4-9. These components are calculated according to equations (3), (4), (5) and (6), using values of ξ (φ) taken from figs. 2 and 3. They are plotted against the pitch angle φ (one complete pitch corresponds to 9^o for Dett. 40/48 and to 11.25^o for Dett. 32/48). The zero line is taken as a radial line.

On examining figs. 4-9 we notice for the velocity distribution that

1. The width of the wake relative to the pitch of the stationary-blades is larger for the configuration Dett. 40/48 than for Dett. 32/48.
2. The form of the wake in each case is similar along the blade length except near the hub and the casing, where it is largely affected by the boundary layer along these two surfaces.
3. The wakes are, ingeneral, shifted by an approximately constant phase angle

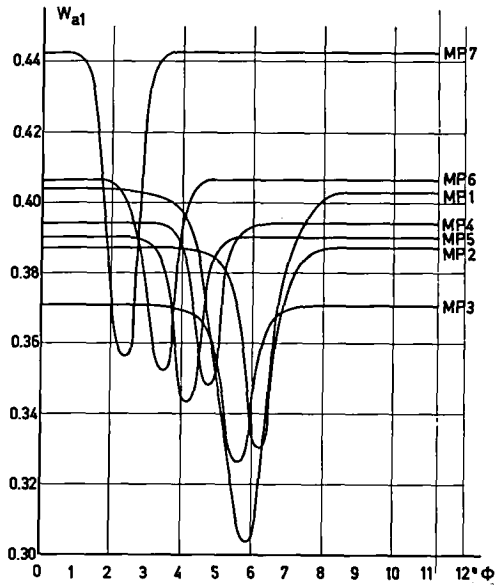

Fig. 4.7 Axial component of the flow-velocity behind a stationary row of blades of the type Dett. 32/48

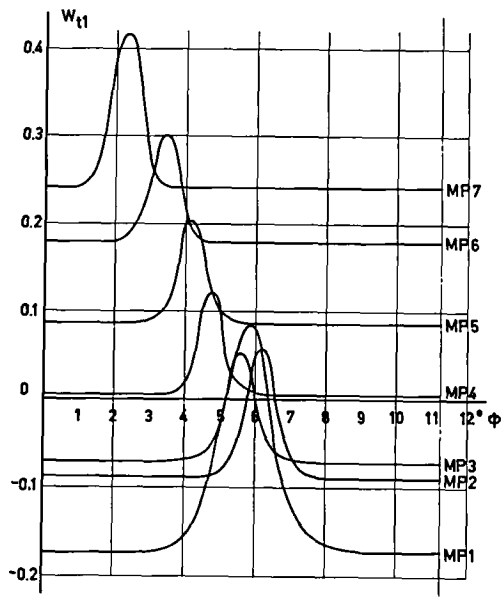

Fig. 4.8 Tangential component of the flow-velocity behind a stationary row of blades of the type Dett. 32/48

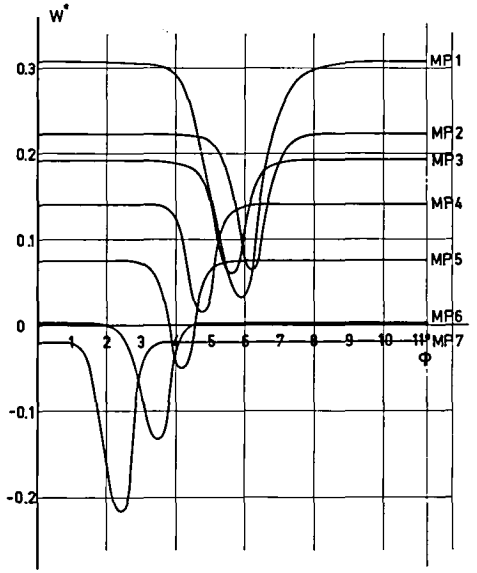

Fig. 4.9 Velocity component causing changes in flow-direction at entrance to the rotating row of blades. Stationary row of blades type Dett. 32/48

(this does not apply to the casing and hub sections). This constant shift can be attributed to the angular deviation of the stationary-blades trailing-edge from the radial direction.

In order to calculate the dynamic force, it is necessary to express these velocity-distributions, which are periodic functions with a period equal to T', in the form of a harmonic series. Since they are given numerically, it is necessary to have a numerical method of calculating the harmonic coefficients. For this purpose the electronic computing machine "ERMETH" was used, for which a library program for harmonic analysis is available [13]. This program is based on the numerical method by Runge for the calculation of the harmonic coefficients of a certain function which is given numerically [15]. The number of coefficients calculated depends on the number of points available to describe the function. However, the shape of the function analysed also affects to a certain extent the number of ordinates required for the harmonic analysis, in order to achieve a certain accuracy. From figs. 4-9 we see that, for the relatively large wake of the configuration Dett. 40/48, we can

Table 4 Harmonic coefficients for the distribution of the axial and tangential components of flow velocity

Blade configuration Dett. 40/48

MP	n	0	1	2	3	4	5	6
1	a_n	0.36000	0.02735	0.00449	-0.00695	-0.00050	0.00203	-0.00053
	b_n		-0.02215	0.01278	0.00173	-0.00321	0.00020	0.00113
	c_n	-0.13700	-0.07590	-0.01257	0.02010	0.00088	-0.00533	0.00132
	d_n		0.06280	-0.03670	-0.00450	0.00950	-0.00098	-0.00233
2	a_n	0.34400	0.01150	-0.00585	0.00155	0.00009	-0.00023	0.00007
	b_n		-0.00164	0.00212	-0.00159	0.00084	-0.00037	0.00024
	c_n	-0.09460	-0.03380	0.01683	-0.00416	0.00043	0.00062	-0.00016
	d_n		0.04520	-0.00594	0.00468	-0.00266	0.00107	-0.00045
3	a_n	0.33400	0.00948	-0.00297	-0.00051	0.00069	-0.00018	0.00002
	b_n		-0.00432	0.00459	0.00220	0.00049	-0.00012	0.00006
	c_n	-0.09350	-0.03000	0.00950	0.00158	-0.00247	0.00103	-0.00050
	d_n		0.01357	-0.01431	0.00695	-0.00149	-0.00011	0.00029
4	a_n	0.35457	0.00805	0.00161	-0.00323	0.00070	0.00023	0.00008
	b_n		-0.00878	0.00676	-0.00079	-0.00097	0.00017	0.00001
	c_n	-0.02995	-0.02324	-0.00459	0.00918	-0.00196	-0.00075	0.00001
	d_n		0.02541	-0.01950	0.00220	0.00276	-0.00064	-0.00005
5	a_n	0.35800	-0.00076	0.00700	0.00221	-0.00143	-0.00180	-0.00061
	b_n		-0.00103	-0.00164	0.00372	0.00216	-0.00008	-0.00137
	c_n	0.04090	0.00316	-0.01965	-0.00616	0.00400	0.00565	0.00263
	d_n		0.02980	0.00520	-0.01048	-0.00646	-0.00028	0.00353
6	a_n	0.37500	-0.01211	0.00119	0.00463	0.00415	0.00270	0.00134
	b_n		-0.01546	-0.01262	-0.00592	-0.00193	0.00002	0.00037
	c_n	0.12750	0.03000	-0.00185	-0.01052	-0.01045	-0.00799	-0.00455
	d_n		0.03830	0.03135	0.01605	0.00641	0.00077	-0.00141
7	a_n	0.43100	-0.01725	-0.00494	-0.00011	-0.00069	-0.00280	-0.00311
	b_n		0.01350	0.01140	0.00488	0.00041	-0.00029	0.00109
	c_n	0.17350	0.03745	0.01100	0.00076	0.00248	0.00626	0.00630
	d_n		-0.0304	-0.02565	-0.01145	-0.00156	0.00002	-0.00187

Table 5 Harmonic coefficients for the distribution of the axial and tangential components of the flow velocity

Blade configuration Dett. 32/48

MP	n	0	1	2	3	4	5	6
1	a_n	0.38800	0.02895	-0.02140	0.01437	-0.00877	0.00470	-0.00219
	b_n		0.00201	-0.00290	0.00279	-0.00215	0.00159	-0.00139
	c_n	-0.13200	-0.07450	0.05560	-0.03775	0.02320	-0.01270	0.00628
	d_n		-0.05310	0.00800	-0.00756	0.00535	-0.00400	0.00378
2	a_n	0.38200	0.01015	-0.00769	0.00463	-0.00192	0.00006	0.00091
	b_n		0.00316	-0.00539	0.00625	-0.00586	0.00472	-0.00338
	c_n	-0.07480	-0.02650	0.02008	-0.01205	0.00492	-0.00001	-0.00261
	d_n		-0.00824	0.01399	-0.01600	0.01467	-0.01150	0.00805
3	a_n	0.36700	0.00855	-0.00755	0.00624	-0.00497	0.00389	-0.00299
	b_n		-0.00032	0.00056	-0.00067	0.00071	-0.00072	0.00070
	c_n	-0.05940	-0.02366	0.02100	-0.01745	0.01390	-0.01084	0.00826
	d_n		0.00085	-0.00150	0.00182	-0.00193	0.00194	-0.00192
4	a_n	0.39020	0.00645	-0.00366	0.00031	0.00239	-0.00373	0.00366
	b_n		-0.00354	0.00581	-0.00614	0.00473	-0.00243	0.00017
	c_n	0.01424	-0.01619	0.00926	-0.00090	-0.00590	0.00937	-0.00937
	d_n		0.00886	-0.01455	0.01545	-0.01204	0.00634	-0.00067
5	a_n	0.38600	0.00529	0.00034	-0.00475	0.00532	-0.00277	-0.00035
	b_n		-0.00555	0.00710	-0.00414	-0.00046	0.00338	-0.00347
	c_n	0.09750	-0.01282	-0.00077	0.01155	-0.01303	0.00676	0.00097
	d_n		-0.01735	0.01015	0.00112	-0.00833	0.00850	0.00850
6	a_n	0.40100	0.00284	0.00727	-0.00620	-0.00196	0.00516	-0.00175
	b_n		-0.00915	0.00505	0.00466	-0.00616	0.00028	0.00358
	c_n	0.19050	-0.00634	-0.01620	0.01389	0.00442	-0.01168	0.00381
	d_n		+0.02036	-0.01129	-0.01040	0.01387	-0.00057	-0.00816
7	a_n	0.43500	-0.00462	0.01210	0.01010	-0.00416	-0.00872	-0.00098
	b_n		-0.01500	-0.00821	0.00815	0.01011	-0.00098	-0.00660
	c_n	0.25800	0.00930	-0.02420	-0.02030	0.00640	0.01770	0.00190
	d_n		0.03000	0.01652	-0.01632	-0.02043	0.00204	0.01346

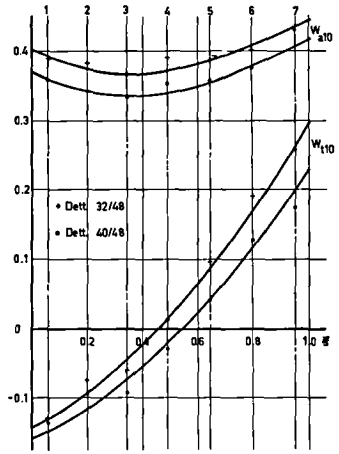

Fig. 4.10 Mean velocity-components as calculated by harmonic analysis

represent the function accurately enough by dividing the pitch (period) into 16 equal divisions. In the second case of Dett. 32/48, we must, however, use 30 equal divisions to obtain a similar accuracy in the results, on account of the relatively small width of the wake.

In the calculation of the dynamic force we are interested in the first three harmonics; we shall, therefore, consider only the first six harmonic orders of the velocity distribution calculated. It is expected that harmonic orders higher than the sixth will have only a negligible effect on the first three harmonic components of the dynamic force. Tables 4 and 5 give the harmonic coefficients a_n, b_n, c_n and d_n (see equations (2.35) and (2.36), and the definitions of the coefficients which follow), for the first six harmonics. The mean velocity components W_{a10} and W_{t10} are also given in these two tables (a_0 and c_0 respectively).

The harmonic coefficients given in tables 4 and 5 will be used according to the method given in chapter 2 for the calculation of the axial and tangential components

of the dynamic force. The fact that these coefficients are calculated from a measured velocity distribution can be seen in fig. 10, in which the mean axial and tangential components of the flow velocity, as calculated from the harmonic analysis (a_0 and c_0 in tables 4 and 5), are plotted for the different sections (MP 1-7), i.e. along the blade length ξ . It can be seen how the different points are scattered on either side of the drawn curves. This scatter is mainly due to discrepancies in the measurement of the velocity distribution. We shall, however, accept the coefficients as calculated and given in tables 4 and 5, without trying to correct them according to fig. 10. This will naturally affect the value of the dynamic force calculated, but we can correct it. This procedure is justified by the fact that higher harmonic orders of the dynamic force are not seriously affected by the zero harmonic order of the velocity distribution (a_0 and c_0) as will be seen later. Consequently the effect of the scatter in the measured values of the mean velocity-distribution will be smaller for the calculated force components of the first and higher orders. The correction will be easier for the forces than for the velocities.

Table 6 Velocity component W_1^* required for the calculation of the upper limit of the dynamic force.

MP	1	2	3	4	5	6	7
Dett.40/48	0.1049	0.0362	0.0143	0.0361	0.0303	0.0265	0.0532
Dett.32/48	0.0809	0.0300	0.0254	0.0202	0.0204	0.0235	0.0361

The velocity component W_1^* required for the calculation of the upper limit of the dynamic force (see 2.4.2) is given in table 6, for both blade configurations.

In order to be able to examine the effect of each of the harmonic coefficients of the velocity distribution on the calculation of the dynamic force, and particularly their effect on the first three harmonic components, we must study fig. 11. This figure shows the degree of convergence of the harmonic series representing the velocity distribution at entrance to the moving row of blades. The amplitudes of the different harmonics between 1 and 6 are defined by

$$r_a \equiv \sqrt{a_n^2 + b_n^2}$$

$$r_t \equiv \sqrt{c_n^2 + d_n^2} \qquad (7)$$

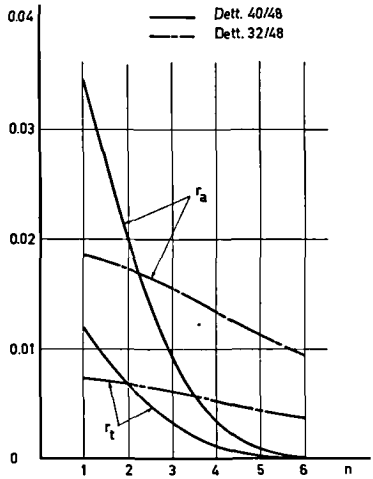

Fig. 4.11 Amplitudes of the different harmonic components of the relative flow-velocity at entrance to the moving row

and have been plotted for the mean blade radius of both configurations (MP 4), since only a qualitative analysis of the two types is needed. For the most part, this is a comparison between the convergence properties of the two cases, which are expected to affect the relative values of the different harmonic orders of the dynamic force, as will be seen later. Fig. 11 shows that the convergence of the harmonic amplitudes for the configuration Dett. 40/48 is stronger than for the other configuration. It follows therefore that the harmonic components of the dynamic force can be expected to show the same tendency. However, it is difficult to make any quantitative statements about these components, since they depend so much on shape and configuration of the moving blades.

The calculation of the transformed harmonic coefficients A_n, B_n, C_n and D_n (see equations (2.39-42)) will be discussed together with the calculation of the dynamic force.

4.3. Determination of the blade form-parameters

It has been shown in chapter 2 how the axial and tangential components of the dynamic force depend on the shape of the moving blades and the configuration of both the moving and the stationary blades. This relation has been given in the form of the two parameters K_a and K_t , which are defined according to chapter 2, equations (11) and (16), as

$$K_a \equiv 2\,R \int_0^{\hat{S}} \left[\frac{R}{B} - \sin\beta\right] dS$$

$$K_t \equiv 2\,R \int_0^{\hat{S}} \cos\beta \; dS \qquad (8)$$

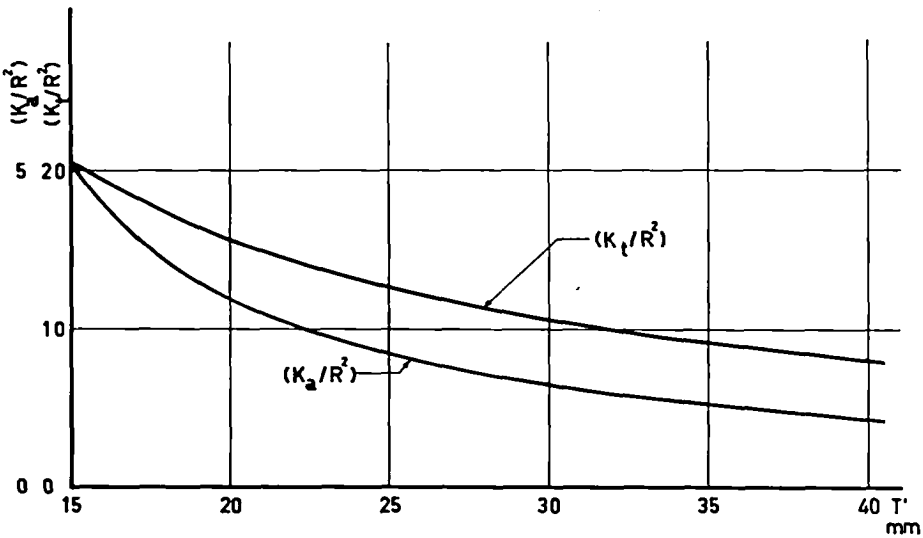

Fig. 4.12 Axial and tangential form-parameters for Dettmering blade

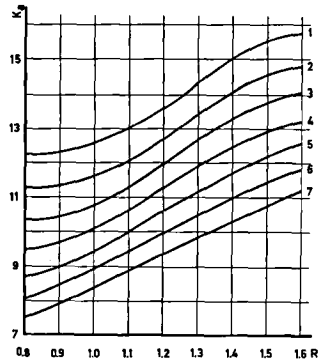

Fig. 4.13 Turbine-blade form-parameter "K_a" for the calculation of the dynamic force. Stationary row type Dett. 40/48

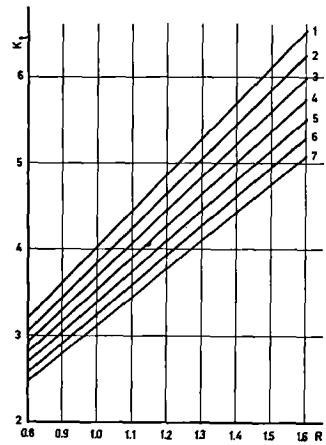

Fig. 4.14 Turbine-blade form-parameter "K_t" for the calculation of the dynamic force. Stationary row type Dett. 40/48

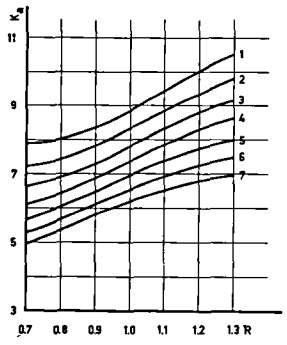

Fig. 4.15 Turbine-blade form-parameter "K_a" for the calculation of the dynamic force. Stationary row type Dett. 32/48

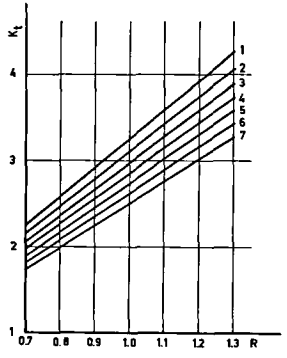

Fig. 4.16 Turbine-blade form-parameter "K_t" for the calculation of the dynamic force Stationary row type Dett. 32/48

It can be seen that they depend on the shape of the mean stream line of the blade channel, which in turn depends on the form and pitch of the blades. The calculation of these parameters for our example has been done by drawing the potential flow pattern for the different blade configurations (different pitches). We can consider the mean stream line in this case to be a good approximation to the actual one (small differences may be caused by the unsteady character of the flow), particularly since the flow pattern has been drawn to a large scale (10:1). The calculation is done for different pitches covering the range required for the minimum and maximum pitches anywhere along the length of the moving-blades. This range corresponds to the minimum and maximum pitches examined in Dettmering's report and are given by

$$T''_{min} = 15.52 \text{ mm} \qquad T''_{max} = 40.46 \text{ mm}$$

The ranges for the pitch ratio R corresponding to the above pitches are as follows

Dett. 40/48	$R_{min} = 0.8$	$R_{max} = 1.6$
Dett. 32/48	$R_{min} = 0.7$	$R_{max} = 1.3$

(these values have been rounded for simplicity)

From the form of equation (8) it is quite simple to prove that K_a/R^2 and K_t/R^2 are functions only of the pitch of the moving blades T''. The values of these functions as calculated according to the above procedure are shown in the two curves in fig. 12, and are used to calculate the form parameters for any section along the blade length (in our case MP 1-7), and for different pitch ratios R . The pitch ratio and the pitch of the moving-blades are calculated according to the stationary-blades configurations and the pitch-ratio range given. The corresponding values of K_a/R^2 and K_t/R^2 are then taken from fig. 12, and multiplied by R^2 to give the required form parameter.

Figs. 13-16 show the form parameters K_a and K_t for the two configurations used, and for different pitch ratios.

4.4. Calculation of the dynamic force

The dynamic force on the turbine blade in our example will be calculated according to the method described in chapter 2. This method involves the determination of the various harmonic orders of the axial and tangential components of the dynamic force, and requires a knowledge of the velocity distribution at entrance to the moving row of blades. The necessary form of this velocity distribution to suit our analysis has already been established in 4.2. The values of the directional components of the dynamic force depend also on the shape of the moving blades, as well as on the configuration of both

the moving and stationary blades (see chapter 2). This latter effect is expressed by the form parameters calculated according to chapter 2, and given for the two configurations (Dett. 40/48 and Dett. 32/48) in figs. 13-16. The dynamic forces will be calculated for the pitch-ratio ranges given in 4.3.

In order to cover this wide range of pitch ratios and to cope with the complexity of the numerical calculation of the dynamic force, it was necessary to use a fast computing machine; the electronic computer "ERMETH" [13] was used for this purpose, and a special program has been written for the calculation of the dynamic forces. Thus it was possible to complete the analysis in a relatively short time.

The main problem during the programming and calculation was that of setting the upper limit of the dynamic forces. Before stating the results of the computation it is necessary to explain the conditions under which the upper limit has been calculated, as well as to choose a simple method for its computation.

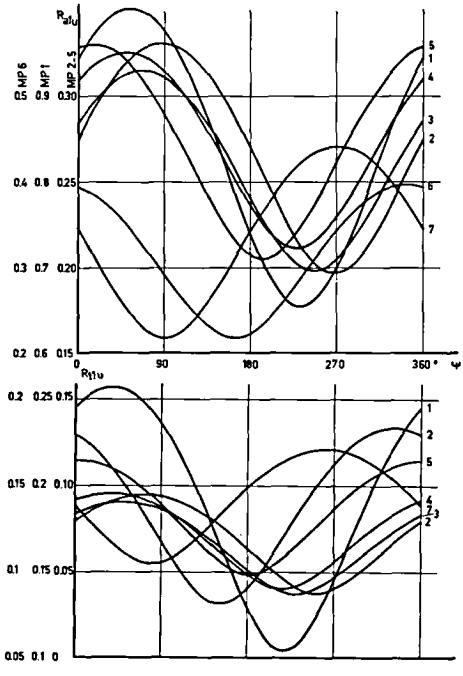

Fig. 4.17 First harmonic amplitude of the upper limit of the dynamic force
Blade type Dett.40/48 Pitch ratio = 0.8

4.4.1. Choice and calculation of the upper limit

It has been explained in 2.4.2 how the upper limit of the dynamic force may be calculated. This depends, as is seen from equations (2.56) and (2.57), on the harmonic velocity component W_1^*, which represents the first harmonic amplitude of the flow-velocity component responsible for changes in flow direction at entrance to the moving row of blades. It depends also on the phase shift between the unsteady flow-direction changes at entrance and exit to the moving-blades row Ψ. In other words, for a certain given velocity distribution, the upper limit of the dynamic force depends on the phase angle Ψ. According to equations (2.56) and (2.57) a maximum value of the upper limit can be calculated, which corresponds to a certain phase angle denoted by Ψ_{max}. A preliminary calculation was done to study the changes in the upper limit corresponding to different values of the phase angle Ψ. The final aim of this study is to find the simplest method of calculating the upper limit of the dynamic force.

A specific blade configuration has therefore been chosen (Dett. 40/48, R = 0.8 and 1.2), and the corresponding upper limit has been calculated with the phase angle varying between 0 and 2π. In figs. 17 and 18 the relative first-harmonic amplitudes of the upper limit of the axial and tangential components are plotted as a function of the phase angle Ψ. These relative amplitudes are defined for the axial and tangential components respectively as follows.

$$R_{a1_u} \equiv \frac{\sqrt{\left(F_{a1} + \Delta F_{a1}\right)^2 + \left(F'_{a1} + \Delta F'_{a1}\right)^2}}{F_{a0}}$$

$$R_{t1_u} \equiv \frac{\sqrt{\left(F_{t1} + \Delta F_{t1}\right)^2 + \left(F'_{t1} + \Delta F'_{t1}\right)^2}}{F_{t0}} \qquad (9)$$

On studying these two figures, we can see that the maximum value of the upper limit corresponds for each section (MP 1-7) to a certain phase angle Ψ_{max}, as expected; however, the value of this phase angle differs along the blade length (Ψ_{max} is not the same for each of the coaxial surfaces of measurement, MP 1-7). This means that the phase shift between the unsteady flow-direction changes at entrance and exit of the moving-blades row is not the same for all the sections along the blade.

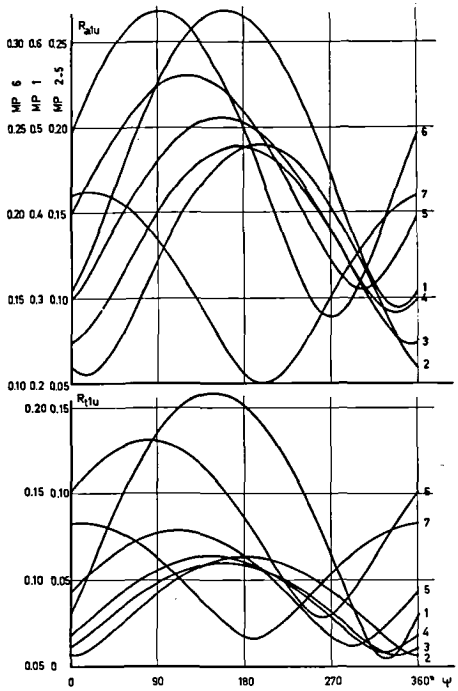

Fig. 4.18 First harmonic amplitude of the upper limit of the dynamic force

Blade type Dett. 40/48

Pitch ratio = 1.2

It seems, however, physically unreasonable that the flow along the blade channel should change between each radial section in order to achieve the maximum conditions corresponding to Ψ_{max}. For simplicity, we will assume therefore that Ψ_{max} has the same value for all radial sections. It then becomes necessary to choose a certain phase angle Ψ_{max} for which the upper limit is calculated at all sections along the blade length.

The choice of this phase angle can depend upon the actual meaning of the upper limit, and the calculation of the vibratory stresses. The first condition allows our choice to be of an approximate character, since the upper limit is considered only as the boundary to a certain range within which the actual value of the first harmonic of the dynamic force lies, rather than an exact value for this force component. This fact makes the choice of the phase angle Ψ_{max} very flexible. From figs. 17 and 18, we can see that the maxima of the upper limit of the dynamic force lie within a certain range of Ψ, so we should therefore, choose Ψ_{max} inside this range. We will assume for simplicity of calculation that Ψ_{max} corresponds to the maximum amplitude of the upper limit for one of the coaxial surfaces (MP 1-7). The question is only, which of these surfaces should be chosen? The answer is very simple and depends on the second condition, i. e. the calculation of the vibratory stresses. The upper limit must be chosen so that its resulting radial distribution along the blade length yields the largest possible vibratory stresses for the blade. These vibratory stresses depend,

as was shown in chapter 3, on the energy added to the blade, most of which is added at the blade tip (for the first mode of vibration). It might therefore be expected that the chosen Ψ_{max} should correspond to one of the sections near the blade tip.

The calculation of the upper limit of the dynamic force is based on the above analysis. The phase angle Ψ_{max} is calculated for either MP 6 or MP 7 and the corresponding upper limit is found for all other sections. In order to limit the number of results given we shall try to find out for which of the two surfaces (MP 6 or MP 7) we should calculate the phase angle Ψ_{max}. For this prupose, the radial distribution of the first harmonic amplitude of the dynamic force for Dett. 40/48 and Dett. 32/48 has been plotted in figs. 19 and 20 respectively (R = 8.0). Lower and upper limits have been given, the upper limit corresponding to Ψ_{max} for both MP 6 and MP 7 .

In the first case we can see that the effect of the casing is so strong that it shifts the phase angle Ψ_{max} (MP 7) far away from other maxima, as seen in fig. 17. As a result, and as shown in fig. 19, the radial distribution of the first harmonic amplitude of the upper limit corresponding to MP 7 is even smaller than the lower limit along most of the blade length. On the other hand, Ψ_{max} corresponding to MP 6 yields a higher radial distribution as shown. This fact leads us to choose Ψ_{max} correspon-

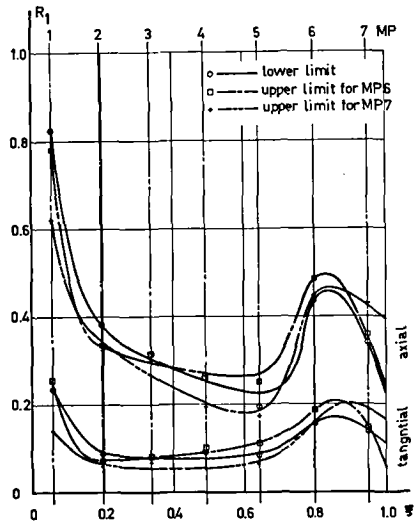

Fig. 4.19 First harmonic amplitude of the axial & tangential components of the dynamic force
Stationary row type Dett. 40/48, Pitch ratio = 0.8

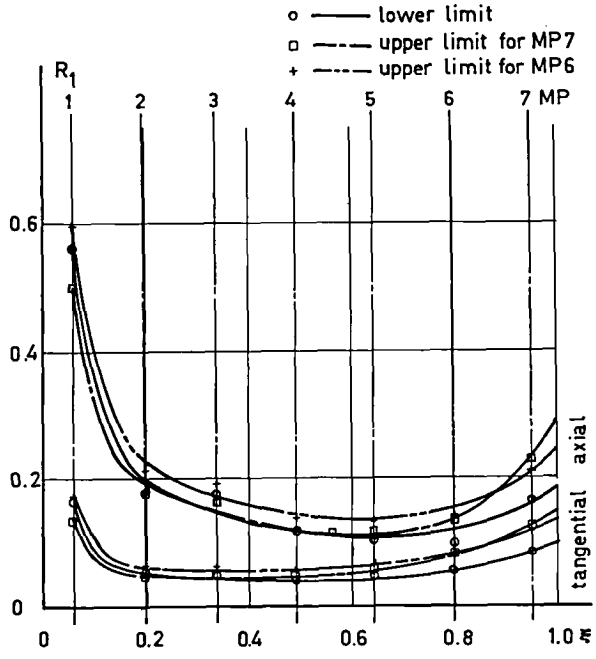

Fig. 4.20 First harmonic amplitude of the axial & tangential components of the dynamic force
Stationary row type Dett. 32/48, Pitch ratio = 0.8

ding to the coaxial plane MP 6_{η} for the configuration Dett. 40/48.

In fig. 20 for Dett. 32/48, we can see, however, that the difference between the two distributions, corresponding to Ψ_{max} for MP 6 and MP 7, is quite small. The calculated vibratory stresses can be expected to be very nearly the same, and, therefore, either of them could be used. For the second configuration (Dett. 32/48) we will choose Ψ_{max} corresponding to the coaxial section MP 7 .

The fact that the above analysis is done only for a single pitch ratio (R = 0.8) should not disturb us, because according to chapter 2, the radial distribution of the dynamic force is expected to be similar for a given stationary-blades configuration, and only the force level or absolute value varies with different pitch ratios. This fact will be seen later when discussing the main results.

4.4.2 Radial distribution of the dynamic force

The radial distribution of the dynamic force is required for the calculation of the vibratory stresses. The results obtained for the harmonic components of the dynamic force can be given either as the sine and cosine coefficients F_{an}, F'_{an}, F_{tn} and F'_{tn}

or in the form of harmonic amplitudes and phase angles. The latter are related to the former by the following relations:

For the amplitude of the lower limit, we may write

$$R_{an_1} \equiv \frac{\sqrt{F_{an}^2 + F_{an}'^2}}{F_{a0}}$$
$$R_{tn_1} \equiv \frac{\sqrt{F_{tn}^2 + F_{tn}'^2}}{F_{t0}} \qquad (10)$$

and for the phase angle we have

$$\varphi_{an_1} \equiv \tan^{-1}\left(\frac{F_{an}}{F_{an}'}\right)$$
$$\varphi_{tn_1} \equiv \tan^{-1}\left(\frac{F_{tn}}{F_{tn}'}\right) \qquad (11)$$

For the upper limit, we can write similar expressions with the upper limit coefficients.

The radial distribution of the harmonic amplitudes and phase angles are given in figs. 21-30 for various pitch ratios, for the two configurations Dett. 40/48 and Dett. 32/48. The pitch ratio range has been chosen according to 4.2, making use of the common range for the two configurations. This range varies between R = 0.8-1.3.

Figs. 21-25 give the radial distribution for the configuration Dett. 40/48 and for the pitch ratios R = 0.8, 0.9, 1.1, 1.2, and 1.3. The pitch ratio R = 1.0 is not given because according to the theory, only the upper limit of the first harmonic order exists, the other harmonics being zero. These figures show the harmonic amplitudes and phase angles of the first three orders plotted against the non-dimensional blade length coordinate ξ (ξ varies from zero at the blade hub section to unity at the tip). Fig. 26-30 show the same for the configuration Dett. 32/48.

Studying these figures, we can deduce that:

1. The radial distribution of the harmonic amplitudes is nearly constant along the middle part of the blade length, whereas at both the hub and the tip ends it varies

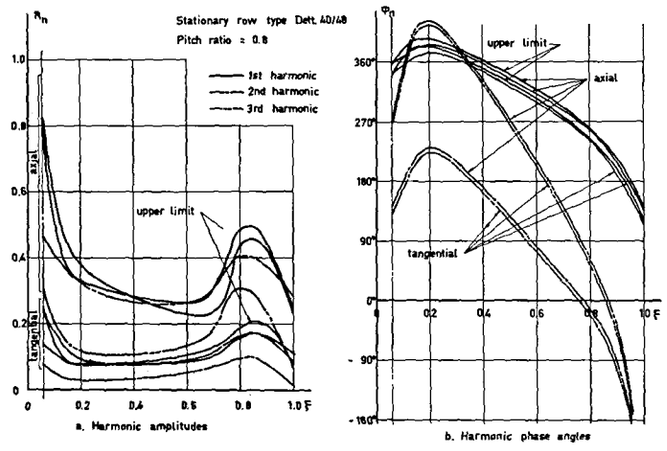

Fig. 4.21

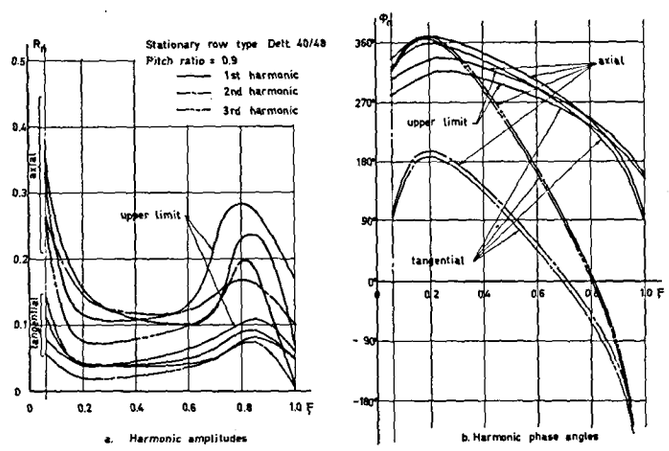

Fig. 4.22

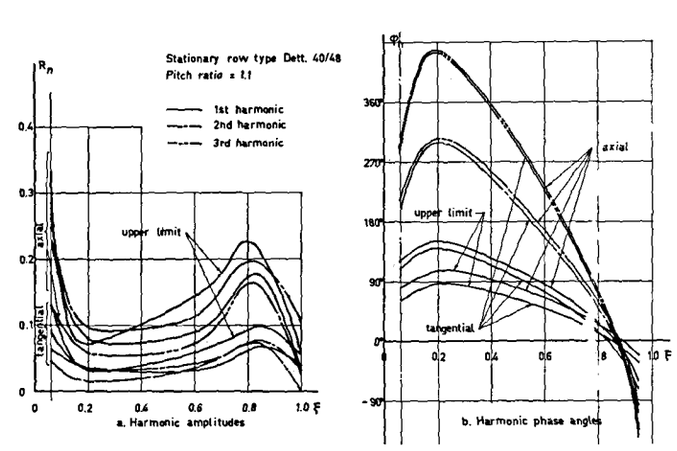

Fig. 4.23

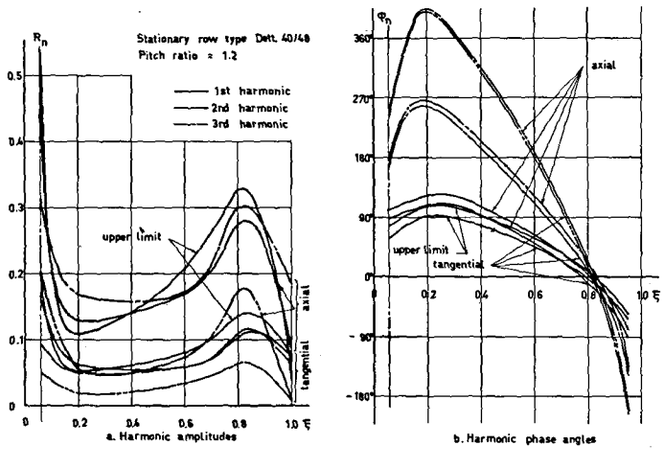

Fig. 4.24

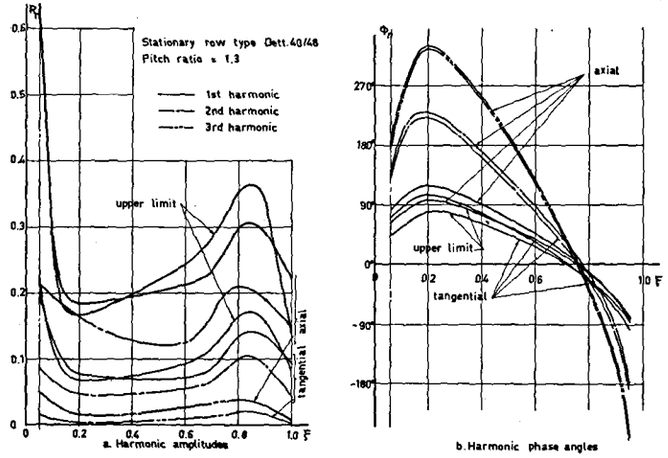

Fig. 4.25

Figs. 4.21....25 Harmonic amplitudes & phase angles for the axial & tangential components of the dynamic force

Leer - Vide - Empty

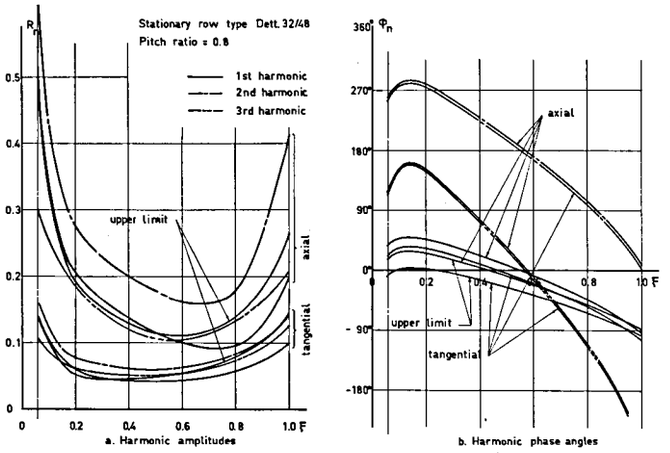

Fig. 4.26

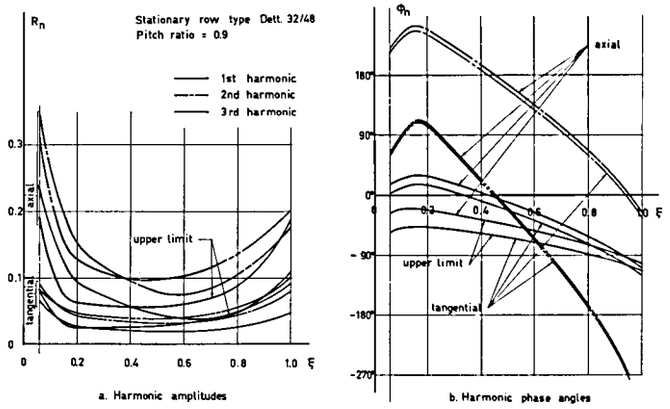

Fig. 4.27

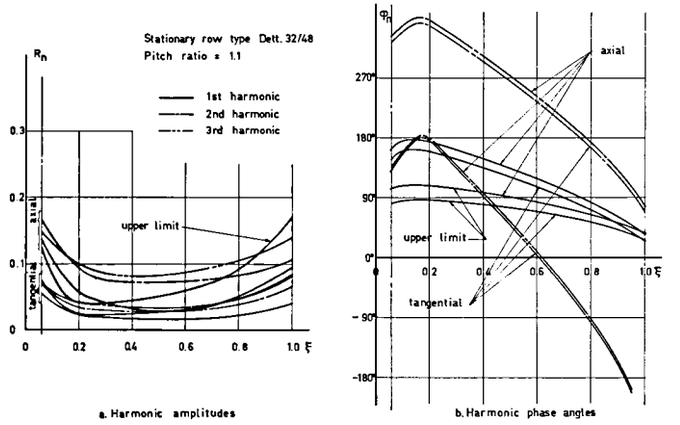

Fig. 4.28

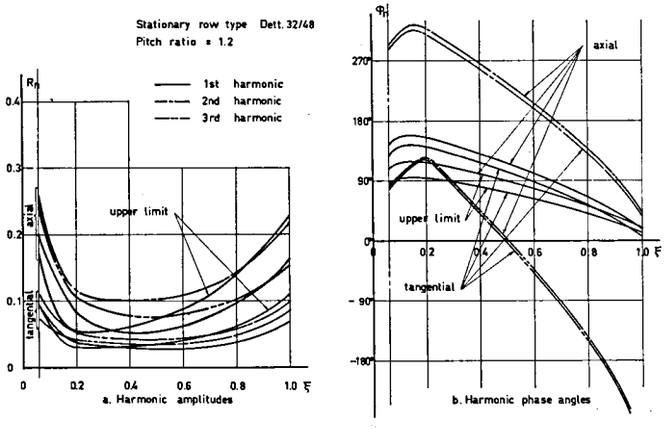

Fig. 4.29

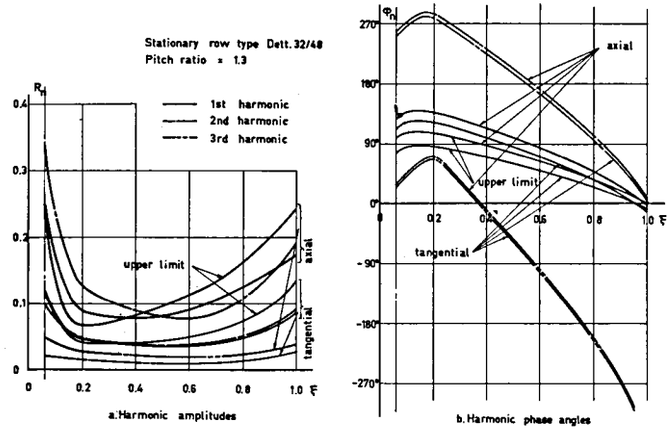

Fig. 4.30

Figs. 4.26....30 Harmonic amplitudes & phase angles for the axial & tangential components of the dynamic force

Leer - Vide - Empty

strongly. This can be attributed to the velocity distribution before the moving row of blades, as shown in figs. 4-9. The magnitude of any harmonic amplitude R_n is proportional to the shape of the velocity-wake, and especially to its height, we can therefore see at once from figs. 4-9 the cause of this resulting radial distribution of the different amplitudes of the dynamic forces. The wake height and form for both row configurations are nearly constant along the middle part of the blade length. Hub and casing walls affect the wake form and consequently the dynamic-force harmonic amplitude. This can be seen very clearly in the difference between the radial distributions at the tip section (MP 7) for Dett.40/48 and Dett.32/48. The decrease of the amplitudes at this section relative to the adjacent section (MP 6) for Dett. 40/48 is due to the similar decrease in the velocity-wake heights, whereas in the case of Dett. 32/48 both the amplitudes R_n and the wake height increase towards the tip section.

2. The radial distribution of R_n for a given configuration is similar for the different pitch ratios. On the other hand, the absolute values of these harmonic amplitudes vary according to the pitch ratio and as expected in 2.3.2. These variations will be discussed in detail later in this chapter.

3. The radial distribution has been drawn according to calculations based on the measurements of the velocity components discussed in 4.2. The distribution is extended to the tip section of the blade ($\xi = 1$) by means of extrapolation. This can be partly justified by the fact that MP 7 lies very near to the tip (see 4.1). Extrapolation to the hub section is not as accurate as for the tip section, because of the steepness of the radial distribution of R_n at this section. This part of the distribution near the hub is, however, not necessary for the calculation of the vibratory stresses, since the energy added to the blade at this part near the hub is negligible, due to the small deflection.

4. In the first case (Dett. 40/48), the first harmonic amplitude of the dynamic force is relatively large, whereas in the second case, the second and third harmonics possess amplitudes as large as the first. This phenomenon is attributed to the relative width of the velocity-wake with respect to the pitch of the stationary blades, which is larger for the first configuration than for the second one. These results are also explained by the values of the different harmonic amplitudes of the velocity distribution, as shown in fig. 11.

5. Along most of the blade length the upper limit amplitudes of the first harmonic lie for both configurations above the lower limit. This is consistent with the analysis of 4.4.1. This part in which the upper limit exceeds the lower is important for

the calculation of the vibratory stresses, since most of the energy is added to the blade in this part, whereas only a negligible amount of energy is added to the other part (near blade's hub-section).

6. The phase angle φ_n is found to be proportional to the phase shift between the different wakes in the velocity distributions shown in figs. 4-9. The radial distribution of the phase angle φ_n along the blade length is approximately linear in the middle part (most of the blade length), and drops suddenly near the hub (see velocity distribution); furthermore, a slight drop is also to be seen near the tip section. This distribution can be directly attributed to the relative positions of the velocity wakes shown in figs. 4-9.

7. A slight difference can be noticed between the phase angle of the axial and tangential components of the dynamic force. This difference grows smaller for higher harmonic orders and is negligible compared with the total phase-angle range.

8. The phase angle distribution of the upper limit differs slightly from that of the lower limit. This difference is mainly due to the part added to the lower limit of the dynamic force to form the upper limit. This part need not necessarily have the same phase angle as the lower limit.

9. The ratio between the range of variations in the phase angle φ_n along the blade length for the first, second and third harmonic orders respectively is approximately 1:2:3. This is due to the fact that the periods of these orders possess geometrically the inverse ratio to each other, and since φ_n depends on the geometrical distribution of the velocity-wakes position, it ought to vary in the range corresponding to the above ratio.

10. The absolute value of the phase angle varies for the different pitch ratios, but the distribution-form and range remain very approximately the same. The variation of the absolute value of φ_n can be attributed to the choice of the origin point of the coordinate-system, which is chosen according to the stationary blades.

In order to explain the variations in the absolute values of the different harmonic amplitudes, we must plot the different harmonic amplitudes of the axial and tangential components of the dynamic force against the pitch ratio R. As before, only the first three harmonic orders will be chosen, and the analysis will be done for only one radial section of the blade length, other sections being considered similar. We choose the mean section of the blade length MP 4 for this purpose. The pitch-ratio ranges for which the dynamic force will be given are chosen according to 4.4.2.

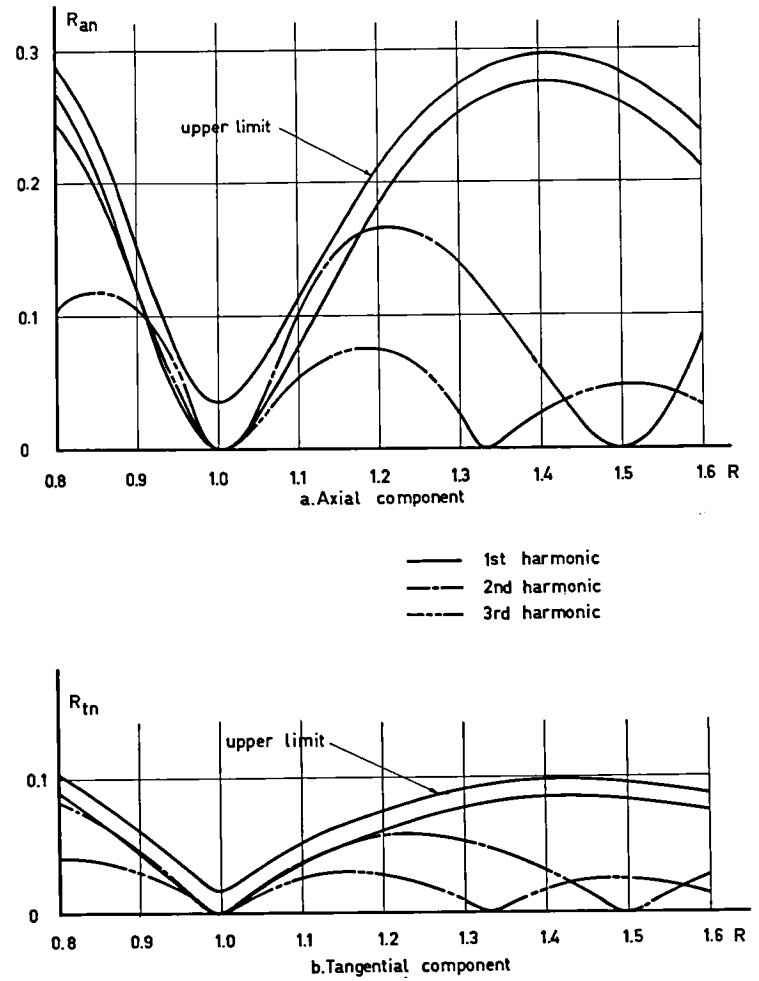

Fig. 4.31 Harmonic amplitudes of the axial & tangential components of the dynamic force for stationary row type Dett. 40/48 & different pitch ratios

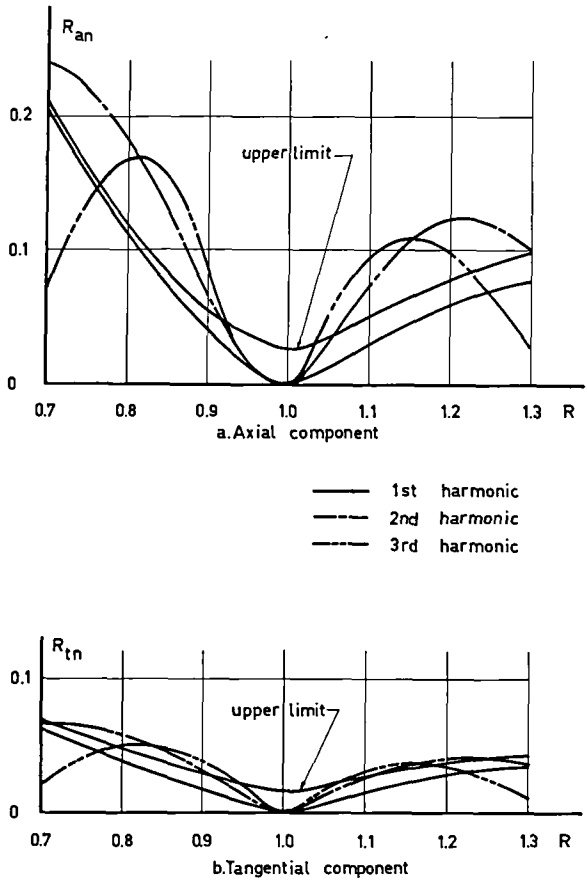

Fig. 4.32 Harmonic amplitudes of the axial & tangential components of the dynamic force for stationary row type Dett. 32/48 & different pitch ratios

Figs. 31 and 32 give the results for the two configurations 40/48 and 32/48 respectively. From these two figures, in which both the axial and the tangential components of the harmonic amplitude R_n has been plotted, we can see that:

1. The amplitudes of the different harmonics depend to a great extent on the pitch ratio R , as expected (for a particular configuration). For each harmonic order, there are certain pitch ratios at which the amplitude is zero, as expected by the analysis in 2.3.2.
2. The amplitudes of the first and second order harmonics of the first configuration (Dett. 40/48) are higher than those of the second configuration, whereas that of the third order is lower. This is mainly due to the shape of the velocity wake at entrance to the moving row of blades and can be seen from the converging character of the different velocity harmonic-amplitudes shown in fig. 11.
3. The upper-limit difference of the first order is relatively small. This means that the approximation in its calculation is of minor importance to the absolute value of the dynamic force.

4.4.3. Mutual effects of the different harmonic orders on the dynamic force

It is of great importance to study the effect of the different harmonic orders on each other, in other words, to study the effect of higher and lower orders of the velocity distribution on a certain harmonic order of the dynamic force. In order to be able to do this, we will choose a certain pitch ratio for which all harmonic orders of the dynamic force have relatively large amplitudes, and study these mutual effects for the mean section MP 4. The different harmonic coefficients F_{an}, F'_{an}, F_{tn} and F'_{tn} will be calculated for the first three orders. In each case a certain higher or lower harmonic order of the velocity distribution coefficients a_n, b_n, c_n and d_n will be neglected, thus studying their effects on the calculated coefficients of the given harmonic order.

Tables 7 and 8 give the results of these studies for Dett. 40/48 and Dett. 32/48 respectively (R = 1.2).

Table 7 Harmonic coefficients of the dynamic force as calculated after neglecting higher and lower orders of the velocity distribution harmonics; Dett. 40/48.

n	neglected order	F_{an}	F'_{an}	F_{tn}	F'_{tn}
1	no	0.095326	-0.024138	0.027691	0.004083
	2	0.095326	-0.024139	0.027690	0.004096
	0 & 2	0.094430	0.015717	0.026874	0.003071
2	no	-0.030060	-0.094994	0.001312	-0.025728
	3	-0.030060	-0.094994	0.001315	-0.025727
	1 & 3	-0.030061	-0.094994	0.001327	-0.025729
	0,1 & 3	-0.032945	-0.094761	-0.002058	-0.025454
3	no	-0.045293	-0.016483	-0.012120	-0.001983
	4	-0.045293	-0.016483	-0.012120	-0.001983
	2 & 4	-0.045293	-0.016482	-0.012122	-0.001990
	1,2 & 4	-0.045293	-0.016482	-0.012122	-0.001990
	0,1,2 & 4	-0.045362	-0.015559	-0.013667	-0.000917

Table 8 Harmonic coefficients of the dynamic force as calculated after neglecting higher and lower orders of velocity distribution harmonics; Dett. 32/48.

n	neglected order	F_{an}	F'_{an}	F_{tn}	F'_{tn}
1	no	0.037483	-0.003320	0.014059	-0.001533
	2	0.037484	-0.003319	0.014064	-0.001523
	0 & 2	0.035625	-0.007268	0.012097	-0.005695
2	no	-0.064033	-0.062401	-0.013269	-0.015613
	3	-0.064033	-0.062402	-0.013300	-0.015595
	1 & 3	-0.064032	-0.062402	-0.013297	-0.015598
	0,1 & 3	-0.066140	-0.059868	-0.015523	-0.012917
3	no	-0.000287	0.044501	-0.006676	0.016896
	4	-0.000287	0.044501	-0.006677	0.016896
	2 & 4	-0.000288	0.044501	-0.006684	0.016894
	1,2 & 4	-0.000288	0.044501	-0.006684	0.016894
	0,1,2 & 4	0.001709	0.045010	-0.004676	0.017429

The results in both cases prove that only the same harmonic order of the velocity distribution at entrance to the moving-blades row is responsible for the greatest part of a certain dynamic-force harmonic-component. Higher and lower orders have only negligible effects on the results as shown in both tables. The effect of the zero harmonic order or steady component of the velocity distribution on the different harmonic components of the dynamic force has also been calculated, and given in the tables 7 and 8.

These results are considered very important, since they prove that any particular harmonic component of the dynamic force on a moving turbine blade is governed to a large extent by the same harmonic component of the velocity distribution before entrance to that row of blades, and that the effects of other orders can be neglected.

It is to be noticed too, on studying the two tables together, that the effect of the lower orders is usually larger than that of the higher orders, and this is mostly attributed to the convergence of the velocity-distribution harmonic-coefficients. Furthermore, the mutual effect for the second configuration is larger than the first, but the difference is of no importance to the absolute values of the results.

The effect of the pitch ratio in this study can be seen from the distribution of the increase or decrease among the different coefficients F_{an}, F'_{an}, F_{tn} and F'_{tn}. This can be justified by studying both equations (2.40) and (2.47).

In this way we conclude the calculation of the dynamic-force distribution along the turbine blade length. The results are given in one particular form which is simple to interpret and understand (amplitude and phase angle). The other way of representing the harmonic components of the dynamic force (sine and cosine form) will be used in the calculation of the vibratory stresses according to chapter 3.

4.5. Calculation of the vibratory stresses

The calculation of the vibratory stresses follows the method given in chapter 3. This method is based on a knowledge of the radial distribution of the different harmonic components of the dynamic force, and the natural modes of vibration of the given blade. The energy added to the vibrating blade in resonance is used to calculate these stresses. It is assumed that the maximum bending stress occurs at the hub section of the blade, due to vibration along the weakest direction of resistance (for untwisted blades).

4.5.1. Considerations of harmonic resonance

One of the assumptions made in the calculation of the vibratory stresses is that a condition of resonance exists between a certain harmonic component of the dynamic

force and a natural mode of vibration of the blade being examined (see 3.1). This does not apply to our example, since the measurements of the velocity distribution for both the configurations used (Dett. 40/48 and Dett. 32/48) were made at a single, constant turbine speed (8000 r.p.m.), and this does not correspond to resonance with any natural mode of vibration of the blade.

To avoid this difficulty, we shall consider a geometrically larger or smaller turbine running at a higher or lower speed according to the conditions dictated by the non-dimensional analysis. Doing this results in

a. Changing the natural frequency of the examined blade (constant cross section), since, for geometrically similar blades, the natural frequency is inversely proportional to the blade length [2].

b. Changing the frequency of the exciting force by changing the turbine speed.

It must be noticed, however, that the changes in blade geometry and turbine speed are to be chosen in the correct sense required to achieve resonance. By doing this, some changes may occur in the Reynold's number; however, their effect on the velocity distribution (which must be non-dimensionally the same) can be neglected.

In this manner, we may apply the results obtained in 4.4 for the radial distribution of the different harmonic components of the dynamic force, and calculate the vibratory stresses at any condition of resonance, and for any harmonic order.

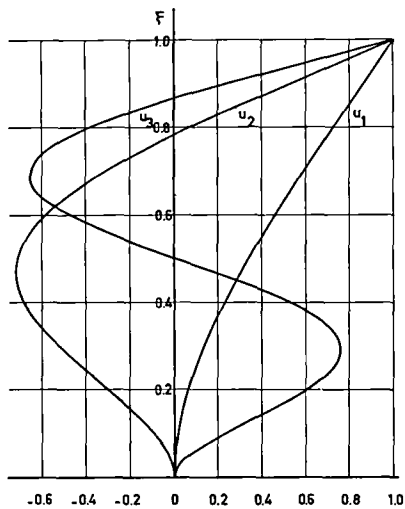

Fig. 4.33 Dynamic deflection-line for a turbine-blade with a constant cross-section, one end fixed and the other free.

4.5.2. Calculation of the dynamic deflection line

One of the main factors in the calculation of the vibratory stresses is the dynamic deflection line, or the displacement of the elastic line of the turbine blade at resonance. This deflection line depends on different factors: a) distribution of the turbine blade cross-section along the blade length, b) fixing of the blade end, and c) harmonic order of the mode of vibration. Our example of the Dettmering profile represents one of the simplest cases. The blade is considered as a non-twisted bar with a constant cross-section, fixed at one end and free at the other. The dynamic deflection line in this case is calculated for the different harmonic orders according to appendix I.

The results for the first, second and third orders are given in table 9 for small intervals of ξ (0.05), such as might be needed for the numerical integration, and are also plotted in fig. 33. In both cases, u_n represents the non-dimensional deflection-line as defined in 3.3.

Table 9 Non-dimensional deflection functions u_n

ξ	u_1	u_2	u_3
0	0	0	0
0.05	0.00428	-0.02523	0.08696
0.10	0.01675	-0.09255	0.22784
0.15	0.03679	-0.18863	0.42445
0.20	0.06380	-0.30083	0.60413
0.25	0.09719	-0.41698	0.72427
0.30	0.13635	-0.52582	0.75632
0.35	0.18071	-0.61736	0.68860
0.40	0.22969	-0.68320	0.52695
0.45	0.28273	-0.71678	0.29322
0.50	0.33928	-0.71359	0.02146
0.55	0.39882	-0.67130	-0.24746
0.60	0.46086	-0.58970	-0.47218
0.65	0.52493	-0.47061	-0.61700
0.70	0.59060	-0.31758	-0.65712
0.75	0.65749	-0.13562	-0.58199
0.80	0.72524	0.06934	-0.39618
0.85	0.79358	0.29099	-0.11762
0.90	0.86225	0.52320	0.22667
0.95	0.93110	0.76075	0.60721
1.00	1.00000	1.00000	1.00000

The calculation of the vibratory-stresses depends also on the factor H_n, defined in 3.3. Its value depends solely on the form of the deflection line, and can be calculated for the different harmonic orders according to equation (3.22) and appendix I. Table 10 gives the value of this factor for the first three harmonic orders.

Table 10 Values of H_n for the first three harmonic orders.

n	1	2	3
H_n	0.87	0.0795	0.0162

4.5.3. Calculation of the dynamic stimulus S_n

The most important factor for the calculation of the vibratory stresses is the dynamic stimulating factor or stimulus S_n . As shown by equation (3.23), the calculation of this factor depends on the radial distribution of the harmonic coefficients of the dynamic force for the given order, and the form of the dynamic deflection line. The harmonic coefficients of the axial and tangential components of the dynamic force F_{an}, F'_{an}, F_{tn} and F'_{tn} are reduced according to 3.2, to the coefficients F^*_n and $F^{*\prime}_n$, which are required in equation (3.23) to calculate the stimulus. In the numerical integration for the stimulus it was found necessary to use small intervals of ξ_i (0.05), especially for the second and third orders, when the harmonic coefficients pulsate frequently along the blade length, due to the large range of the phase angle φ_n (this range can be seen in figs. 21-30).

The results of the calculation of the stimulus are plotted in figs. 34 and 35 for both configurations and for different pitch ratios. Fig. 34 shows that the stimulus for the first harmonic order is larger than that for the second and third orders. On the other hand studying fig. 35 shows the reverse of the latter phenomenon.

The absolute value of the stimulus for the third harmonic order for the configuration Dett. 32/48 is seen from fig. 35 to be relatively high (up to approximately 0.30). This is not, however, dangerous, because the vibratory stresses depend also on the factor H_n , which is small for this harmonic order. This will be shown later in this chapter when studying the distribution of $D_{n\,max}$.

A very important factor in the calculation of the stimulus is of course the phase

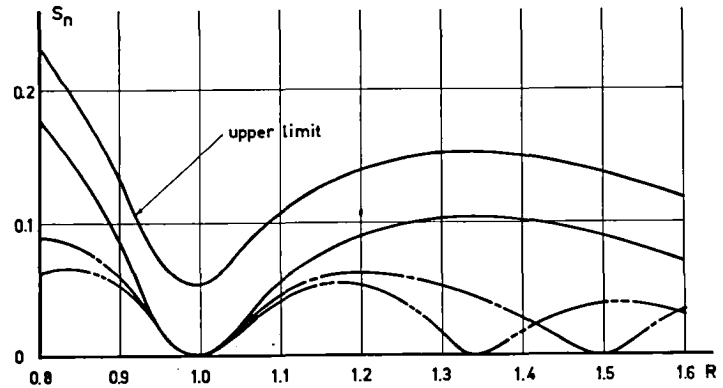

Fig. 4.34 Dynamic stimulating factor for stationary row type Dett. 40/48.

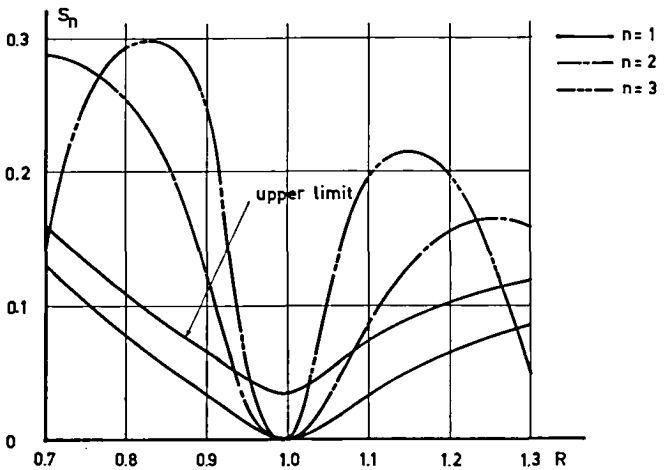

Fig. 4.35 Dynamic stimulating factor for stationary row type Dett. 32/48.

angle φ_n . This angle determines the ratio between F_n^* and $F_n^{*'}$ for the different sections along the blade length. It, therefore, affects the amount of energy added to the vibrating blade in each harmonic order, and consequently the value of the stimulus; it is probably due to this fact that the third harmonic order of the stimulus for Dett. 32/48 is relatively high.

The vibratory stresses in the turbine blade depend on the different factors discussed above, and in order to obtain a better idea about their values in our case, it is useful to calculate the stress ratio factor $D_{n\,max}$, which gives the ratio of the maximum vibratory bending-stress for a certain harmonic order n to the static bending stress under the same conditions (definition in equation (3.24)). The value of the logarithmic decrement δ is essential for this calculation. We shall choose a 13% Ni steel for our blade, which has a logarithmic decrement $\delta = 0.02$ [2]. This value of δ is considered to be on the high side for the different steels used for turbine blades.

The stress ratio $D_{n\,max}$ is calculated for the two configurations of our example, and for the first three harmonic orders. It is plotted for both configurations, and for each order separately. The results obtained are shown in figs. 36, 37 and 38, for the first, second, and third orders respectively. From these figures we can see that, in general, the first order stress-ratio for Dett. 40/48 is higher than that for Dett. 32/48, whereas for the second and third orders it is lower. This is largely due to the distribution of the dynamic stimulus, shown in figs. 34 and 35. Furthermore, the steady bending stresses when at resonance with the first mode of vibration are largely magnified to give the vibratory stresses (up to 30 times). This can even be higher in the case of other steels used for turbine blades, possessing a smaller δ . On the other hand the magnification of the steady stresses for higher orders (second and third) is relatively small, as shown in figs. 37 and 38.

If a trial is made to select the most suitable range of moving-blade pitches for the optimum aerodynamic conditions, we can find according to Traupel [2], that, for the Dettmering blade the optimum chord/pitch ratio should lie between 1.19 and 1.45. This corresponds to the following pitch ratios in our analysis.

Dett. 40/48	$R \cong 1.1 - 1.3$
Dett. 32/48	$R \cong 0.9 - 1.1$

It is clear, on examining fig. 36, that, to attain a low vibratory-stress level, the second configuration is better than the first. This is due to

1. The first order vibratory-stress level is lower for the second configuration.
2. The calculated pitch range of the optimum aerodynamic conditions for the second

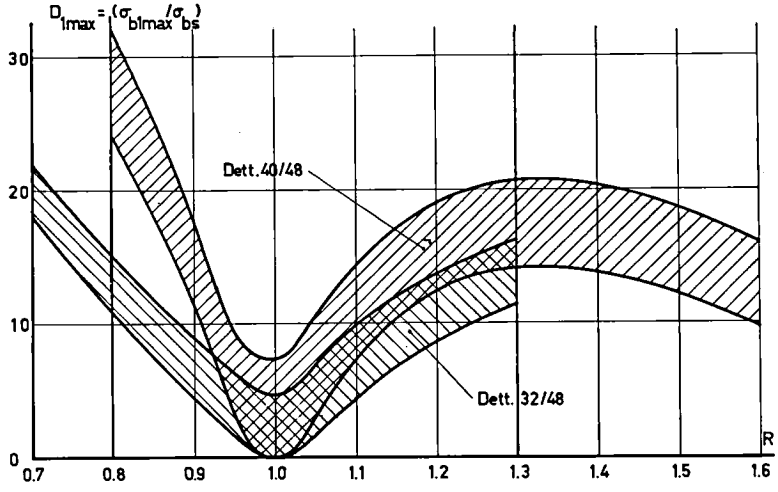

Fig. 4.36 Maximum stress-ratio for the first order harmonic resonance

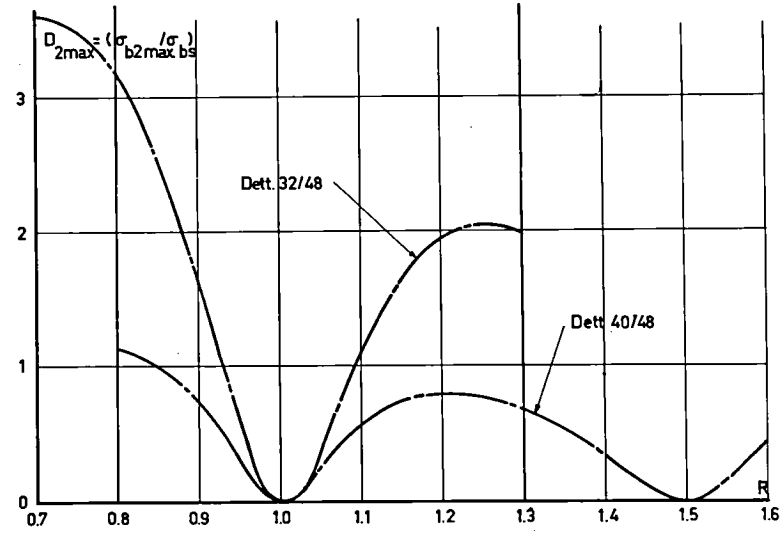

Fig. 4.37 Maximum stress-ratio for the second order harmonic resonance

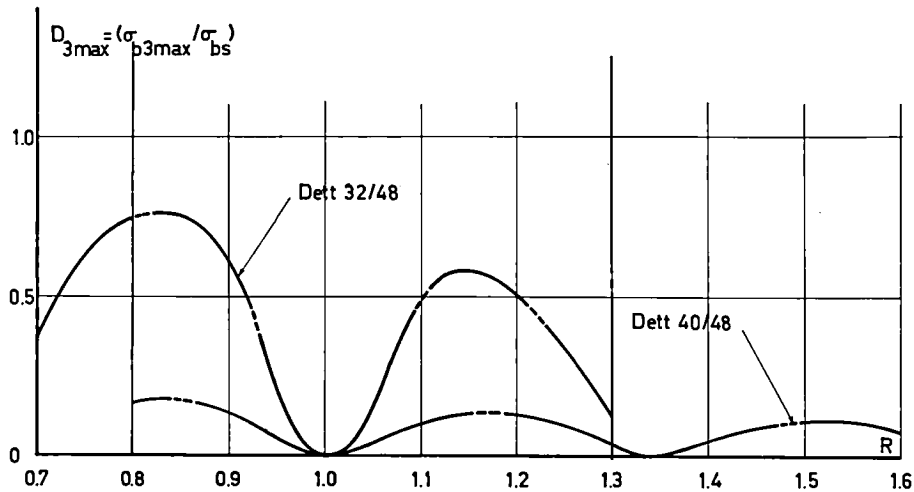

Fig. 4.38 Maximum stress-ratio for the third order harmonic resonance

configuration corresponds to a lower vibratory-stress level, as seen in fig. 36.

It should be stated here that, according to the Dettmering report, the configuration Dett. 32/48 is aerodynamically better than Dett. 40/48.

4.6. Concluding remarks

In this chapter, the dynamic forces and vibratory stresses have been calculated according to the theory established in chapters 2 and 3 respectively. The calculations have been done for a certain specific example, which was chosen according to the conditions stated at the start. The main purpose of this example was to win a qualitative but still precise look at the application of the theory established. By allowing different pitch ratios as parameters the solution has been given a more or less general form, which can be expected to help in future studies.

The ultimate aim of the theory and calculated numerical example was to study the vibratory stresses in a turbine blade. It was seen that these stresses are proportional to the energy added to the vibrating blades. This energy depends on the radial distribution of the dynamic-force along the blade length, and the mode of vibration of the blade (the dynamic deflection line).

It has been found that the dynamic forces depend on the aerodynamic conditions existing before the moving row of blades (velocity distribution) as well as on the shape and configurations of both the moving and the stationary rows (form-parameters). The stationary-row configuration affects mainly the form of the velocity distribution (wake shape) which in turn affects to a large extent the dynamic force, whereas the pitch ratio R , which depends on configurations of both rows, changes the level of the dynamic force, as shown in 4.4.2.

The dynamic deflection line depends purely on design factors and can be calculated, once the blade shape and method of fixing to the rotor have been decided. It can be calculated analytically for simple cases such as the example chosen, otherwise it becomes necessary to use relatively tedious graphical and numerical methods for the general and complicated cases of a twisted blade with a variable cross-section distribution. This latter case is more probable for turbine blades, which are liable to run in resonance with some exciting-force frequencies.

The results obtained show that it is possible to calculate the vibratory stresses at resonance more accurately than recent estimations based on statistical data. It has been shown that the assumptions for the radial distribution of the dynamic force such as have been made before are very approximate.

The vibratory stresses have been found to be very high in the first order, although they can sometimes be neglected for higher orders. The first order stress-level is found to be equal to, if not greater than, the centrifugal stresses on the blade, moreover it possesses a dangerous alternating character.

The theory established enables the turbine blade designer to estimate the maximum vibratory stress which might occur in a turbine blade, if it was forced to run in resonance with some exciting force harmonic frequencies.

APPENDIX I

Calculation of the dynamic deflection lines for a bar with constant cross-section, fixed at one end and free at the other:

The solution of this problem is given in [2], and it is only necessary to change it to suit our analysis.

The deflection at any distance ξ from the fixed end of the bar for any harmonic order n is given by

$$Y_n(\xi) = C_{n1}(\sin \varkappa_n \xi - \sinh \varkappa_n \xi) + C_{n2}(\cos \varkappa_n \xi - \cosh \varkappa_n \xi) \quad (1)$$

where the following condition applies for the relation between the two constants,

$$\frac{C_{n1}}{C_{n2}} = \frac{\sin \varkappa_n - \sinh \varkappa_n}{\cos \varkappa_n + \cosh \varkappa_n}$$

Thus we can write

$$C_{n2} = A_n C_{n1} \quad (2)$$

where

$$A_n \equiv \frac{\cos \varkappa_n + \cosh \varkappa_n}{\sin \varkappa_n - \sinh \varkappa_n} \quad (3)$$

Substituting equation (2) in (1) we get

$$Y_n(\xi) = C_{n1} \left\{ (\sin \varkappa_n \xi - \sinh \varkappa_n \xi) + A_n (\cos \varkappa_n \xi - \cosh \varkappa_n \xi) \right\} \quad (4)$$

Choosing the deflection at the free end as a reference value, we can define the non-dimensional deflection u_n by

$$u_n(\xi) \equiv \frac{Y_n(\xi)}{Y_n(1)} \tag{5}$$

Substituting $\xi = 1$ in equation (4) we find

$$Y_n(1) = C_{n1} \left\{ \frac{-2 \sin \varkappa_n \sinh \varkappa_n}{\sin \varkappa_n - \sinh \varkappa_n} \right\} \tag{6}$$

Substituting equations (4) and (6) in (5) we can write

$$u_n(\xi) = B_n \left\{ (\sin \varkappa_n \xi - \sinh \varkappa_n \xi) + A_n (\cos \varkappa_n \xi - \cosh \varkappa_n \xi) \right\} \tag{7}$$

where

$$B_n \equiv \frac{\sin \varkappa_n - \sinh \varkappa_n}{-2 \sin \varkappa_n \sinh \varkappa_n} \tag{8}$$

giving the dynamic deflection line for any harmonic order n. Differentiating equation (7) once and twice with respect to ξ we get

$$u_n'(\xi) = \varkappa_n B_n \left\{ (\cos \varkappa_n \xi - \cosh \varkappa_n \xi) - A_n (\sin \varkappa_n \xi + \sinh \varkappa_n \xi) \right\} \tag{9}$$

$$u_n''(\xi) = -\varkappa_n^2 B_n \left\{ (\sin \varkappa_n \xi + \sinh \varkappa_n \xi) + A_n (\cos \varkappa_n \xi + \cosh \varkappa_n \xi) \right\} \tag{10}$$

BIBLIOGRAPHY

[1] Sabastiuk, A. & Sisto, F. — A survey of aerodynamic excitation in turbomachines. Trans. ASME, 78 (1956), pp. 555-564.

[2] Traupel, W. — Thermische Turbomaschinen, Bd. I & II. First edition, Springer (1958-1960).

[3] Kemp, N.H. & Sears, W.R. — The unsteady forces due to viscous wakes in turbomachines, Journ. of Aero. Sc. (1955), pp. 478-483.

[4] Nolan, R.W. — Vibration of marine-turbine blading. Trans. ASME 72 (1950), pp. 439-446.

[5] Forshaw, J.R. — Gas turbine principles and practice, Ch. 12 Vibration. (Cox, H.R.). Newnes (1955).

[6] Trumpler, W.E. & Owens, H.M. — Turbine-blade vibration and strength. Trans. ASME 77 (1955), pp. 181-194.

[7] Prohl, M.A. — A method for calculating vibration frequency and stress of a banded group of turbine buckets. Trans. ASME 80 (1958), pp. 169-180.

[8] Weaver, F.L. & Prohl, M.A. — High frequency vibration of steam-turbine buckets. Trans. ASME 80 (1958) pp. 181-194.

[9] Kaufmann, W. — Technische Hydro- und Aeromechanik. 2 edition (1958), Springer.

[10] Zerkowitz, G. — Der Antriebsatz der mehrdimensionalen Strömungslehre nebst technischen Anwendungen. Zeitschrift für das ges. Turbinenwesen, 27 (1916). p.43.

[11] Tolstow, G.P. — Fourierreihen. Deutscher Verlag der Wissenschaft.

[12] Rosard, D.D. — Natural frequencies of twisted cantilever beams. Journ. of appl. mechanics, 20 (1953), p. 241.

[13] Waldburger, H. — Gebrauchsanleitung für die ERMETH (Elektronische Rechenmaschine der ETH). Inst. für Angew. Mathematik ETH.

[14] Dettmering, W. Experimentelle Untersuchungen an einer axialen Turbinenstufe. Forschungsbericht des Landes Nordrhein-Westfalen Nr. 908, Westdeutscher Verlag (1960).

[15] Zurmühl, R. Praktische Mathematik, 3rd edition, Springer (1961).

Zusammenfassung

Der Zweck dieser Arbeit ist die Abschätzung der periodischen Kräfte auf eine Turbinenschaufel, die sich aus der periodischen Geschwindigkeitsverteilung hinter einem vorgeschalteten Schaufelkranz ergeben. Zunächst wird die Strömung eines inkompressiblen Mediums für ein einzelnes Element von unendlich kleiner radialer Ausdehnung betrachtet. Unmittelbare Einflüsse der Reibung werden dabei vernachlässigt, d.h. es wird nur der durch die Reibung im vorgeschalteten Kranz gestörte Charakter der Zuströmung berücksichtigt. Das führt zu einer einfachen Formulierung der Kontinuitäts-, Impuls- und Energie-Gleichung. Der so gewonnene Ausdruck für die Kraft kann nun längs der Schaufel integriert werden. Die Untersuchung zeigt, wie diese periodische Gesamt-Kraft vom Charakter der Störungs-Zonen (Geschwindigkeits-Dellen) und der Geometrie der Schaufelgitter abhängt. Für die weitere Untersuchung erweist es sich als zweckmässig, die Kräfte in eine Fourier-Reihe zu zerlegen.

Auf Grund dieser Unterlagen wird es möglich, die Deformation und somit die Beanspruchung einer Schaufel im Resonanz-Fall zu berechnen, sobald die Material-Dämpfung bekannt ist. Eine aerodynamische Dämpfung wird nicht eingeführt, da sie sich unter den gegebenen Voraussetzungen als klein erweist.

An durchgerechneten Beispielen wird gezeigt, welche Amplituden bei den verschiedenen Schwingungs-Ordnungen zu erwarten sind. Insbesondere zeigt es sich, dass man die erste Ordnung etwa richtig abschätzen kann, wenn man annimmt, die periodische Kraft-Amplitude betrage im Maximum ca. 20% des Mittelwertes der Schaufelkraft.

CURRICULUM VITAE

As a citizen of the U.A.R. (Egypt) I was born in Cairo on the 10th January, 1937. At the age of five I began my school career and continued it in the primary and secondary schools of Cairo. In July 1953 I passed the leaving examination of the secondary schools, qualifying for admission to the University. At Cairo University, I studied engineering from 1953 to 1958, graduating from the mechanical engineering department in June 1958. After my graduation I was appointed as an assistant in the mechanical engineering department of Cairo University, where I was mainly concerned with problems of steam turbines and thermal power-stations.

Winning a scholarship offered by the government of the United Arab Republic, I came to Switzerland in October 1959 to continue my studies in the branch of thermal turbomachines. I was admitted as a listening student to the Federal Institute of Technology in Zürich (ETH). After two academic terms I sat the admission examination. Passing this examination in November 1960 successfully, I was allowed to begin my research under the guidance of Prof. Dr. W. Traupel, professor of thermal turbo-machines in the Federal Institute of Technology (ETH). During the last few years (1960 to 1964), while I was preparing my thesis, I kept in contact with various Swiss and German Industrial Concerns for the development and production of thermal turbomachines.